AD/A-004 226

ACOUSTIC FLUCTUATIONS DUE TO SHALLOW WATER THERMAL MICROSTRUCTURE

James Burgess Hagen

Naval Postgraduate School
Monterey, California

September 1974

AD/A004226

REPORT DOCUMENTATION PAGE		READ INSTRUCTIONS BEFORE COMPLETING FORM
1. REPORT NUMBER	2. GOVT ACCESSION NO.	3. RECIPIENT'S CATALOG NUMBER
4. TITLE (and Subtitle) Acoustic Fluctuations Due to Shallow Water Thermal Microstructure		5. TYPE OF REPORT & PERIOD COVERED Master's Thesis; September 1974
		6. PERFORMING ORG. REPORT NUMBER
7. AUTHOR(s) James Burgess Hagen		8. CONTRACT OR GRANT NUMBER(s)
9. PERFORMING ORGANIZATION NAME AND ADDRESS Naval Postgraduate School Monterey, California 93940		10. PROGRAM ELEMENT, PROJECT, TASK AREA & WORK UNIT NUMBERS
11. CONTROLLING OFFICE NAME AND ADDRESS Naval Postgraduate School Monterey, California 93940		12. REPORT DATE September 1974
		13. NUMBER OF PAGES ~~154~~ 153
14. MONITORING AGENCY NAME & ADDRESS(if different from Controlling Office) Naval Postgraduate School Monterey, California 93940		15. SECURITY CLASS. (of this report) Unclassified
		15a. DECLASSIFICATION/DOWNGRADING SCHEDULE

16. DISTRIBUTION STATEMENT (of this Report)

Approved for public release; distribution unlimited.

17. DISTRIBUTION STATEMENT (of the abstract entered in Block 20, if different from Report)

18. SUPPLEMENTARY NOTES

PRICES SUBJECT TO CHANGE

19. KEY WORDS (Continue on reverse side if necessary and identify by block number)

Acoustic Fluctuations
Thermal Microstructure
Shallow Water Thermal Microstructure

20. ABSTRACT (Continue on reverse side if necessary and identify by block number)

    Simultaneous measurements of waves, orthogonal water particle velocities, temperature, conductivity and acoustic phase and amplitude measurements at 20 and 40 kHz over horizontal and vertical, 2m paths were made at the NUC oceanographic tower, San Diego in April 1974.

    Four stochastic models for acoustic propagation including geometric, Born, Rytov and Debye approximation models were

DD FORM 1473 EDITION OF 1 NOV 65 IS OBSOLETE
1 JAN 73
(Page 1)   S/N 0102-014-6601 |

UNCLASSIFIED

(153)

(20. ABSTRACT   continued)

tested.   The Krosil'nikov - Obhukov formulation of the Born
approximation yielded reasonable results.   Diffulty in
establishing scales obviated good results from the Rytov and
Debye models.

Taylor thermal microscales from spatial correlation
analyses determined vertically across the thermocline varied
from 6.8 to 178 cm.   The measured variance of the index of
refraction ranged from 4.5×10^{-4} to 2.7×10^{-3}.

Temporal stochastic analyses showed horizontal acoustic
path losses were ten times vertical losses because of
diffraction effects.   The primary mechanisms for acoustic
variability were internal and surface waves pumping the
thermocline up and down.

Acoustic Fluctuations Due to
Shallow Water Thermal Microstructure

by

James Burgess Hagen
Lieutenant, United States Navy
B.S.E.E., University of Colorado, 1966

Submitted in partial fulfillment of the
requirements for the degree of

MASTER OF SCIENCE IN OCEANOGRAPHY

from the

NAVAL POSTGRADUATE SCHOOL
December 1974

Author _____

Approved by _____

Thesis Advisor

_____

Second Reader

_____

Chairman, Department of Oceanography

_____

Academic Dean

3

ABSTRACT

Simultaneous measurements of waves, orthogonal water particle velocities, temperature, conductivity and acoustic phase and amplitude measurements at 20 and 40 kHz over horizontal and vertical, 2m paths were made at the NUC oceanographic tower, San Diego in April 1974.

Four stochastic models for acoustic propagation including geometric, Born, Rytov and Debye approximation models were tested. The Krosil'nikov - Obhukov formulation of the Born approximation yielded reasonable results. Difficulty in establishing scales obviated good results from the Rytov and Debye models.

Taylor thermal microscales from spatial correlation analyses determined vertically across the thermocline varied from 6.8 to 178 cm. The measured variance of the index of refraction ranged from 4.5×10^{-4} to 2.7×10^{-3}.

Temporal stochastic analyses showed horizontal acoustic path losses were ten times vertical losses because of diffraction effects. The primary mechanisms for acoustic variability were internal and surface waves pumping the thermocline up and down.

TABLE OF CONTENTS

LIST OF TABLES

LIST OF FIGURES

ACKNOWLEDGEMENTS

I. INTRODUCTION

A. HISTORY

A continuing program of in situ ocean microstructure research has been conducted at the United States Naval Postgraduate School (NPS) since 1971. Under this program, a series of three annual experiments dedicated to the study of the complex temporal and spatial relationships between multiple parameters measured in shallow water have been conducted by the Department of Oceanography. Each of these experiments has been restricted in scope to measurements inside a 9 m^3 volume of water and to oceanographic phenomena which occur in the frequency range 0.001 to 2.5 Hz.

B. OBJECTIVES

In this thesis, initial analysis of certain parameters measured in the latest of these experiments is reported. Primary emphasis is given to stochastic temperature relationships affecting high frequency (20 kHz) CW sound transmission over a short path. The particular objectives of this experiment were to investigate the dependence of acoustic phase and amplitude fluctuations on the magnitude and characteristics of the ocean thermal structure and the intensity of the related turbulence.

10

II. THEORY

The description of oceanic turbulence by stochastic
techniques has followed developments in the atmosphere.
One of the principal difficulties in application of the
theoretical methods provided from atmospheric research has
been determination of the range of applicability of certain
turbulence models in terms of ocean parameters. Another
has been the application of these models to sound propagation
in a manner similar to the relationships developed for
electromagnetic wave propagation in the atmosphere as
summarized by Strohbehn [1968]. Historically, attempts to
resolve these difficulties have been interconnected since
their primary relevance is to acoustic prediction which
motivated the research.

A. STOCHASTIC MODELS FOR THE MEDIUM

Three expected value techniques which have been applied
to turbulence calculations in the ocean are 1) the spatial
correlation (autocorrelation) function, 2) the structure
function and 3) a "piecewise correlation" function.
Application of each technique requires a statistically
homogeneous medium but the order above indicates their
relative applicability to increasingly less stringent
stationarity requirements. The function form for each is
listed below.

11

The autocovariance function, $R_x(\rho)$:

$$R_x(\rho) = E[T(x)T(x+\rho)] \ . \tag{1}$$

The structure function, $D_x(\rho)$

$$D_x(\rho) = E\{[T(x) - T(x+\rho)]^2\} \ . \tag{2}$$

The piecewise correlation function, $R'_x(\rho)$

$$R'_x(\rho) = E[1 - \frac{E\{[T(x) - T(x+\rho')]^2\}}{2 R_x(0)}$$

$$= E[1 - \frac{D_{\tilde{x}}(\rho')}{2 R_x(0)}] \ . \tag{3}$$

E indicates expected value and ρ is the spatial lag. For completely stationary processes, the structure function and the "piecewise correlation" function reduce to

$$D_x(\rho) = 2[R_x(0) - R_x(\rho)] \ , \tag{4}$$

and $\qquad R'_x(\rho) = E[1 - D_x(\rho)'/2R_x(0)] = R_x(\rho')/R_x(0).$

$$\tag{5}$$

The stationarity difficulties often encountered in the use of $R_x(\rho)$ are partly overcome by the use of $D_x(\rho)$ because the large scale effects in the ocean are differentially filtered out [Black 1965]. The piecewise correlation function

12

can be applied to measurements which have only "piecewise
stationarity." This makes it the most powerful tool of the
three techniques. "Piecewise stationarity" is defined as
stationarity (in the ordinary sense) over a sufficient
record length for which the structure function and variance
can be calculated. This method was proposed by Whitmarsh,
Skudrzyk and Urick [1957].

Various analytical equations have been used to approxi-
mate the form of the auto covariance function used to describe
the environment. Liebermann [1951] used a simple exponential
form in his early experiments. Others have used a Gaussian
form with some success [Stone and Mintzer 1953]. Use of the
exponential form yields the best fit to experimental data
above certain spatial lags, but it underpredicts the number
of "small" turbulent blobs. This undesirable effect is
eliminated by the use of the Gaussian form.

Kolmogorov [1941] predicted a 2/3 power law dependence
for the structure function for turbulent flow in which there
was a decoupling of the energy producing and energy diss_pa-
tion regions. Batchelor [1953] transformed this result and
demonstrated that in wave number space energy spectra have
a wave number to the -5/3 power law dependence. This was
first verified convincingly by Grant et al. [1962] for ocean
measurements and Pond et al. [1963] for atmospheric measure-
ments. Ocean measurements do not always show the dependence
since the ocean tends to be stratified much more intricately
structured than the atmosphere which makes the recording of

continuous stationary data unlikely. However the -5/3 power law depends not so much upon isotropy as upon the clear separation of scales of energy production and energy dissipation in which a cascade of energy from larger to smaller scales occurs. Whether or not such a form is ubiquitous in the ocean is not as significant as the presence of horizontal sheets which could cause multiple reflection layers. Very sharp, multiple thermal layers have been reported in the Arctic [Denner 1971], for example.

Recently it has been shown that surface wave effects can be removed from ocean turbulence measurements with the result that purely turbulent flow remains and a -5/3 power relationship may be observed [Thornton and Boston 1974]. These findings were based upon measurements both in and around the thermocline and showed that anisotropy was not a critical difficulty, provided additional energy sinks or sources did not result (e.g. in the thermocline).

Unfortunately, other energy contributions to the turbulence spectra do exist. Microstructure related turbulence from salt-fingering is one form [Gregg 1973, Denner 1971]. Billow turbulence resulting from shear instabilities related to internal waves has also been reported by a number of investigators [Woods and Wiley 1972, Gregg 1973, Powell 1974]. Further, the existence of the internal wave itself could be expected to add energy at low frequencies as could surface wave interaction with the thermocline.

B. WAVE PROPAGATION MODELS

Four methods derived from the Helmholtz equation have been used to describe wave propagation through the turbulent ocean. These are: 1) geometrical optics, 2) the Born approximation [Born 1933], 3) Rytov's method [Rytov 1937], and 4) the Bebye approximation [Frisch 1968]. While it is not a necessary assumption, most applications of these methods presume that the ocean is homogeneous so that the scalar wave equation can be used. Such an assumption places a rather severe restriction on the acoustic wavelength, λ, such that

$$\lambda \ll \ell_o \tag{6}$$

where ℓ_o = inner scale of the turbulence. This restriction will be discussed in detail later.

1. Geometrical Optics

The geometrical optics (ray theory) approach is a linearization of the wave equation which assumes only Rayleigh scattering and refraction effects are important. Since diffraction effects are ignored, the high frequency (short wavelength) restriction,

$$\lambda \ll \ell_o^2/L \tag{7}$$

where L = acoustic path length, is placed on the results.

15

One of the first experiments which used a stochastic technique to examine the acoustical effects of small-scale temperature inhomogeneities in the ocean was conducted by Liebermann [1951]. Through the use of the classical optical model, Liebermann was able to predict certain scintillations in sound amplitude observed at sea by the equation:

$$V_I^2 = \frac{8}{15} \sqrt{\pi} \, \alpha^2 \, (L/a)^3 \qquad (8)$$

$$V_I^2 = E[(\frac{\Delta I}{I})^2] \qquad (9)$$

$$\alpha^2 = E[(\frac{\Delta c}{c_0})^2] \qquad (10)$$

where V_I^2 = variance of the sound intensity, I_0 = mean sound intensity, ΔI = the instantaneous deviation of sound intensity from the mean, α^2 = variance of the index of refraction, L = acoustic path length and a = Taylor temperature microscale [Lumley and Panofsky 1964]. Liebermann also showed that sound reverberation encountered in the ocean was larger than that predicted due to thermal inhomogeneities alone. This was substantiated by later developments which have shown that biological scattering, chemical relaxation and bubbles in the near-surface region are important contributors to sound attenuation.

Sagar [1955,1957,1959] was able to show that sonar amplitude fluctuations resulting from temperature measurements could be correlated to sea state. Additionally, he

16

showed that the linear dependence of the variance of sound
pressure level on range [Sheehy 1950] was apparent only when
thermal microstructure was present.

A modified geometrical optics technique has recently
been proposed by Tatarski [1967]. The method is similar to
the classical one except the path length is described as
the eikonal or total path length, θ. However, one would
assume that this would modify the restriction on the results
to

$$\lambda \ll \ell_o^2/\theta \qquad (11)$$

No application of this method to the ocean has yet been made.

2. Born Approximation

The Born approximation is a perturbation technique
applied to the wave equation which is valid only as long
as the acoustic amplitude fluctuations remain small. This
is not a serious restriction in the ocean, even under the
most severe scattering conditions, but the model only accounts
for a single scattering from a turbulent blob over the
acoustic path length, L. This requires that

$$\lambda \ll \alpha \sqrt{aL} \qquad (12)$$

The geometrical optics results are a special, high frequency
case included in this model.

17

Stone and Mintzer [1962, 1965] conducted a series
of laboratory experiments from which they demonstrated
solutions to the Born Model which predict the variance of
normalized sound pressure level, V^2, in a low frequency
region (wave region) and in the ray theory region. For
the wave region they showed:

$$V^2 = \frac{1}{2} \sqrt{\pi} \, k_o^2 \, \alpha^2 \, a \, L \quad \text{(Gaussian } R_x(\rho)) \quad (13)$$

$$V^2 = \alpha^2 \, k_o^2 \, a \, L \quad \text{(Exponential } R_x(\rho)) \quad (14)$$

$$V^2 = E\left[\left(\frac{\Delta P}{P_o}\right)^2\right] \quad (15)$$

$$\lambda \ll 2\pi a \quad (16)$$

$$\lambda \ll 2\pi L \quad (17)$$

$$k_o = 2\pi/\lambda \quad (18)$$

Where P_o = mean sound pressure level and ΔP = pressure level
difference from the mean. For the ray region, no solution
is possible if the exponential form of the spatial correlation
function is used since the solution is divergent. But they
showed that the following equation results from use of the
Gaussian correlation function:

18

$$v^2 = \frac{4}{15} \sqrt{\pi} \; \alpha^2 (L/a)^3 \qquad\qquad (19)$$

Neubert and Lumley [1970] used data from the above experiments to compare with atmospheric data based upon the same model. Their results showed that the turbulent scales for air and water are of the same order of magnitude for "similar" turbulent flows. They were also able to better define the limit on wave length specified in relation (6), such that

$$\lambda \leq a/5[\sigma_k(u/c_0)]^{\frac{1}{2}} \qquad\qquad (20)$$

$$a^2 = \lambda_g^2/\sigma_k \qquad\qquad (21)$$

$$R_t^2 \approx 15(\eta_g/\lambda_g)^4 \qquad\qquad (22)$$

where:

λ_g = Taylor turbulence microscale,

σ_k = Prandtl number for the medium,

u = local turbulent velocity,

c_0 = mean speed of sound in the medium,

R_t = Richardson number,

19

and

η_g = Kolmogorov turbulence microscale.

In addition, they found a restriction on acoustic frequency
was necessary, though it was usually less restrictive than
(20). This restriction is

$$f \geq 750[\sigma_k(R_t)^{\frac{1}{2}}]^{\frac{1}{2}}/\lambda_g \quad (sec^{-1}) \tag{23}$$

It follows from (6) and (20) that

$$\ell_o \simeq O\{a/50[\sigma_k(u/c_o)]^{\frac{1}{2}}\} \quad (cm) \tag{24}$$

which lends additional meaning to relations (6), (7) and
(11).

Whitmarsh, Skudrzyk and Urick [1957] conducted
experiments in the ocean which largely agree with Stone's
and Mintzer's laboratory results. However, they noted the
variance in sound pressure level due to thermal scattering
varied directly as the acoustic frequency and as the range
squared in the Kolmogorov turbulence range. This result is
obviously in the intermediate range between the ray and
wave solution regions suggested by Stone and Mintzer.

They also observed that the turbulent patches were
not spherical, but were spheroidal in shape. In this case,
a simple transform to cylindrical coordinates shows that the

Taylor microscale, a, must be replaced such that

$$a^2 = (b^2/3)(2 + c^2/b^2) \qquad (25)$$

where b = narrower dimension and c = longer dimension of the turbulent patch. This has the effect of reducing the focusing length of an individual turbulent "lens" which, in turn, increases the effective ray solution region.

The following expression for the variance of the sound pressure level, V^2, has been presented as valid over the entire wave and ray regions [Krasil'nikov and Obhukov, 1956[:

$$V^2 = k_o^2 \alpha^2 a L[1 - 1/D\tan^{-1}D] \qquad (26)$$

$$D = \pi L/k_o a. \qquad (27)$$

For this result, the wave region is defined when

$$\lambda \gg 2a^2/L \qquad (28)$$

and the ray region is defined for

$$\lambda \ll 2a^2/L. \qquad (29)$$

21

3. Rytov's Method

Rytov's method (method of smooth perturbations) is the method used by Tatarski [1961] to develop a stochastic wave model for the atmosphere. It includes the geometrical optics and Born approximation methods as special cases and includes multiple scattering effects as well. Unfortunately, the scattering effects are included such that they cannot be parameterized directly in terms of the turbulence.

Either the spatial correlation or structure function may be used with this method as dictated by considerations regarding the stationarity of measurements to be analyzed. The restriction

$$\lambda \ll \sqrt[3]{l_o^4/L} \tag{30}$$

is necessary for reasonable solutions of the resultant equations. It is also necessary to compute the range of validity of the perturbation expansion when this method is used. This calculation will not be discussed, but Strohbehn [1968] suggested that the method is valid as long as the variance in the normalized log-amplitude of the sound pressure level is less than 0.8. He also argued that the results from sound phase calculations should be less restricted than those for amplitude.

Black [1965] applied this model to certain data from the CHAIN experiment. One important conclusion he reached

was that the standard deviation of the fluctuation in sound intensity through a turbulent medium, σ_s, and the principal period, T_s, of its fluctuation can be predicted by the equations:

$$\sigma_s = 12.7 \, C_n \, L^{\frac{11}{12}} \, \lambda^{-\frac{7}{12}} \tag{31}$$

$$T_s = \pi\sqrt{\lambda L}/2\nu_n \tag{32}$$

$$c^2n = C_T^2/4T_o^2 + C_s^2/1000S^2 + C_v^2/c_o^2 \approx C_T^2/4T_o \tag{33}$$

$$C_T^2 = D_T(L)/L^{\frac{2}{3}} \tag{33a}$$

$$C_s^2 = D_s(L)/L^{\frac{2}{3}} \tag{33b}$$

$$C_v^2 = D_v(L)/L^{\frac{2}{3}} \tag{33c}$$

where:

ν_n = absolute value of the medium's mean velocity across the acoustic path,

T_o = mean absolute temperature (°C),

S = mean salinity in parts per thousand,

C_o = mean speed sound (m/sec),

$D_T(L)$ = value of the temperature structure function at range L,

$D_s(L)$ = value of the salinity structure function at range L,

$D_v(L)$ = value of the turbulence structure function at range L.

The values for C_n which Black observed were:

In thermocline:	$5.2 \times 10^{-4} m^{-1}$
Near surface:	$1.0 \times 10^{-4} m^{-1}$
Below thermocline:	$2.1 \times 10^{-5} m^{-1}$.

4. Debye Approximation

The Debye approximation to the wave equation is the most general model currently available for the description of the turbulent ocean effects on sound transmission [Neubert 1970]. It contains Rytov's method as part of its solution and it reduces to the Born model when the single scattering condition

$$\lambda \gg 2 \pi \, \alpha \sqrt{\alpha L} \tag{34}$$

is applied. The resultant equation from the model,

$$v^2 \approx 2 \, \alpha^2 \, k_o^2 \, L_e \, L \tag{35}$$

where L_e = the Eulerian integral scale (e.g. the largest turbulent scale), has no special long range nor high frequency restrictions. In other words, it is good when the cumulative effects of small, continuous fluctuations of the local turbulent velocity strongly affect phase at longer ranges. No use has been made of this model in the ocean to date.

C. MODEL APPLICATION

Stewart and Grant [1962] conducted a turbulence experiment near the surface in the presence of large waves. They showed the Taylor microscale, a, was on the order of 6 cm which corresponds to the results (6.4 cm) Neubert and Lumley [1970] calculated from Sheehy's [1950] data. Since these measurements correspond well and fit the conditions of the current NPS experiment, the Neubert and Lumley values were used to provide a rough basis for further analysis. These values, coupled with experimental parameters, are shown in Table 1.

The limits of applicability of each of the wave models and the associated value of V^2 calculated on the basis of this data is shown in Table 2. It would appear from the latter table that the Debye approximation and perhaps the Born model for the wave region (if the limit imposed by relation (6) is not too strong) would be most applicable in this case. The large difference in V^2 resultant from the Born model compared to that from the Debye model could be the result of poor definition of the micro and integral scales.

One should also note that the acoustic near-field criteria for a piston source imposes an additional requirement on the wavelength:

$$\lambda > r^2/L \tag{36}$$

where r = radius of the transmitter active disc. Since relation (36) requires $\lambda > 0.6$ cm, geometrical optics and Rytov's method can be immediately discarded.

TABLE 1

PARAMETER VALUES FOR MODEL TESTING

Parameter	Assumed Value	Source
C_o	1505 m/sec	Experiment
u/C_o	7×10^{-5}	NL
L_e	40m	NL
λ_g	6.4 cm	NL
R_t	6300	NL
σ_k	7	NL
$\alpha^2 a$	5.0×10^{-7}	S
L	200 cm	Experiment
f	20 khz	Experiment
λ	7.5 cm	Experiment
C_n	$1.0 \times 10^{-4} m^{-1}$	B
u	10.5 cm/sec	C
η_g	258 cm	Equation 22
a	2.4 cm	Equation 21
ℓ_o	2.2 cm	Equation 24
α	4.6×10^{-4}	C
k_o	$0.84 \ cm^{-1}$	Equation 18
D	130	Equation 27
r	10.88 cm	Experiment

NL = Neubert and Lumley [1970]

S = Sheehy [1950]

B = Black [1965]

C = Calculated from above data.

TABLE 2

RESULTS FROM MODEL TESTING

Model	V^2	Most Restrictive Limit
Geometric	5.8×10^{-2} (19)	$\lambda \ll 1.1 \times 10^{-2}$ cm (7)
Born (Gaussian form)	6.3×10^{-5} (13)	$1.0 \times 10^{-2} \ll \lambda \ll 15$ cm (12,16)
Born (Exponential form)	7.1×10^{-5} (14)	$1.0 \times 10^{-2} \ll \lambda \ll 15$ cm (12,16)
Born (Neubert Limits)		$\lambda \leq 20.9$ cm (18)
Born (K-O)	7.1×10^{-5} (26)	$\lambda \gg 2.9 \times 10^{-2}$ cm (28)
Rytov	1.1×10^{-2} (31)	$\lambda \ll 0.5$ cm (30)
Debye ($L_e = 40$m)	2.4×10^{-1} (35)	None
Debye ($L_e = 3$ m)	1.8×10^{-2} (35)	None

HOMOGENEOUS ASSUMPTION

$\lambda \ll 2.2$ cm (6)

ACOUSTIC FAR-FIELD CRITERION

$\lambda > 0.6$ cm (36)

Note: Numbers in parenthesis refer to applicable equation.

III. EXPERIMENT AND DATA ANALYSIS

A. EXPERIMENT

Measurements were taken from May 24 to 26, 1974 from the Naval Undersea Research and Development Center's (NUC) oceanographic research tower located 1.6 km off Mission Beach San Diego, California. The tower is a stable, three-tiered concrete and steel structure built into sandy bottom in water of 18.5 m mean depth. It provides enclosed spaces for electronic equipment and open-deck working areas for handling instruments. Winch controlled trolleys are available on three sides of the structure on which devices may be lowered to within 1 m of the bottom. Instruments for this experiment were installed on an aluminum and steel frame attached to a trolley on the west side of the tower which faced the predominant swell. A schematic view of the experiment layout is shown in Figure 1.

Basic meteorological and oceanographic data were available from equipment permanently installed on the tower. A bathythermograph trace obtainable from the north side of the structure facilitated placement of the instrument frame in the desired vertical position with respect to the thermocline.

The general environmental conditions encountered were moderate winds, sea and swell from the West. Light winds to 5 kts, overcast skies and swell to 1 m were usual in the
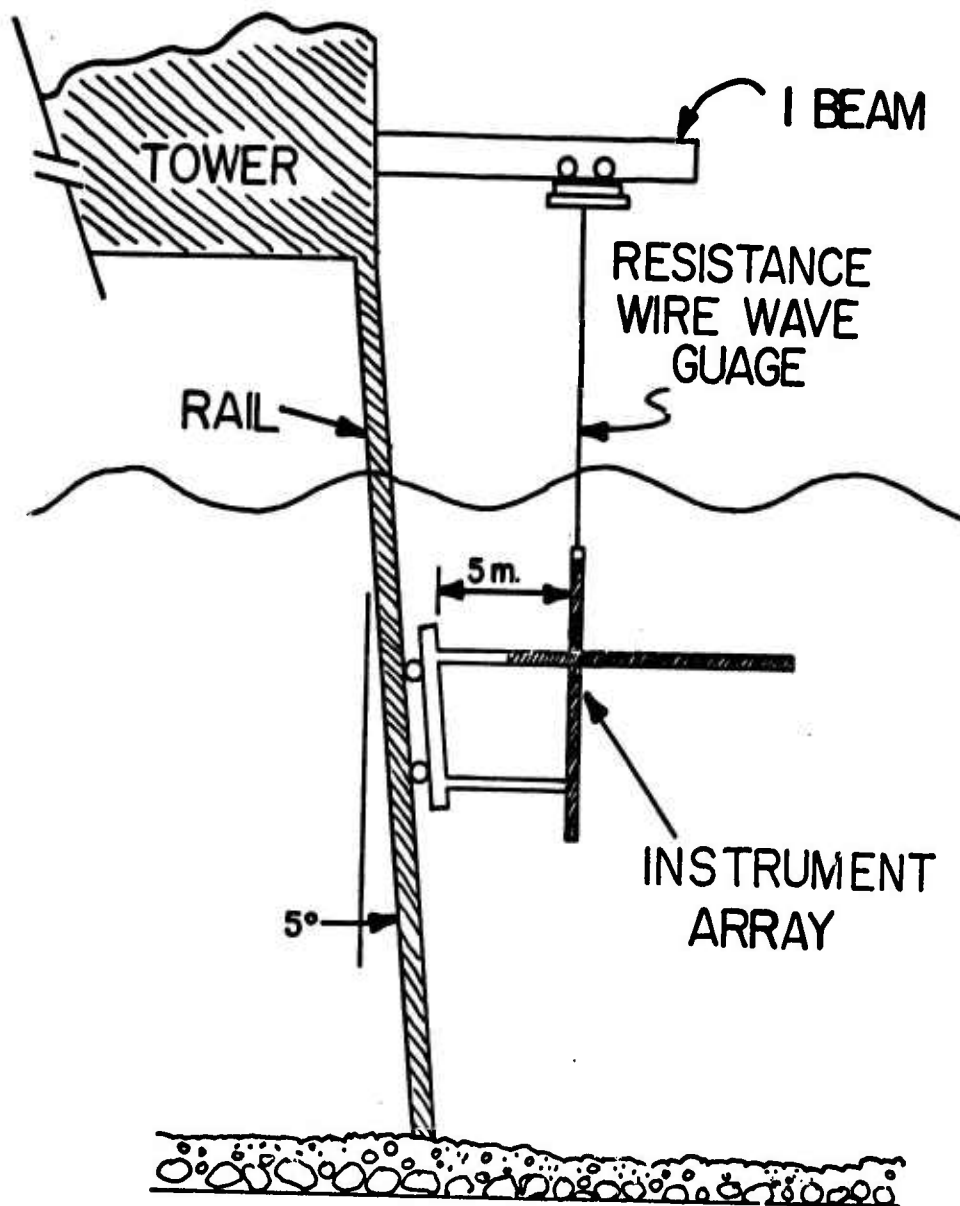
FIGURE I.   SCHEMATIC DIAGRAM OF EXPERIMENT LAYOUT.

morning (see Table 3). In the afternoon, winds increased to 15 kts and seas of 0.75 m with accompanying swell of 1 m was common. The diurnal variation in thermocline depth was approximately 12 m.

1. Instruments

Temperature measurements were made with Fenwell Electronics Inc. type k496, double-bead thermistors which exhibit low self-heating and well-matched, high-resolution characteristics. Calibration of the thermistors, together with associated circuitry, was conducted in the laboratory under closely controlled, stable conditions. A Hewlett-Packard HP-2801A quartz thermometer with an accuracy of $\pm .006°C$ was used as a temperature standard and a decade box was used as a resistance standard. The same decade box was used to calibrate the thermistor array in the field to eliminate resolution difficulties resulting from the poor overall accuracy of the decade box.

Water particle velocities were measured using Marsh-McBirney electromagnetic flowmeters (models 721 and 722). Since these flowmeters were calibrated by the manufacturer only for steady flow conditions, each probe was recalibrated for unsteady flow by oscillating it in a water tank at rates corresponding to expected experiment velocities.

A Baylor Co. wave staff system, model 13528R, was used to measure sea surface elevation. Calibration was

TABLE 3

DAILY METEOROLOGICAL AND OCEANOGRAPHIC DATA AT 1000 HR.

METEOROLOGICAL DATA

Date	Winds Speed/Dir.	Temp(°C)	Wet Bulb Temp (°C)	Dry Bulb Temp (°C)	Dew Point (°C)	Relative Humid.(%)	Pressure (mb)
24 Apr	4kts/270°	14.93	11.1	13.9	8.9	71	1018.0
25 Apr	0	15.32	11.1	13.9	8.9	71	-
26 Apr	3kts/165°	14.60	11.1	13.9	8.9	71	1020.5

SURFACE DATA

Date	Bucket Temp(°C)	Avg. Swell Height (m)	Swell Period (Sec)	Swell Direction	Secchi Depth (m)	"Red Tide" Present
24 Apr	14.30	0.24	15	090°	4	YES
25 Apr	13.32	0.49	11	090°	4	YES
26 Apr	13.50	0.85	8	090°	5	NO

BATHYTHERMOGRAPH DATA (°C)

Date	Surface	3m	6m	9m	12m	15m	18m
24 Apr	14.2	13.6	12.25	11.6	11.3	11.2	11.15
25 Apr	13.2	12.7	11.3	10.9	10.8	10.8	10.8
26 Apr	13.6	13.4	12.65	11.6	10.9	10.7	10.7

accomplished at the NUC tower by successively shorting out sections of the sensor active element while measuring output voltage.

A Naval Research Laboratory, Underwater Sound Reference Division (USRD) type F-33 general purpose unidirectional transducer was used as a CW sound transmitter. It features two piezoelectric ceramic arrays mounted coaxially which, when excited in parallel, exhibit exceptional directivity. This was desired to reduce interference from surface, bottom and equipment frame reflections. The beam widths (-3db down) for 20kHz and 40kHz were 20° and 10° respectively. USRD type F-50 lead zirconate-titanate omnidirectional transducers were used as receivers.

The sonar array was calibrated in an anechoic test tank filled with fresh water and the hydrophone calibrations compared satisfactorily with calibrations previously performed at USRD. The frequency standard used was a Hewlett-Packard HP-2801A quartz thermometer configured as a frequency meter and the voltage standards were an RMS calibrated Fluke digital voltmeter and a Hewlett-Packard model HP 3400A RMS voltmeter. Phase measurements were conducted using a Dranetz model 305 phase meter. Calibration and accuracy measurements for the peripheral equipment associated with the sound arrays were taken concurrently with transducer calibration.

The instrumentation accuracy, response and limitations are summarized in Table 4.

TABLE 4

INSTRUMENT SUMMARY

Measurement	Band	Accuracy	Time Constant	Limiting Parameter
Absolute Temperature	10–16°C	±0.014°C	150 msec	thermistor linearity
Temperature Variation	±2°C	±0.006°C	150 msec	calibration standard
Particle Velocity	0–3m/sec	±0.074 m/sec	200 msec	velocimeter linearity
Surface Elevation	0–4.5m	±0.020m	unknown	wave gage linearity
Sound Pressure Level	0–66dB/1μb	±1.4dB/1μb	< 1 msec	band-pass filter linearity
Sound Amplitude Variation	0–1%	±0.005%	< 1 msec	calibration of peripheral instruments
Sound Phase	0–360°	± 1° (30cm) ± 5° (60cm)	< 1 msec	visual reading of average phase shift
Sound Phase Variation	±180°	±0.2°	< 1 msec	sensitivity of peripheral equipment

2. Instrument Arrangement

Two arrays of thermistors were mounted on one side of the equipment frame in a common vertical plane. Seven thermistors were mounted along a horizontal member and 7 were mounted along a vertical member as shown in Figure 2. The instrumentation and abbreviated notation used in the text is given in Table 5. One thermistor in the vertical array was common to the horizontal array. The thermistor probes were spaced in an approximate geometric progression so that a maximum number of spatial combinations could be achieved for adequate definition of the spatial correlation and structure functions with a limited number of probes. The minimum spacing (5.0 cm) was determined by the physical size of the thermistor mounts. This was compatible with the smallest wavelengths which could be measured within the time constant of the thermistor. Maximum thermistor spacing was determined by physical constraints on the length of the support pipe to prevent strumming.

Three velocimeters were placed so that the horizontal and vertical particle velocities could be measured in the same plane as the thermistor arrays. Additionally, they were placed in a vertical line directly under the Baylor wave gage with the horizontal component measured from the west. The temperature and particle velocity devices were offset 29 cm from the support frame by mounting brackets to minimize false turbulence effects generated by the frame.

34
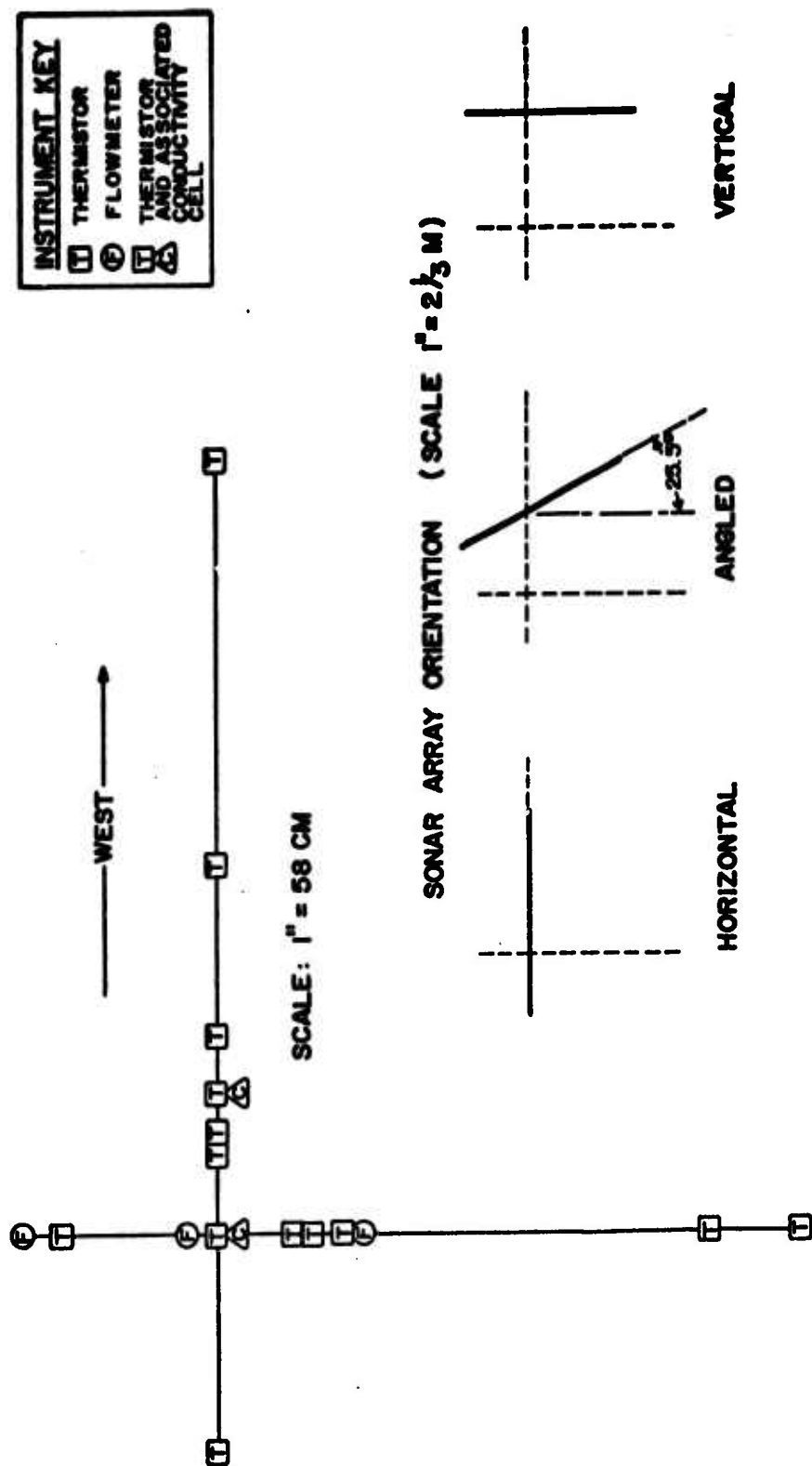
FIGURE 2. RELATIVE POSITIONS OF INSTRUMENTS ON FRAME (SIDE VIEW) INSERTS SHOW SONAR ARRAY CENTERLINE POSITION RELATIVE TO FRAME BAYLOR WAVE GAGE WAS LOCATED DIRECTLY ABOVE VERTICAL ARRAY DEVICES.

TABLE 5

CHANNEL ABBREVIATIONS

Data Channel	Abbreviation	Order in Fig. 2
Vertical Temperatures	TMV1-TMV7	From Bottom
Horizontal Temperatures	TMH1-TMH7	From West
Sound Amplitude	SAM1-SAM3	From East
Sound Phase	SPH1-SPH2	or From Top
Sea Surface Elevation	WAVE	-
Horizontal Flow Velocity	FVAY-FVCY	From Bottom
Vertical Flow Velocity	FVAX-FVCX	From Bottom
Conductivity	SAL1-SAL2	From West

The sonar array was separately mounted on a tripod base which pivoted vertically around the main equipment frame but which was held rigid by clamps during recording periods. This arrangement facilitated horizontal and vertical sound path measurement (Figure 2). The centerline of the transmitted sound beam was 57 cm away from the vertical plane of the thermistor arrays to minimize unwanted reflections from the other instruments.

Three F-50 receivers were placed along the center of the transmitted beam outside the near field at 2.0, 2.3 and 2.9 m from the transmitter face. The minimum separation (30 cm) was selected to maximize the number of wavelengths through which the lowest frequency (20kHz) sound would travel between receivers and to remain near the lower spatial scales of the measured temperature. The maximum sound path length of 2.9 m was selected to minimize reflections from the frame and mountings.

3. Pre-recording Signal Processing

The signals from the wave height and particle velocity devices were recorded directly. All other signals were processed through a combination of filters, amplifiers and dc bias removal devices to maximize signal-to-noise (S/N) ratio before recording.

a. Temperature Circuitry

Each of the horizontal and vertical temperature arrays was connected to a separate temperature array drawer

37

which contained Wheatstone bridge networks, amplifiers and calibration facilities for seven channels (see Figure 3). The Wheatstone bridge network provided the capability to match the response of each channel. Additionally, balance adjustments were provided to adjust the operating point of the amplifiers to the mean temperature so that distortion during recording was minimized.

b. Sonar Circuitry

As shown in the block diagram (Figure 4), signals from the F-50 transducers were amplified and then band-pass filtered at the operating frequency. The signal was then processed through a second-detector-type demodulator. The dc bias was removed from the detected signal and the amplitude modulation (AM) signal was then amplified and low-pass filtered.

Dranetz type 305 phase meters were connected between the band-pass filter outputs from receiver hydrophones one and two and, similarly, between hydrophones two and three. The dc bias was removed from the output of each phase meter and the signal was then amplified and low-pass filtered.

Before each run the dc bias setting was made and the rms voltage from each band-pass filter output and mean phase shift read from each phase meter was recorded. This technique allowed much higher signal amplification to be used prior to recording because the signal amplifiers were not saturated by the large dc segment of the signal.

38
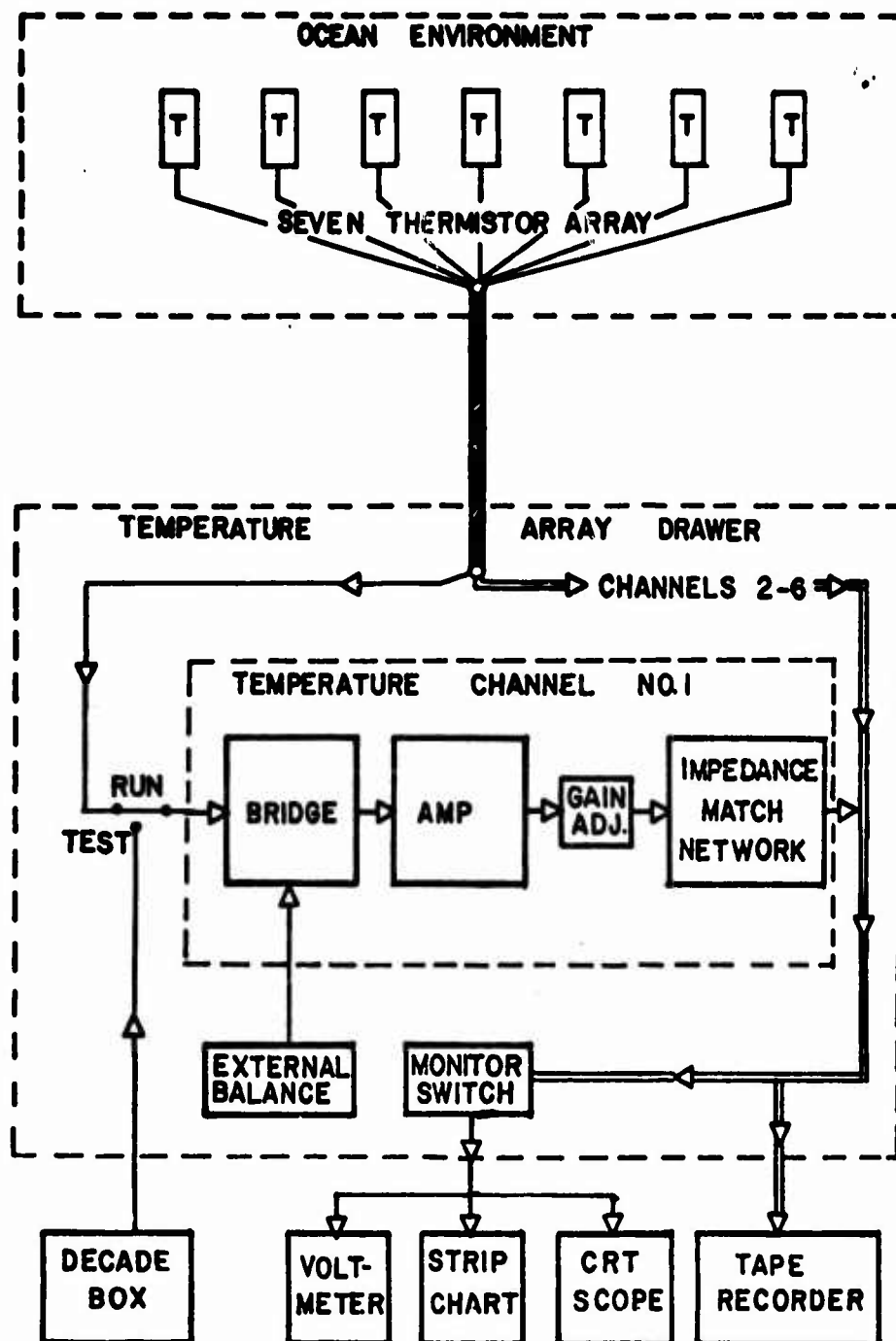
FIGURE 3.   BASIC TEMPERATURE MEASUREMENT
CIRCUIT BLOCK DIAGRAM. ONLY I OF THE 7 CHANNELS IS
SHOWN IN THE TEMPERATURE ARRAY DRAWER FOR CLARITY.
TWO IDENTICAL ARRAY DRAWERS WERE USED DURING THE
EXPERIMENT.
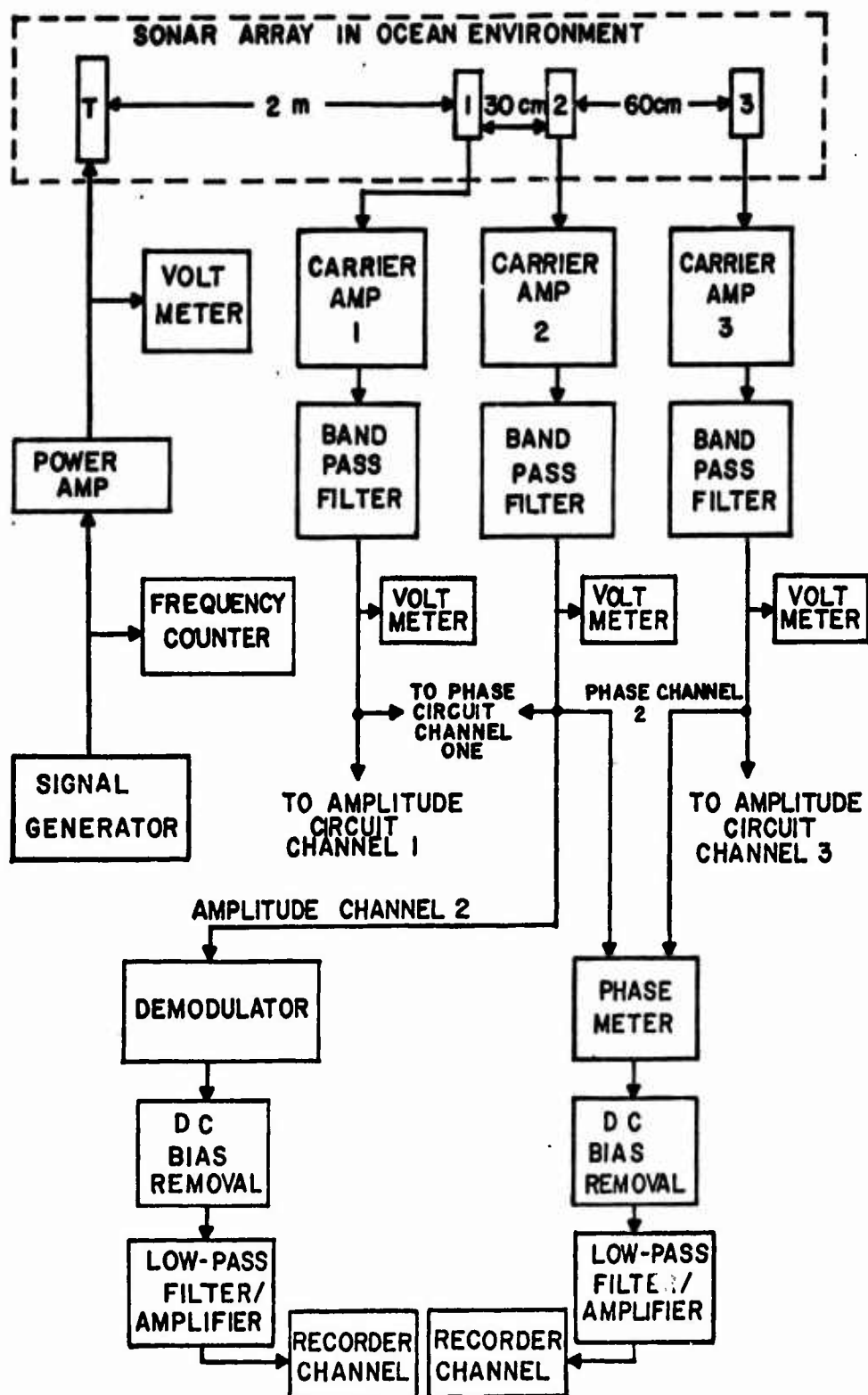
FIGURE 4. BASIC SONAR PHASE AND AMPLITUDE
MEASUREMENT BLOCK DIAGRAM. TWO PHASE CHANNELS AND
THREE AMPLITUDE CHANNELS WERE USED, HOWEVER ONLY
ONE OF EACH IS SHOWN FOR CLARITY.

4. Experimental Procedure

Twelve data recording runs of 29 to 73 minutes duration were taken at various depths above, in and below the thermocline. A total of 28 channels of data were recorded for each run including 2 channels dedicated to experimental conductivity devices [Kane 1974]. Surface elevation, vertical and horizontal particle velocities, temperature, sound amplitude modulation, sound phase modulation and conductivity were measured simultaneously.

Run depths were selected on the basis of a BT trace taken just before the run, but the final run depth was chosen to optimize the degree of fluctuation in temperatures monitored from the vertical thermistor array. The sonar array was held in a fixed position during each recording run. Runs were made with the sonar array oriented horizontally, vertically and at an angle with respect to the support structure. This allowed data to be obtained at various attitudes through and along the thermocline. A summary of all twelve runs is given in Table 6.

A Sabre III and a Sangamo model 3500, both 14 channel FM tape recorders, were used to record the analog data. A timing pulse was recorded on one channel of each recorder at the beginning of each run to provide temporal continuity between recorders.

The analog recordings were digitized using a hybrid system including a Scientific Data System model 5000 analog

TABLE 6

SUMMARY OF RUNS

Run Number	Start Date/Time	Total Run Time (min)	Mean Run Depth (m)	Position Relative to Layer	Height of Sea (m)	Height of Swell (m)	Sonar Freq. (kHz)	Sonar Array Orientation
1	24/1814	72	7.53	Above	0.3	0.9	20	Horizontal
2	24/2134	30	12.03	In	0.3	0.9	20	Horizontal
3	24/2304	29	8.93	Below	0.5	1.1	20	Horizontal
4	25/0845	26	5.35	Below	0.1	0.9	20	Horizontal
5	25/1020	33	5.81	Below	0.0	0.8	20	Horizontal
6	25/1056	58	6.11	In	0.1	1.2	40	Horizontal
7	25/1230	31	12.69	Below	0.5	1.5	40	Horizontal
8	25/1541	37	5.68	Above	0.2	0.8	20	Horizontal
9	25/1651	54	9.63	Above	0.3	0.8	40	Horizontal
10	26/1244	38	5.33	In	0.2	0.9	20	Vertical
11	26/1601	66	7.59	Above	0.2	1.1	20	Angled
12	26/1729	73	10.44	In	0.2	0.9	20	Angled

computer and a Xerox Data Systems model 9300 digital computer. Digital data preparation and analysis was performed on an IBM model 360 computer. The digitizing data rate used was 25Hz, however 60Hz electronic noise was coupled into the signal, so low-pass filters were used to remove it. Additionally, noise spikes which existed in some channels were removed by a digital editing routine. Data handling capacity was improved by reducing the number of samples by five using an inverse transform, numerical low-pass filter [Davidson 1970]. The latter reduced the analysis Nyquist frequency to 2.5Hz. The linear trend and remaining dc bias were also removed before analysis.

Spectral analysis was performed on 26.6- minute segments of certain data sets. This choice dictated a minimum detectable frequency of 0.00625Hz. A standard lag time of 5% of the record length was chosen which resulted in 40 degrees of freedom for each computed spectrum. The resultant 80% confidence limits of the chi-squared distribution were between 0.73 and 1.30 of the measured spectral estimates. A Parzen window was applied to the correlation function during the spectra calculations to minimize the effect of finite record length on the spectral analysis.

IV. EXPERIMENT RESULTS

During this experiment, the primary factors influencing
the results were the sea state, the thermocline gradient and
the position of the instruments with respect to the thermo-
cline. The sea state remained nearly constant throughout
the recording periods although the peak of the swell showed
a gradual shift to higher frequencies. The thermocline
depth and gradient continuously fluctuated under the influence
of internal waves which are characteristic of the waters off
San Diego during this time of year. In order to resolve
some of the effects of the thermolcine variability, analyses
in and above the layer were required. Experiment runs one
and two were chosen for this purpose. Additionally, run
12 was examined to check the results since: 1) it included
data in and above the thermocline in a single record; 2) the
thermocline gradient was intermediate between the gradient
encountered in runs one and two; 3) the sonar array was
angled toward the vertical rather than horizontal during the
run and 4) the run was conducted two days after runs one
and two under slightly different sea conditions.

A. ENVIRONMENT

The thermocline migrated diurnally from near the surface
in the morning to about 14m in the evening. It was generally
diffuse near the surface but near the bottom it was compressed
so that a very sharp thermal gradient (2°C/m) was created.

Superimposed upon this effect was an apparent four-hourly
dilation and contraction of the isotherms.

Figures 5-9 show representative bathythermograph (BT)
traces taken periodically during the experiment. The traces
are plotted so that the 12°C mark corresponds to the time
the BT was taken. Recording run envelopes in depth and time
are included to show the position of the instrument array
relative to the thermocline. The 11°, 12° and 13°C isotherms
are shown to indicate the relative intensity of the tempera-
ture gradient during the runs. Figure 9 is an expanded
time plot for BT's taken during run 12 which shows a large
internal wave having a 36 min period; this was observed
throughout the experiment.

The four-hourly variation in the thermocline gradient
probably was caused by internal wave interference effects
since analysis showed that these variations were associated
with periods of high temperature variance but not with sur-
face waves nor heat budget considerations.

Surface slicks presumably associated with internal waves
were seen propagating from the West at certain intervals
during the experiment. A typical example of the effect of
these waves is shown in the vertical temperature analog
records of run number 12 (Fig. 10). The large 36 min wave
peak passing the vertical temperature array is shown by the
dramatic temperature decrease which occurred at about 1800.
Nine and 1.5 min period, small-amplitude internal waves
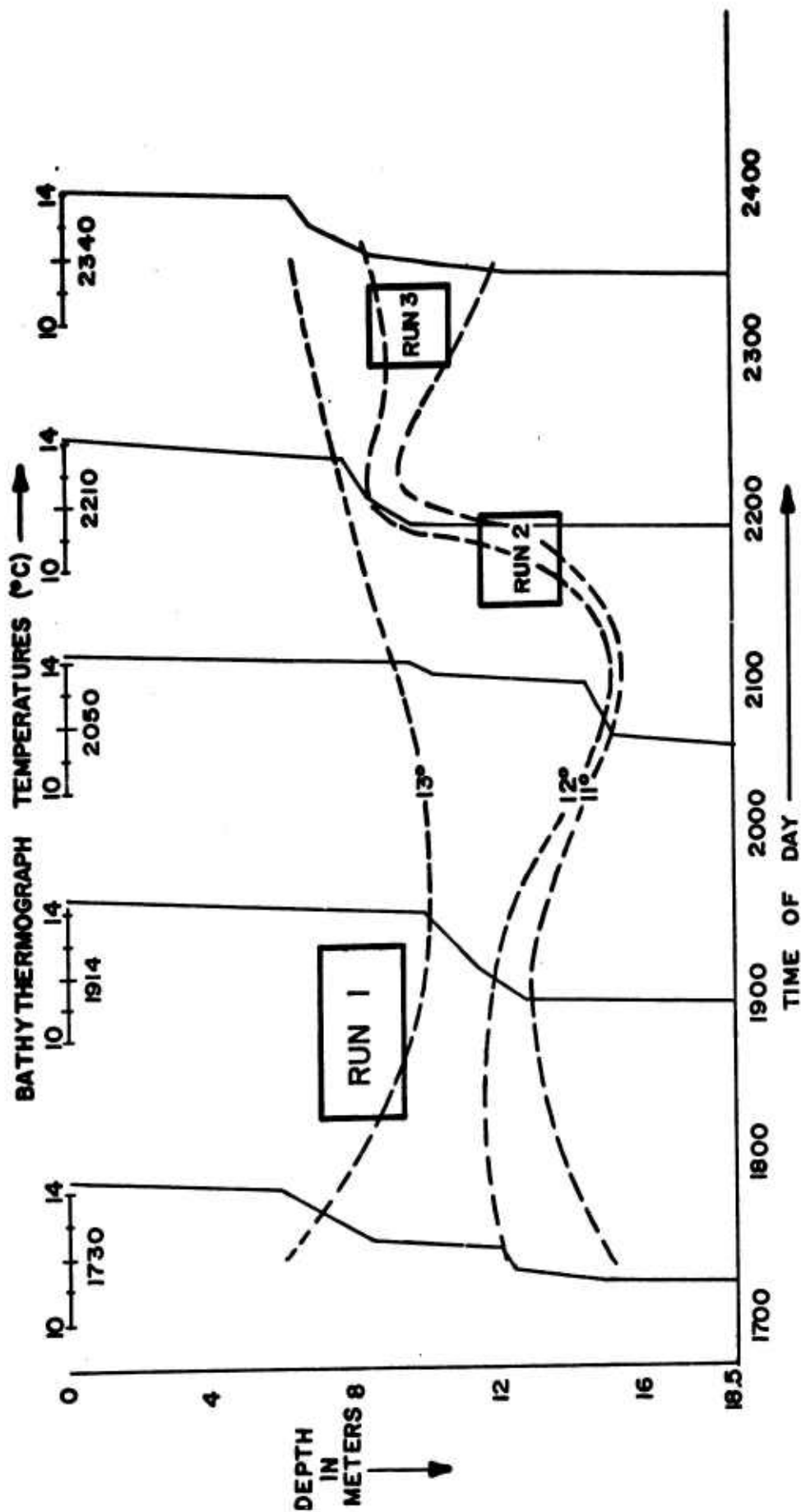
FIGURE 5. BATHYTHERMOGRAPH TRACES FOR 24 APRIL 1974. TYPE OF THE TRACE IS LOCATED AT THE 12°C TEMPERATURE MARK. RECORDING RUN ENVELOPES IN DEPTH AND TIME ARE INCLUDED TO SHOW THE POSITION OF THE INSTRUMENT ARRAY RELATIVE TO THE THERMOCLINE. THE 11°, 12° AND 13° C ISOTHERMS ARE SHOWN TO SHOW THE RELATIVE INTENSITY OF THE TEMPERATURE GRADIENT DURING THE RUNS.
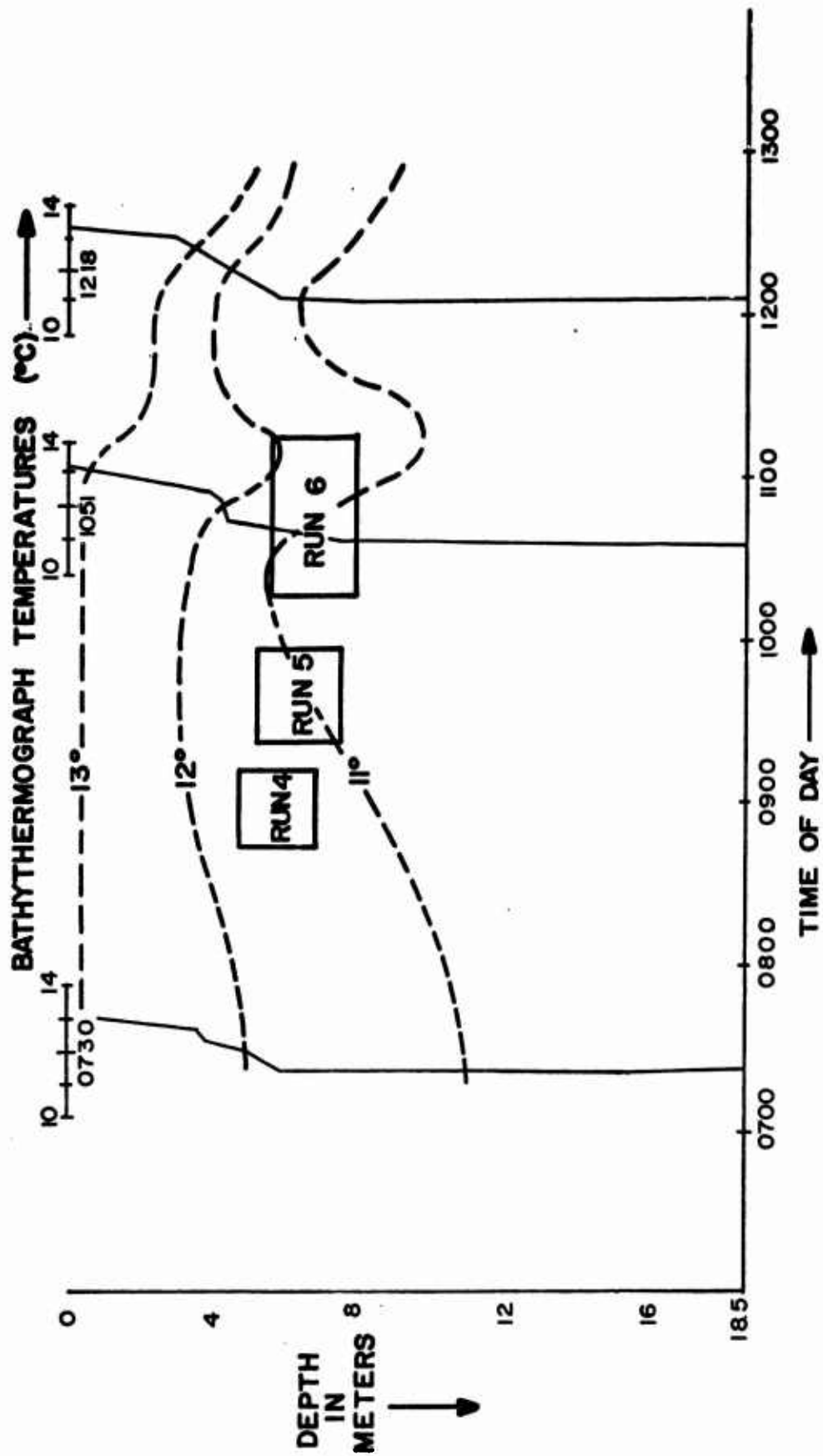
FIGURE 6. BATHYTHERMOGRAPH TRACES FOR THE MORNING OF 25 APRIL.

47.
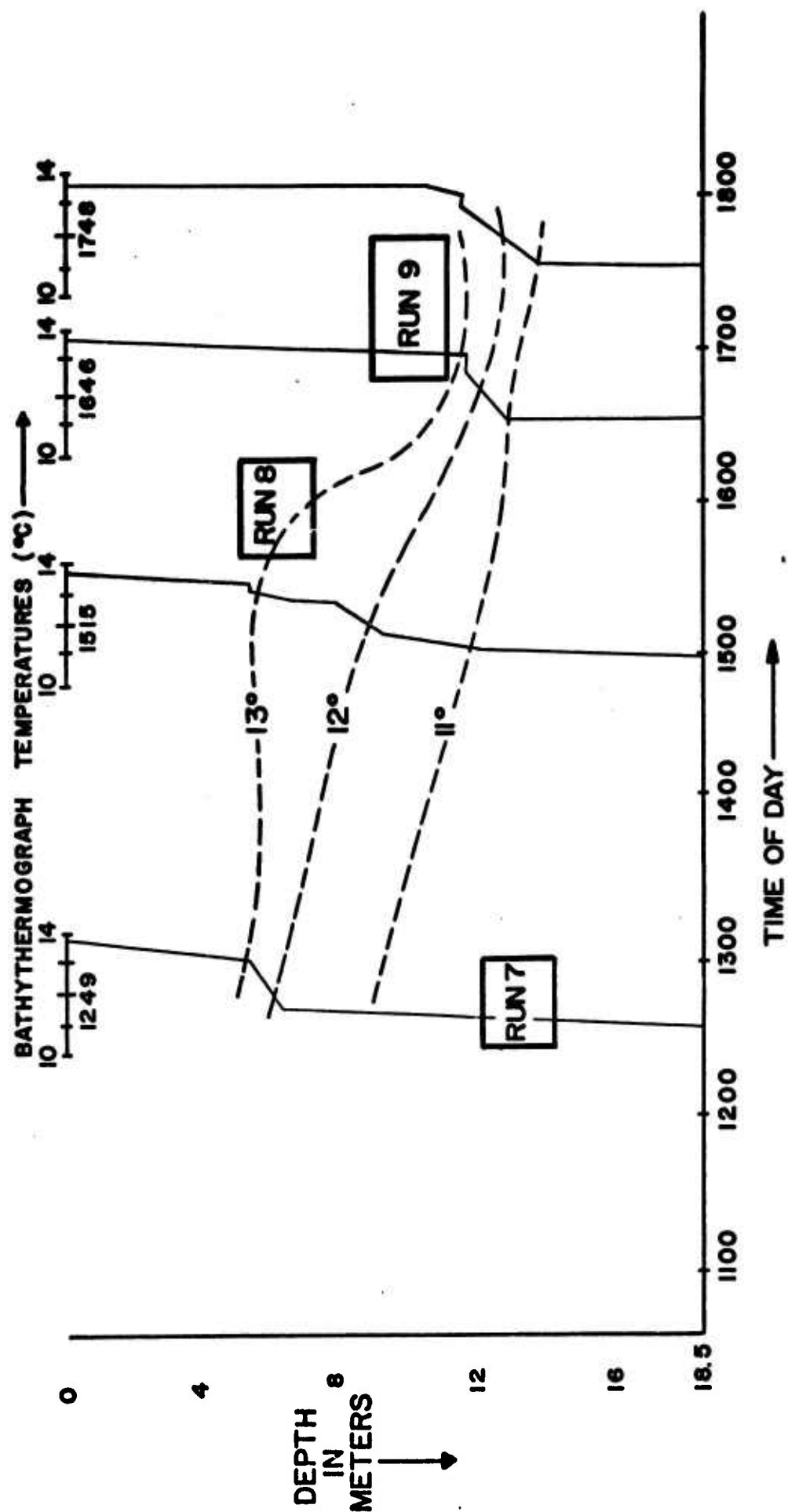
FIGURE 7. BATHYTHERMOGRAPH TRACES FOR THE AFTERNOON OF 25 APRIL.

48
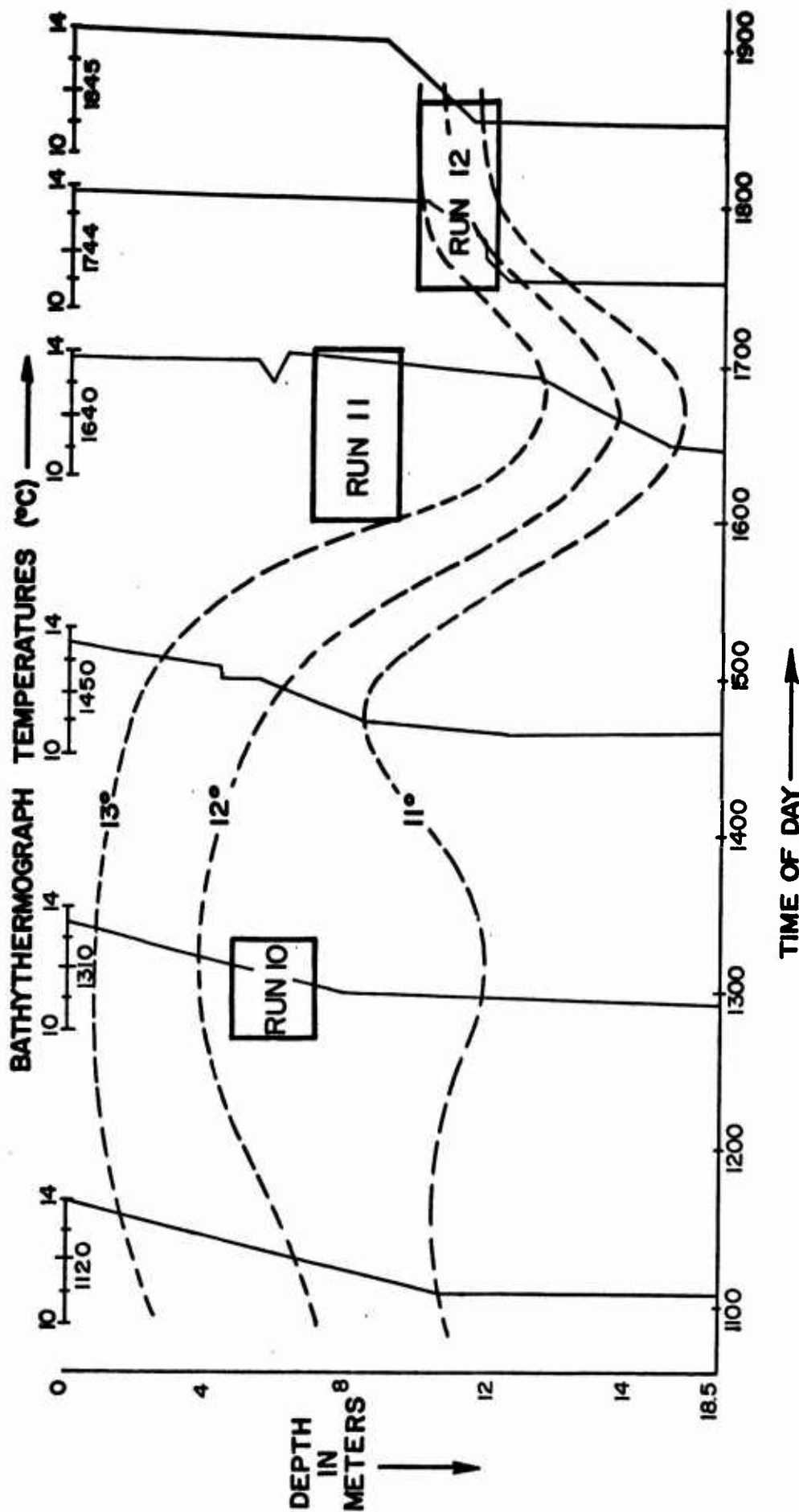
FIGURE 8. BATHYTHERMOGRAPH TRACES FOR 26 APRIL.

49
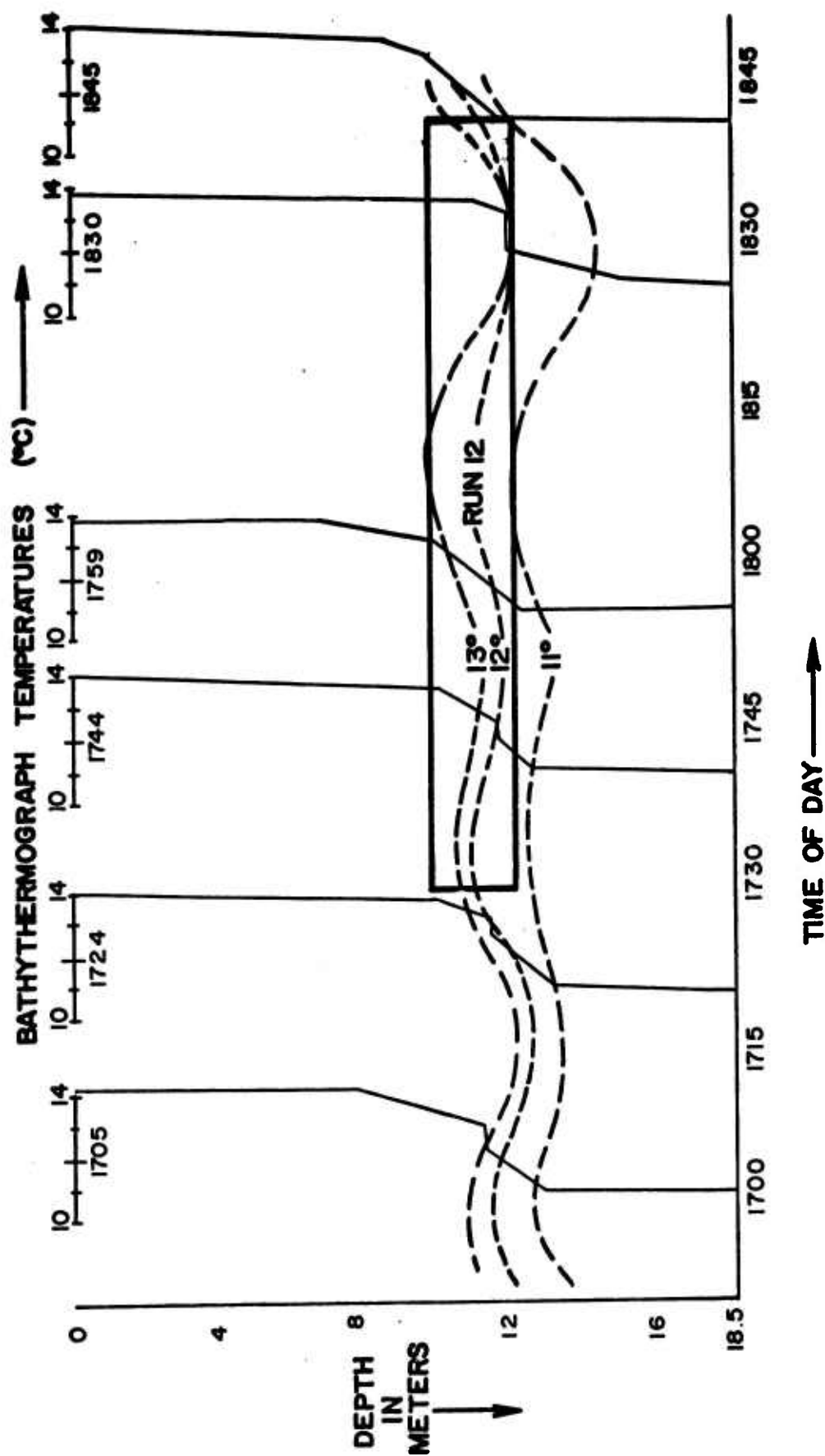
FIGURE 9. SHORT TIME INTERVAL BATHYTHERMOGRAPH TRACES FOR THE PERIOD OF RECORDING RUN 12, 26 APRIL.

50

CHANNEL NAME

1805, 26 APR

DEPTH

TMV7 — 9.9m

TMV6 — 10.44m

+0.72°c

TMV5 — 10.70m

11.5min

TMV4 — 10.74m

TMV3 — 10.9m

TMV2 — 12.25m

Figure 10. Effect of internal waves on the vertical thermistor array.

51
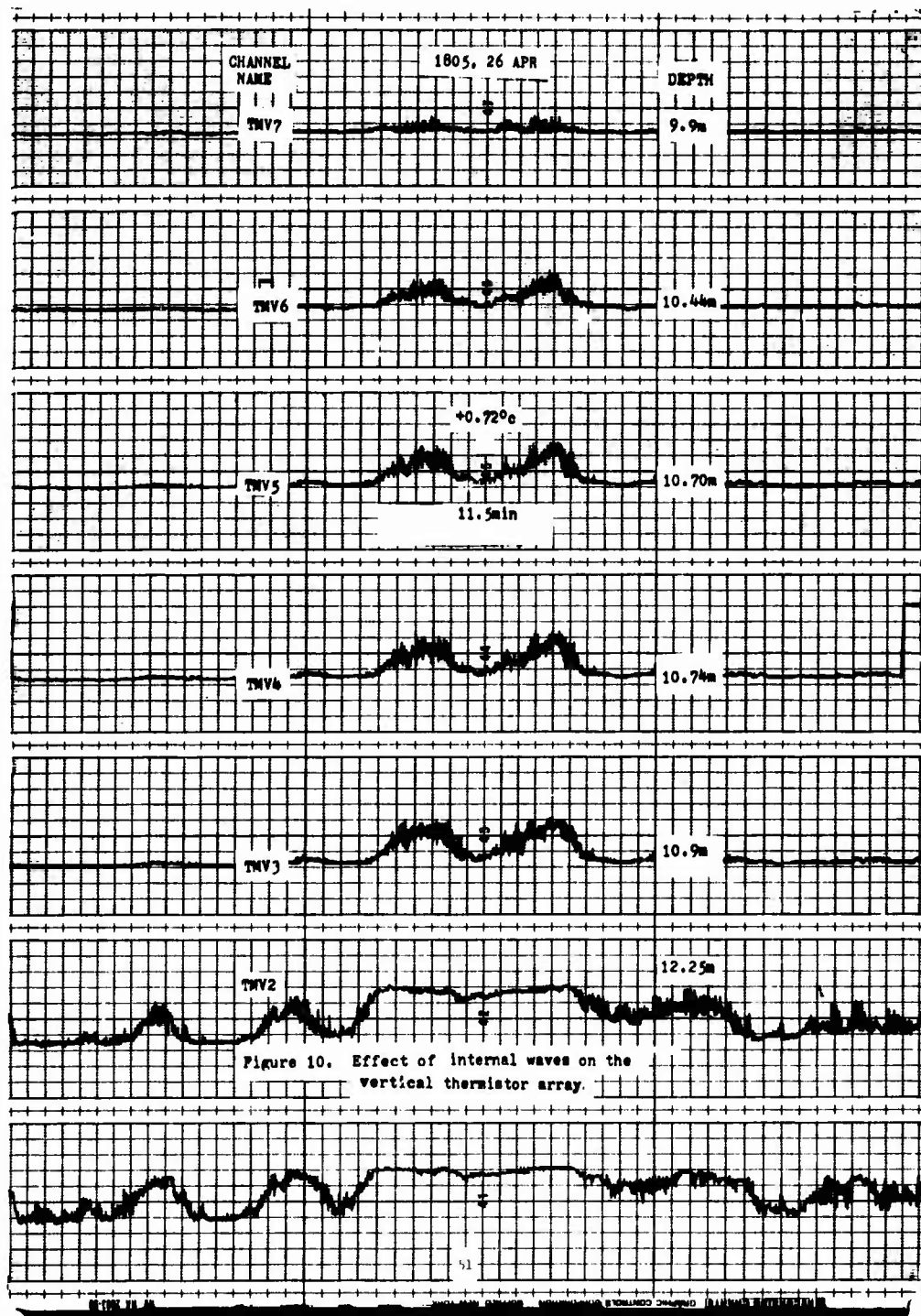
effects are seen superimposed upon the larger internal wave. The "grass" is surface swell related. Spectral analysis showed that a broad band of internal wave periods from 160 secs (maximum detectable by the method) to as low as 30 secs were superimposed on the large wave as well.

Figure 11 shows the resultant sound effects from the internal wave temperature perturbations of Fig. 10 during run 12. The sound array was angled 25° to the vertical in run 12. The sound amplitude modulated signals SAM1 and SAM2 were initially above the layer and were not affected by the turbulent thermocline losses as severely as SAM3 (below the layer). As the layer moved up, the interference and diffraction effects of the turbulent blobs [Whitmarsh and others 1957] in the vicinity of SAM3 were diminished. This is shown by the increase in sound pressure level (about 10^{-3} µb) on the SAM3 analog record.

When the layer moved into the vicinity of SAM1 and SAM2, the sound pressure level at these transducers was reduced by about 6×10^{-4} µb and 3×10^{-4} µb, respectively. The thickness of the "grass" on these plots is an indication of the wave-induced amplitude scintillation effects (~2 to 5 $\times 10^{-4}$ µb) caused by pumping the turbulent blobs back and forth across the sound path. (Similar results occurred when the sound path was horizontal, but the scintillations were then caused by waves pumping the thermocline up and down.) Additionally, the movement of the layer ($\Delta T \approx .3°C$) between SAM1 and SAM2 caused sound phase modulation, SPH1, to phase shift about 30°.

52

Figure 11. Effect of internal wave peak on sound
and particle velocity.

53
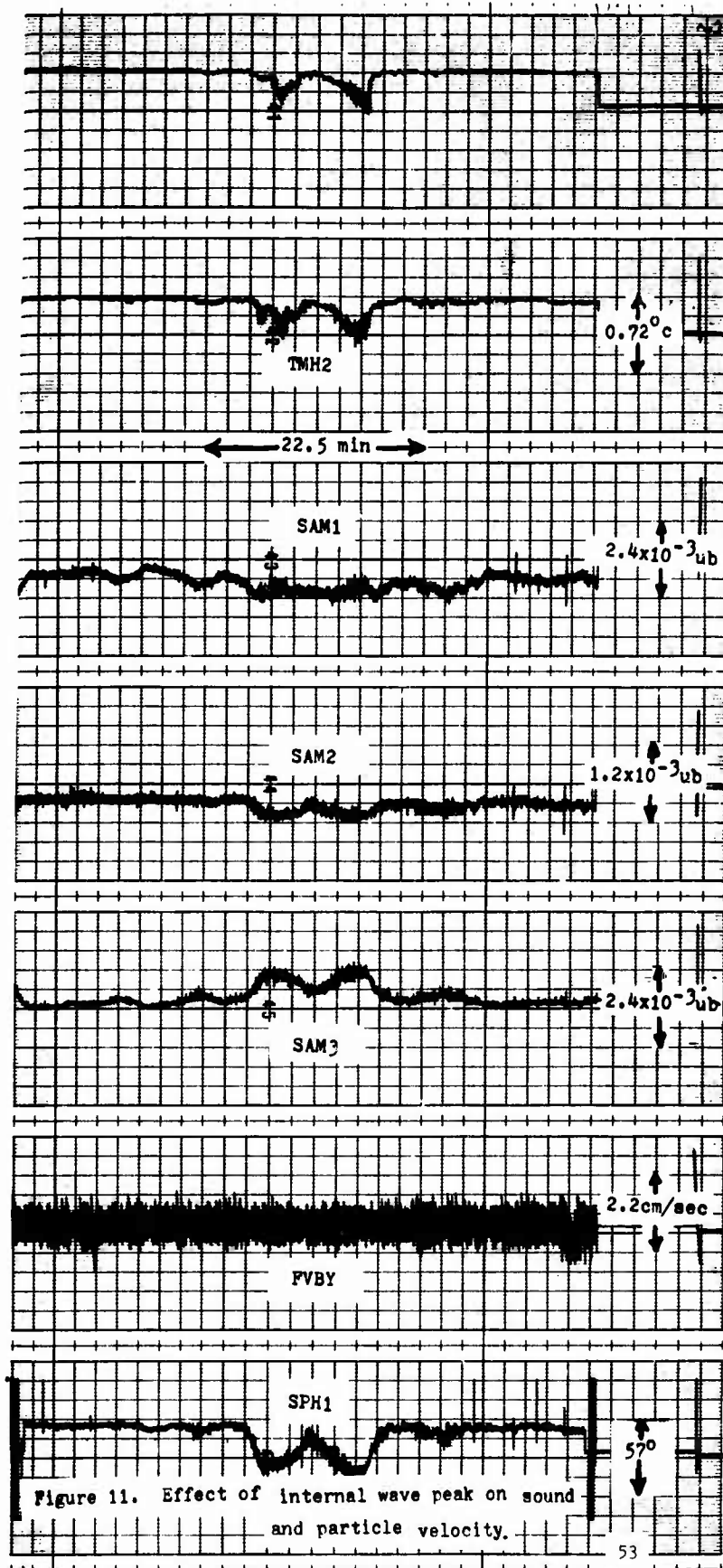
B. TEMPORAL STOCHASTIC ANALYSIS

Time series analyses were performed on 26.67 minute segments of each of the sound channels, the wave record, three temperature records and two water particle velocity records. Analyses included for each signal the calculation of the first and second moments, variance, mean period (calculated from total zero upcrossings), autocorrelation function and autospectrum. Also, the crosscorrelation, quadrature and co-spectra, phase difference, coherence-squared and linear regression analysis were calculated between specific pairs of channels (see Table 7). Examples of cross-spectral analysis results for runs two and 12 are shown in Figs. 12-15. Additional results are given in Appendix A. Thermistor 2 on the horizontal array, TMH2, was selected for temperature comparisons with the sound records because this thermistor was most central to the sound propagation path during the runs.

1. Basic Statistics

Representative basic statistics of temperature, waves, sound amplitude and sound phase are shown in Table 8. By examining the order of magnitude of these statistics in relation to the depth of the run and the proximity to the thermocline, certain qualitative relationships between the parameters can be seen:

1) The magnitude of the temperature variance was determined primarily by proximity to the layer and its mean

TABLE 7

CHANNELS COMPARED IN TEMPORAL STOCHASTIC ANALYSES

		Abscissas For Regression Analyses		
	Channels	TMH2	WAVE	SAL2
	SAM1	X	X	X
	SAM2	X		
Ordinates For Regression Analyses	SAM3	X		
	SPH1	X	X	X
	SPH2	X		
	TMH2		X	X

55

SAMPLE LENGTH ~ 26.67

FREQ. RESOLUTION - .00625 Hz

WAVE VARIANCE - .0998 m²

TMH2 VARIANCE - .4619°C²
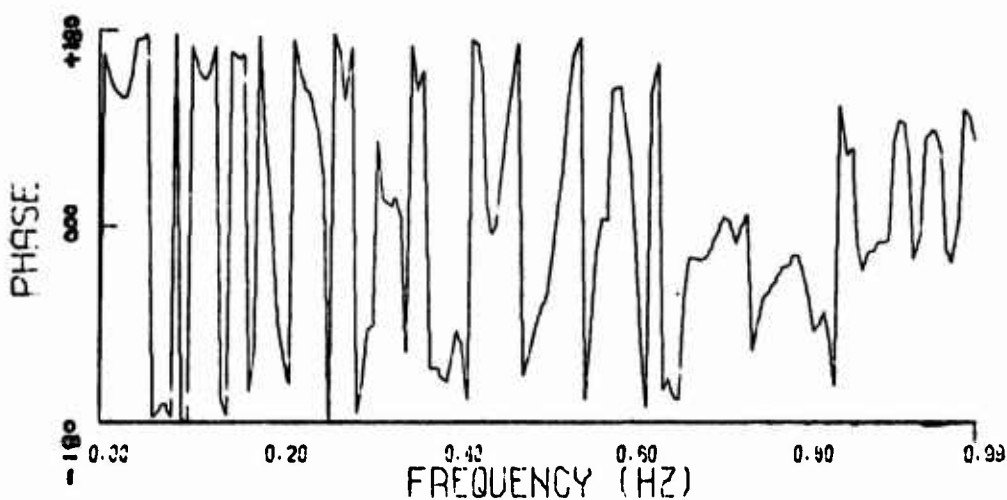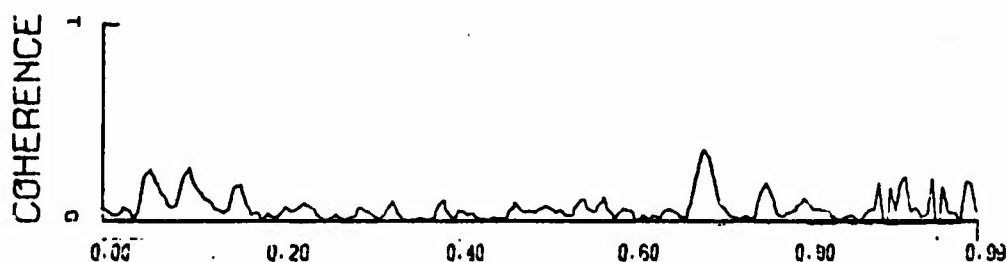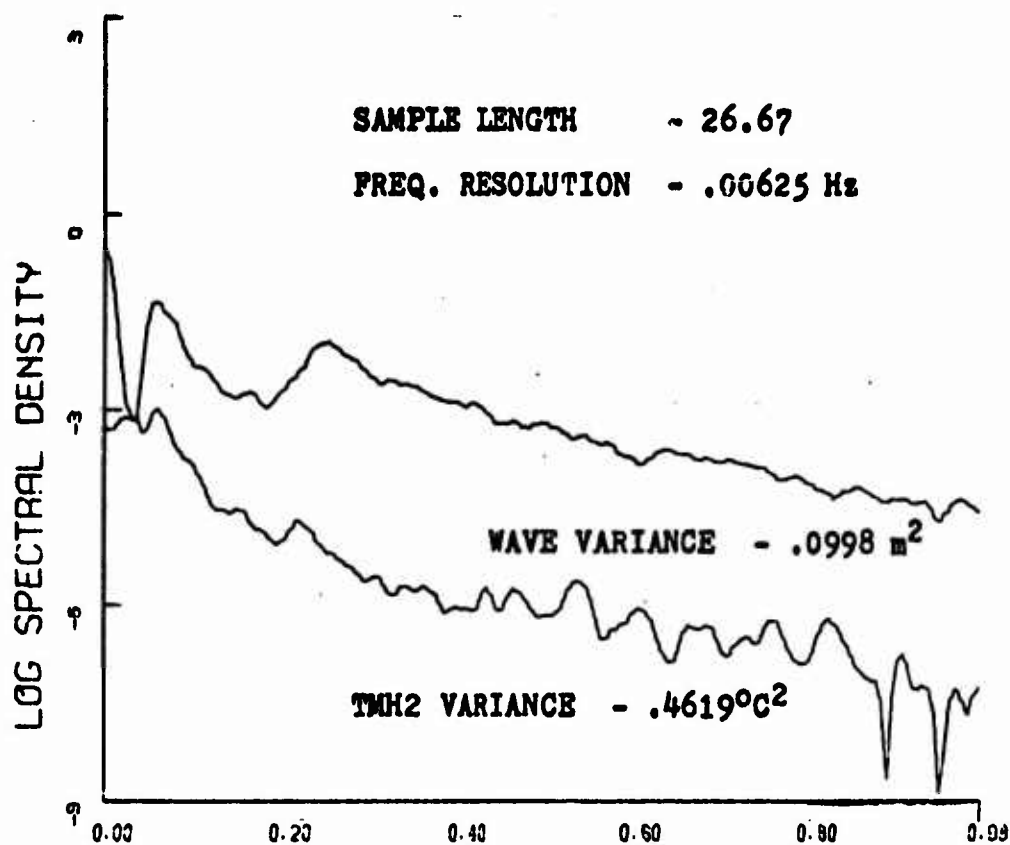
FIGURE 12. Run 2 TMH2 vs WAVE Spectra

56
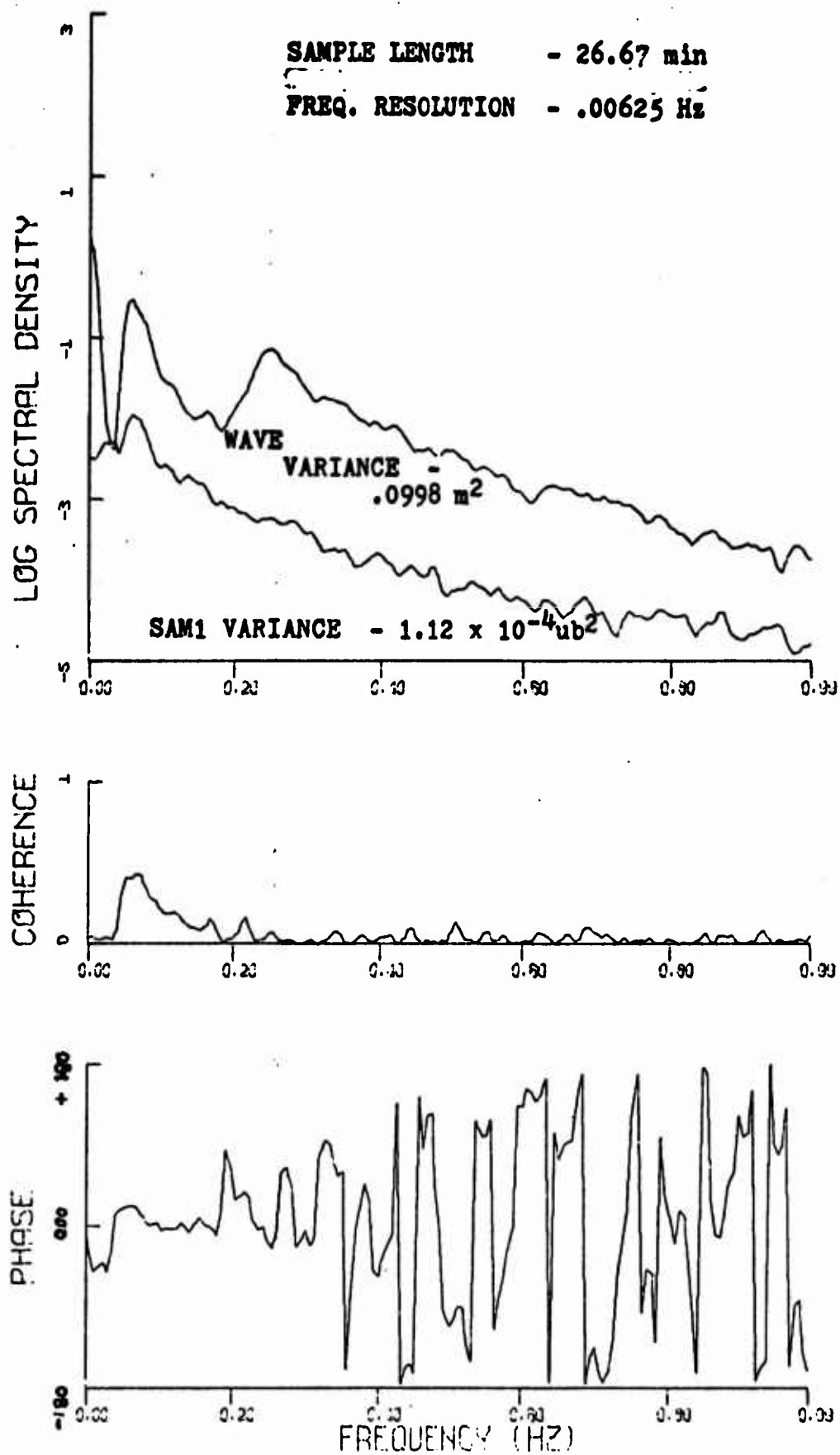
FIGURE 13. Run 2 SAM1 vs WAVE Spectra
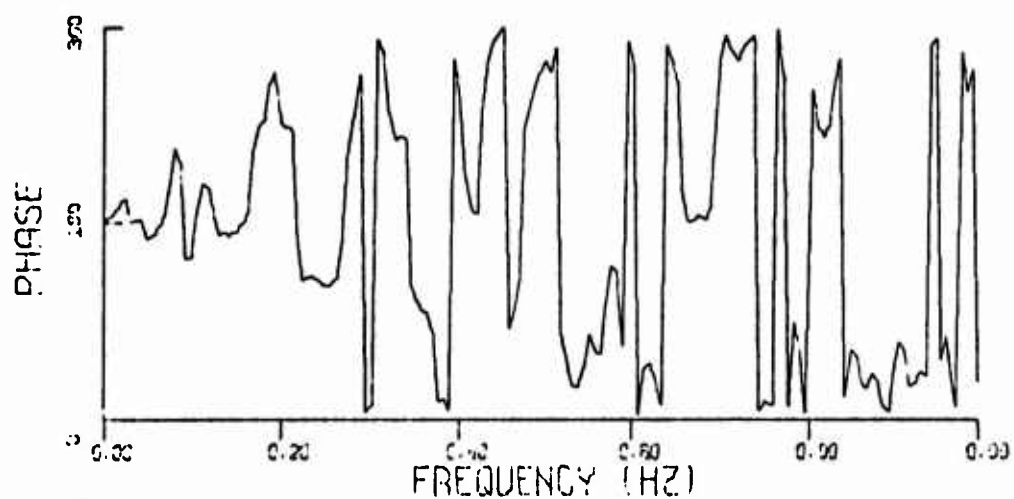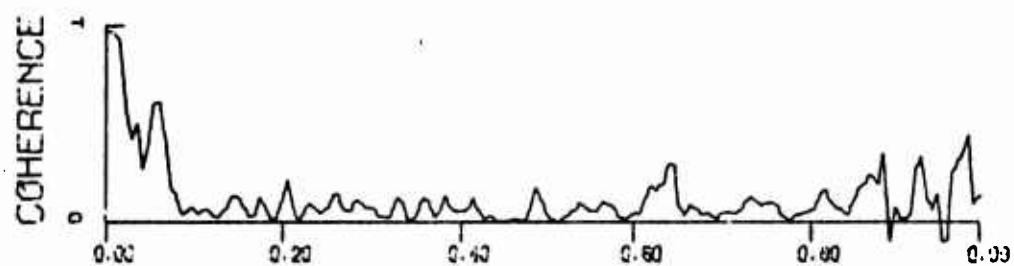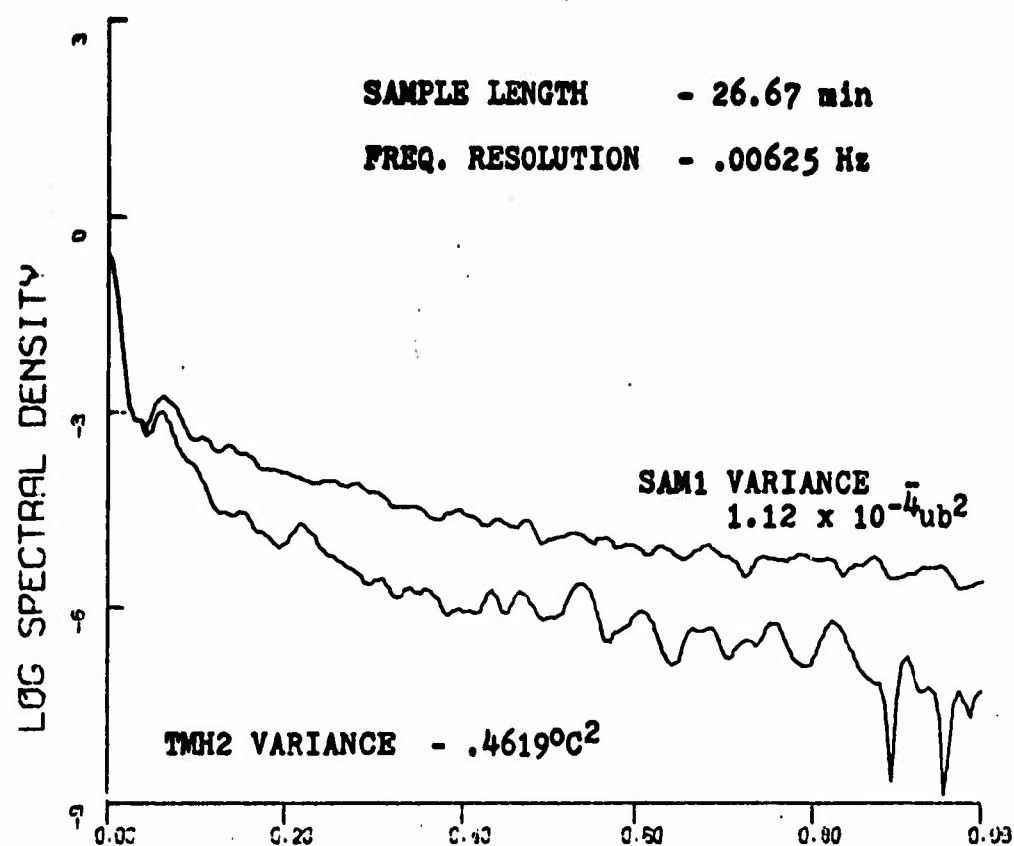
FIGURE 14. Run 2 SAM1 vs TMH2 Spectra
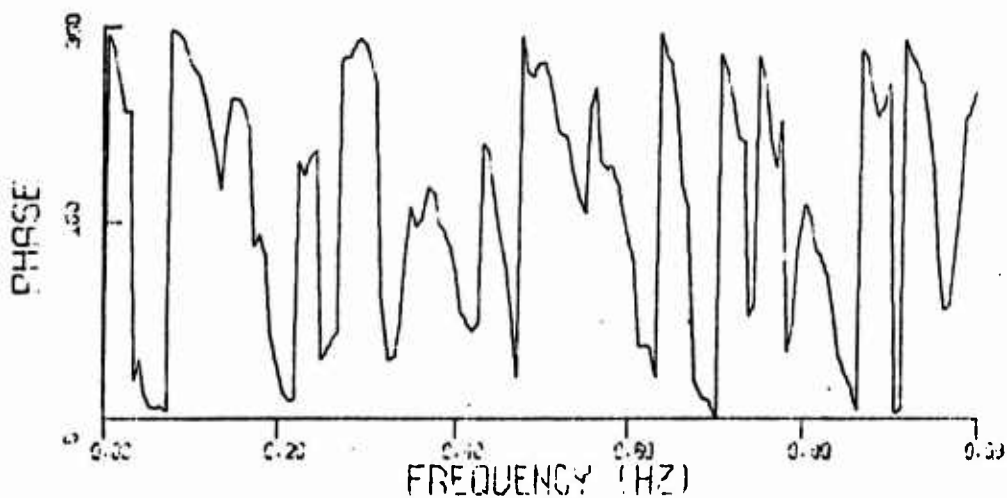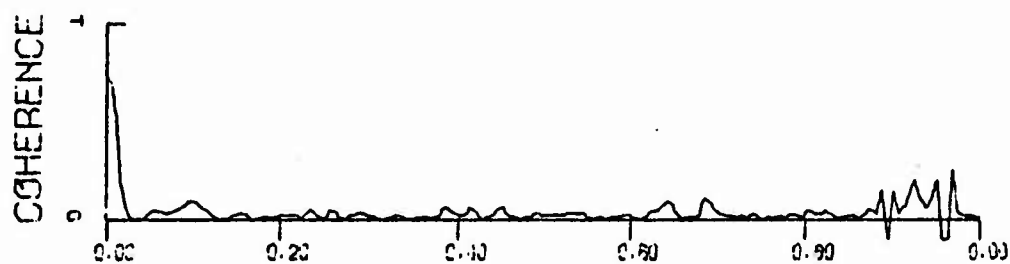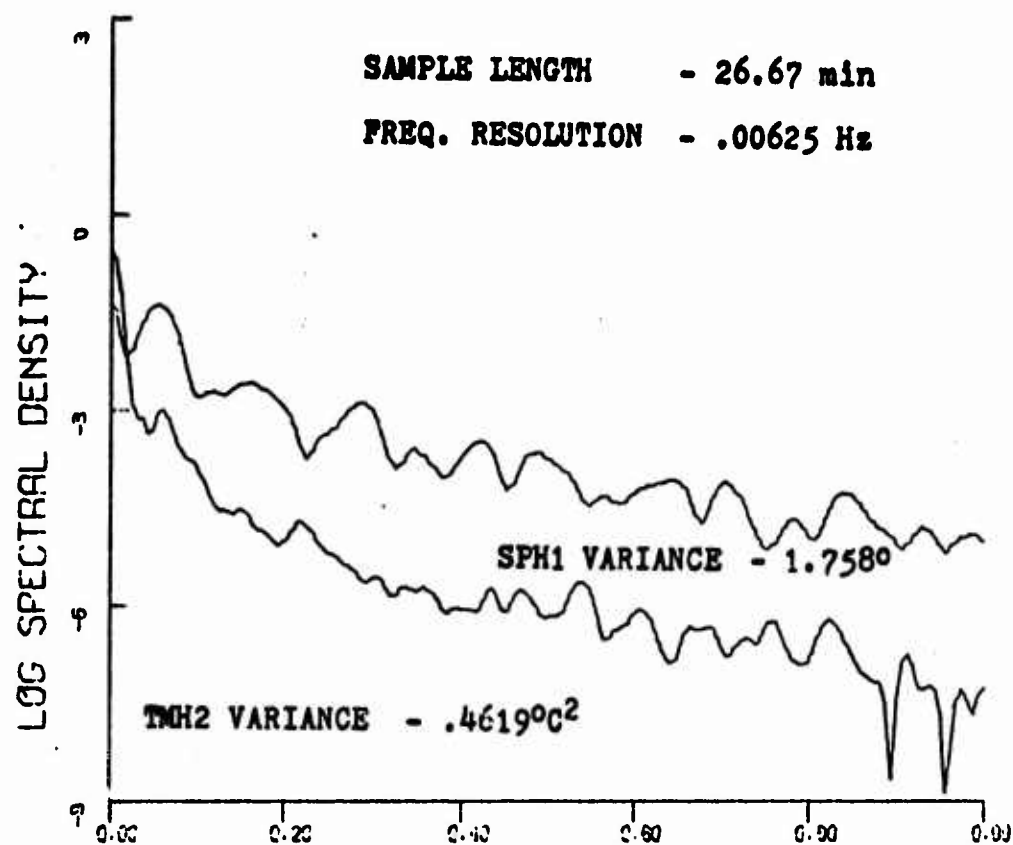
FIGURE 15. Run 2 SPH1 vs TMH2 Spectra

TABLE 8

Time Series Statistical Parameters

Run #/Channel	Average Value	RMS Value	Variance	56 Sec. Minimum Variance	56 Sec. Maximum Variance	Mean Period (sec)
1/TMH2	14.44°C	14.58°C	0.22×10^{-1} °C^2	8.04×10^{-4} °C^2	1.08×10^{-1} °C^2	18.2
2/TMH2	12.00	12.67	4.60×10^{-1}	170.0×10^{-4}	14.3×10^{-1}	178
12/TMH2	13.77	14.02	0.670×10^{-1}	9.94×10^{-4}	3.53×10^{-1}	21.6
1/WAVE	3.88m	4.19m	$0.105 m^2$	$0.098 m^2$	$0.101 m^2$	4.06
2/WAVE	2.50	2.82	0.100	0.046	0.156	4.69
12/WAVE	4.24	4.66	0.177	0.108	0.285	4.69
1/SAM1	0.76μb	0.87μb	$1.12 \times 10^{-4} \mu b^2$	$6.70 \times 10^{-5} \mu b^2$	$8.48 \times 10^{-5} \mu b^2$	7.02
2/SAM1	0.92	1.06	1.88×10^{-4}	4.62×10^{-5}	8.55×10^{-4}	22.86
12/SAM1*	0.62	0.70	4.05×10^{-5}	7.20×10^{-6}	1.11×10^{-4}	4.44
1/SPH1	37.33°	38.74°	2.03°	9.89×10^{-1}°	1.02°	7.37
2/SPH1	17.03	18.35	1.76	0.985×10^{-1}	.146	9.20
12/SPH1*	53.50	56.43	8.71	9.97×10^{-1}	10.8	7.08

RUN	DEPTH(m)	PROXIMITY TO THERMOCLINE(m)
1	7.53	4
2	12.03	0-1
12	10.44	1-2

*Anomalous because sonar array angled 25° to vertical vice horizontal.

period was controlled by surface wave swell until the layer was very close to the thermocline.

2) Sound amplitude variance was controlled by proximity to the thermocline (temperature gradient) when the sonar array was horizontal. The movement of the thermocline with respect to the sound path must therefore be the primary influence on sound amplitudes in this configuration.

3) The amplitude variance when the array was nearly vertical was much smaller than when it was horizontal. This indicated the effect of turbulence proximity to the hydrophone was smaller than the effect of temperature gradient motion over the sound path.

4) Since the mean period of the sound fluctuations was much smaller than the mean period of the swell at depth, turbulent interactions related to the higher frequency internal wave motion of the thermocline were emphasized in the sound measurements.

5) When the sound array was vertically oriented vice horizontal, much larger phase variations occurred even though amplitude variations were smaller. This resulted from the large temperature variations over thepath length caused by waves pumping the thermal gradient up and down. This also showed that the temperature variation effects on sound amplitude and phase were in quadrature.

6) The order of the mean sound phase variances indicates that phase was primarily influenced by surface waves when the

array was horizontal. Since spectral analysis showed that the wave coherence with temperature was very low at the surface wave frequencies, this effect may be bubble related.

2. Spectral Analysis

Cross-spectral analysis of the temperature, waves and sound records for the horizontal sonar runs one and two showed that the sound amplitude changes (Figs. 13 and 14) were in phase with the waves and 180° out of phase with temperature in the regions of highest coherence. This was expected in the stable density structure encountered. Additionally, the coherence squared function (simply referred to as coherence) showed that only the long-period, prominent swell was important to the sound amplitude modulation because the higher frequency wave particle velocities were much more rapidly attenuated with depth.

Sound phase (Fig. 15) was found to vary directly with temperature at the internal wave and surface wave frequencies although coherence at the surface wave frequencies was much smaller than at the internal wave frequencies. This indicated that the turbulence associated with the layer was more important than bubbles or surface wave perturbation of the thermocline in influencing sound speed over the horizontal sound path. A comparison of the coherences of Figs. 12 and 13 shows that the temperature effect is at least as important as bubbles even at the surface wave frequencies.

Similar cross-spectral analyses with the sonar path angles 25° from the vertical (run 12) yielded markedly different results. For the sound path entirely above the layer (SAM1), coherence with temperature was small over all frequencies. Small coherence peaks occurred at 0.15Hz and 0.7Hz which indicated that the vertical motion of the turbulent blobs forced by surface swell had some effect in the angled sound path.

Sound phase coherence with temperature was largest at the internal wave frequencies but smaller, broad-banded coherence at the surface wave frequencies was also observed. This confirmed that the phase was being controlled by the vertical motion of the thermocline.

Most of the sound path associated with SAM2 (2.3m) was not in the thermocline during the majority of run 12. However the hydrophone was near the top of the layer. As a result, its amplitude was in phase with temperature at the internal wave frequencies and coherence at other frequencies was almost zero. This verified that the interference effect of the proximity of the thermocline-associated turbulence to the receiver was theprimary effect on SAM2 variability.

Very high coherence and 180° phase difference between TMH2 and SAM3 at the internal wave and the surface wave frequencies was observed. Since the acoustic path associated with SAM3 generally spanned the thermocline, this indicated that the variability of amplitude across the entire

thermocline was controlled by refraction and diffraction similar to the horizontal case. The effect of diffraction was smaller than for the horizontal case, because the lenticular shape of the turbulent blobs present broader profiles to the vertical sound path. The reduced diffraction effects caused the variance in sound amplitude for run 12 to be an order-of-magnitude less than that for run 1.

3. Regression Analysis

Sound amplitude and phase variances, V^2(SAM) and V^2(SPH), were plotted versus TMH2 variances, V^2(T), and least squares regression analyses were applied to the data. Linear relationships between V^2(SAM) and V^2(SPH) versus V^2(T) were found to exist for runs one and two but not for run 12. This was because of insufficient variability in the portion of run 12 analyzed. The empirical relationship below was developed from the mean regressions calculated for runs one and two:

$$V^2(\text{SAM}) = (0.34 \mu b^2/°C^2)V^2(T)e^{-L/x} \tag{37}$$

where L = acoustic path length and x = the distance required to reduce V^2(SAM) by 1/e (determined empirically). x is near the size of the Taylor microscale.

The derivation of Equation (37), plots of the variances over the run segments and the regression plots are given in Appendix B.

64

C. SPATIAL ANALYSIS

Temperature spatial correlation and structure functions
were calculated directly from ensemble averages of 26.67 min
records from all possible combinations of thermistor pairs
along the vertical thermistor array. Twenty-two spatial
lags with values between 0 and 260 cm were thus determined
from seven thermistors. The value of C_T (see Equation 33a)
and the Taylor microscale as well as the Eulerian integral
scale were derived from the above functions (Table 9).
However, since large variations were seen in these functions
the validity of the calculated scales was questionable.

In an attempt to remove the non-stationary effects
resulting from internal waves, analyses using ensemble
averages of short segments having nearly constant turbulent
intensity were conducted for runs two and twelve. The
segments were chosen so that examples of low, medium and high
turbulent intensity could be examined (Table 10). Because
the thermocline steepness was highly variable along the
vertical thermistor array, however, only the medium inten-
sity correlation function was smooth enough to provide satis-
factory Eulerian integral scales and the structure function
of all samples varied widely. Values of the Taylor microscale,
Eulerian integral scale and C_T^2 generated from hand-smoothed
results are given in Table 11. The correlation function and
structure function values as well as the mean variance for
the vertical array thermistors are given in Appendix C.

65

TABLE 9

Temperature Spatial Scales (cm) for 26.67 min Ensembles

Run #	Taylor[1] Microscale	Taylor[2] Microscale	Eulerian Integral Scale	c_T^2
1	15	40	36	1.45×10^{-4}
2	178	158	175	3.6×10^{-3}
12	60	100	36	8.3×10^{-3}

TABLE 10

Relative Turbulent Intensity for Special Spatial Analyses

Qualitative Intensity	Ensemble Size (min)	TMH2 Mean Variance $(^{\circ}C)^2$	Range $(^{\circ}C)^2$	Run
Low	4.67	0.27×10^{-1}	$\pm0.77\times10^{-2}$	12
Medium	4.67	4.24×10^{-1}	$\pm4.95\times10^{-1}$	2
High	3.73	7.79×10^{-1}	$\pm2.23\times10^{-1}$	2

TABLE 11

Temperature Spatial Scales (cm) for Special Ensembles

Qualitative Intensity	Taylor[1] Microscale	Taylor[2] Microscale	Eulerian Integral Scale	c_T^2
Low	23	6.8	24	3.3×10^{-3}
Medium	71	40	35	4.4×10^{-3}
High	15	20	63	5.4×10^{-3}

Taylor[1] = Taylor microscale from spatial correlation

Taylor[2] = Taylor microscale from structure function

D. APPLICATION OF MODELS

While it is apparent that some of the scale estimates
calculated from the vertical thermistor array may be erron-
eous, it is instructive to apply the theoretical models
for the sound amplitude variance to see which model is
most applicable in the non-stationary case. Table 12 lists
the equations necessary to calculate the basic parameters
for application of the models. For the purposes of this
examination, the values of the Richardson number (R_t), the
Prandtl number (σ_k) and u/c_o were assumed to be the same
as reported by Neubert [1970] (see Table 13 for values).
The speed of sound is used to calculated Wilson's Equation
[Urick 1967].

Tables 13 and 14 list the resultant parameters of each
sample for which scales were determined. It is noteworthy
that the values of the refractive index (α) calculated above
are an order of magnitude above the near surface results
reported by other investigators [Haley 1972, Medwin 1973]
(see Table 15) except in the low turbulent intensity cases.
This is further evidence that the relative influence of the
turbulent thermocline in sound scattering is much greater
than bubbles.

If the order of magnitude of the Taylor microscale is
correct (see Table 13 for comparative values) the values of
$\alpha^2 a$ are one to four orders of magnitude greater than previously

67

TABLE 12

EQUATIONS USED FOR MODEL PARAMETER EVALUATION

Parameter	Equation
c_o	$c_o = 1449 + 4.6T - 0.55T^2 + 0.17d$
α	$\alpha^2 = [4.6^2 v^2(T) + 0.055^2 v^4(T)]/c_o^2$
λ_g	$\lambda_g = a\sqrt{\sigma_k} = 2.65a$
η_g	$\eta_g = \lambda_g^4 (R_t/15) = 2.07 \times 10^4 a^4$
C_n	$C_n^2 = C_T^2/4T_o^2$
ℓ_o^*	$\ell_o^* = 0(2.2/2.4a) = 0(0.9a)$

T = mean temperature (°C)

d = depth (m)

$v^2(T)$ = variance in temperature (°C^2)

a = Taylor microscale (cm)

η_g = Kolmogorov microscale (cm)

* equation for ℓ_o assumes u/c_o is a constant

68

TABLE 13

Experiment Parameter Values for Model Tests

Parameter	RUN 1	RUN 2	RUN 12
c_o (m/sec)	1516	1498	1515
α^-	4.5×10^{-4}	2.1×10^{-3}	7.9×10^{-4}
L (cm)	200	200	200
a (cm)	15	178	60
ℓ_o^*	13.5	160	54
λ (cm)	7.5	7.5	7.5
k_o (cm^{-1})	0.84	0.84	0.84
C_n	1.45×10^{-4}	1.05×10^{-4}	2.4×10^{-4}
L_e (cm)	36	175	36
σ_k	7	7	7
λ_g (cm)	40	472	159
η_g (m)	10.5	21.4	19.2
R_t	6300	6300	6300
$\alpha^2 a$	3.0×10^{-6}	7.9×10^{-4}	3.7×10^{-5}

TABLE 14

Short Sample Parameter Values for Model Tests

Parameter	Low Intensity	Medium Intensity	High Intensity
c_o (m/sec)	1512	1508	1500
α	5.0×10^{-4}	2.0×10^{-3}	2.7×10^{-3}
L (cm)	200	200	200
a (cm)	23	71	15
ℓ_o^*	21	64	13
λ (cm)	7.5	7.5	7.5
k_o (cm^{-1})	0.84	0.84	0.84
C_n	1.05×10^{-4}	1.16×10^{-4}	1.29×10^{-4}
L_e (cm)	24	35	63
σ_k	7	7	7
λ_g (cm)	61	188	40
η_g (cm)	2.8	8.5	1.8
R_t	6300	6300	6300
$\alpha^2 a$ (cm)	5.8×10^{-6}	2.8×10^{-4}	1.1×10^{-4}

TABLE 15

Comparative Values of a, α and $a\alpha^2$

Environment	a (cm)	α	$a\alpha^2$ (cm)	Source
Ocean	60	7.0×10^{-5}	2.94×10^{-7}	Liebermann [1951]
Laboratory	1.1 (min.)	1.2×10^{-4}	1.5×10^{-8}	Stone and Mintzer [1962]
Ocean Mean	–	–	5.0×10^{-7}	Sheehy [1950]
Ocean Mean			1.26×10^{-6}	Sagar [1960]
Bering Sea			3×10^{-10}	Shoemaker
NUC Tower (no bubbles)		3×10^{-5} 2.5×10^{-6}		Haley [1972]
(with bubbles)		6.7×10^{-4}	1.1×10^{-7}	Haley [1972]
Deep Ocean	169	2.55×10^{-5}	3.1×10^{-9}	
	89	0.59×10^{-5}	5.8×10^{-6} to 7.9×10^{-4}	
NUC Tower	6.8–178	4.5×10^{-4} to 2.7×10^{-3}		Tables 13 and 14

reported. This result has a direct relationship (in the Born model) to the variance of sound amplitude.

The variances of sound amplitude calculated by each model previously discussed (Geometric, Born, Rytov, Debye) are presented in Tables 16 - 19. In general, the best fit to the measured sound variances were calculated from the Born model using the Krasil'nikov-Obhukov formulation. A surprisingly good fit to the true variance was also obtained from the geometric model in the mid-intensity range. Because of the above, the stimates of the Taylor microscale seem reasonable.

Since the accuracy of the scales, C_T^2 and L_e, the Eulerian integral scale, is in question, no firm statement can be made about the adequacy of the Rytov and Debye models. However, because L_e is thought to be correct for the mid-intensity ensemble, the Debye model appears incorrect. Presumably, calculation of the structure function and correlation function from the thermistors in the horizontal array over stationary ensembles would resolve this question. Unfortunately, this was not accomplished in time for inclusion in this thesis.

TABLE 16

Geometric Model Experimental Results

$$v^2 = 4/15 \sqrt{\pi} \, \alpha^2 (L/a)^3 \quad ; \quad 7.5 << \ell_o^2/L \quad \text{(cm)}$$

Ensemble	Model v^2	Observed $v^2 (\mu b)^2$	ℓ_o^2/L (cm)
Run 1	4.8×10^{-4}	1.12×10^{-4}	0.91
Run 2	3×10^{-6}	1.45×10^{-3}	128
Run 12	1.1×10^{-5}	4.05×10^{-5}	146
Low Intensity	7.8×10^{-5}	7.1×10^{-6}	2.2
Mid Intensity	4.2×10^{-5}	9.5×10^{-5}	21
High Intensity	8.2×10^{-3}	3.0×10^{-4}	0.85

TABLE 17

Born Model Experimental Results
[Krasil'nikov and Obhukov]

$$v^2 = k_o^2 \alpha^2 a L (1 - 1/D \tan^{-1} D) \quad ; \quad D = \pi L / k_o a$$

Ensemble	Model v^2	Observed v^2	D
Run 1	4.3×10^{-4}	1.12×10^{-4}	50
Run 2	7.9×10^{-4}	1.45×10^{-3}	4.2
Run 12	3.74×10^{-5}	4.05×10^{-5}	12.5
Low Intensity	5.8×10^{-6}	7.1×10^{-6}	32.5
Mid Intensity	2.8×10^{-4}	9.5×10^{-5}	10.5
High Intensity	1.1×10^{-4}	3.0×10^{-4}	50

$$D >> 1 \rightarrow \text{Wave Region}$$

TABLE 18

Rytov Model Experimental Results

$$V^2 = 161\ C_n^2\ L\ 11/6\ -7/6\ ;\quad 7.5 \ll \sqrt[3]{l_o^*/L}$$

Ensemble	Model V^2	Observed V^2	$\sqrt[3]{l_o^*/L}$
Run 1	5.2×10^{-3}	1.12×10^{-4}	5.5
Run 2	2.8×10^{-3}	1.45×10^{-3}	150
Run 12	1.5×10^{-2}	4.05×10^{-5}	35
Low Intensity	2.8×10^{-3}	7.1×10^{-6}	9.9
Mid Intensity	3.4×10^{-3}	9.5×10^{-5}	44
High Intensity	4.2×10^{-3}	3.0×10^{-4}	5.2

TABLE 19

Debye Model Experimental Results

$$V^2 = 2\alpha^2 k_o^2 L_e L$$

Ensemble	Model V^2	Observed V^2
Run 1	2.1×10^{-3}	1.12×10^{-4}
Run 2	0.22	1.45×10^{-3}
Run 12	6.3×10^{-3}	4.05×10^{-5}
Low Intensity	1.7×10^{-3}	7.1×10^{-6}
Mid Intensity	4×10^{-2}	9.5×10^{-5}
High Intensity	0.13	3.0×10^{-4}

V. CONCLUSIONS

The theories of turbulence which have been developed for the ocean require some degree of stationarity in the medium before they may be applied. This paper has examined four basic stochastic models of acoustic wave propagation under the most severe conditions of non-stationarity, e.g. near a sharp thermocline which is being oscillated by both large surface swell and by internal waves.

The experimental conditions specified that the solution form would be in the wave region for which the Born model would be most accurate. The solution of the Krasil'nikov-Obhukov form of the Born model from directly measured, ocean parameters gave reasonable results.

The solution of the Rytov and Debye models for the same conditions yielded results two orders of magnitude higher than was actually measured. Because evaluation of scales was difficult, this was expected even though both models are more general than the Born model and, in fact, contain its solution in a subset. This also showed the determination of the Taylor microscale was more reliable than the determination of the structure constant, C_T^2, or the Eulerian integral scale for measurements across the thermocline.

An attempt was made to apply the correlation function and structure function piecewise to small sections of data which were thought to be relatively stationary. For

75

application across the thermocline, this method did not work well because selection of such sections is very difficult.

The results of the time series analyses showed that the losses over the acoustic path were greatest when the array was horizontal near the thermocline because the diffractive losses were an order of magnitude greater than those for the nearly vertical case. Interference effects due to the proximity of turbulence to the receiving hydrophone accounted for a 0.14% signal loss and scintillations due to surface swell accounted for 0.07% signal modulation. The effects of bubbles were small because the measurements were relatively deep and the acoustic frequency was much lower than the peak bubble resonant frequency. Measured loss over the 2m path was on the order of 5% and phase shifts of up to 30° occurred for these worst-case conditions.

Current sound propagation models based upon empirical data have undoubtedly included these effects in surface scattering or reverberation. But the roughness description for the sea surface used by sonar models is based upon sea state. The losses here described are, instead, related to the swell wave-induced water particle velocities and internal waves.

APPENDIX A

Spectral Analysis Plots

This appendix includes examples of cross-spectral analysis plots so that qualitative comparisons between sound, temperature and waves during the experiment can be made. Included are spectra for 1) sound amplitude versus temperature, 2) sound phase versus temperature, 3) wave-related effects and 4) comparison of one sound channel with another for the same run. The plots included are listed below.

Sound Amplitude Versus Temperature

Run #	Channels Compared
1	SAM1 - TMH2
1	SAM2 - TMH2
1	SAM3 - TMH2
2	SAM1 - TMH2 (see text)
2	SAM2 - TMH2
2	SAM3 - TMH2
12	SAM1 - TMH2
12	SAM2 - TMH2
12	SAM3 - TMH2

Sound Phase Versus Temperature

Run #	Channels Compared
1	SPH1 - TMH2
2	SPH1 - TMH2 (see text)
2	SPH2 - TMH2
12	SPH1 - TMH2

Wave-Related Effects

Run #	Channels Compared
1	TMH2 – WAVE
1	SPH1 – WAVE
2	SAM1 – WAVE
6	TMH2 – FVBY
12	TMH2 – WAVE

Sound Channel Comparisons

Run #	Channels Compared
2	SAM1 – SAM2
2	SAM1 – SAM3
2	SAM2 – SAM3
2	SPH1 – SPH2

RUN 1

FREQUENCY (HZ)

79

RUN 1

LOG SPECTRAL DENSITY

SAM 2

TMH 2

COHERENCE

PHASE

FREQUENCY (HZ)

80

RUN 1

81

RUN 2

FREQUENCY (HZ)

82

RUN 2

LOG SPECTRAL DENSITY

SAM3

TMH2

COHERENCE

PHASE

FREQUENCY (HZ)

RUN 12

LOG SPECTRAL DENSITY

SAMI

TMH2

COHERENCE

PHASE

FREQUENCY (HZ)

84

RUN 12

RUN 12

86

RUN 1

SPHI
TMH2

FREQUENCY (HZ)

87

RUN 2

SPH 2

TMH 2

LOG SPECTRAL DENSITY

COHERENCE

PHASE

RUN 12

LOG SPECTRAL DENSITY

SPHI

TMH2

COHERENCE

PHASE

FREQUENCY (HZ)

RUN 1

FREQUENCY (HZ)

90

RUN I

WAVES

SPHI

RUN 2

LOG SPECTRAL DENSITY (M**2-SECS)

WAVES

SAMI

COHERENCE

PHASE

FREQUENCY (HZ)

92

RUN 6

RUN 12

RUN 2

FREQUENCY (HZ)

95

RUN 2

LOG SPECTRAL DENSITY

SAM3

SAM1

COHERENCE

PHASE

FREQUENCY (HZ)

96

RUN 2

SAM 3

SAM 2

LOG SPECTRAL DENSITY

COHERENCE
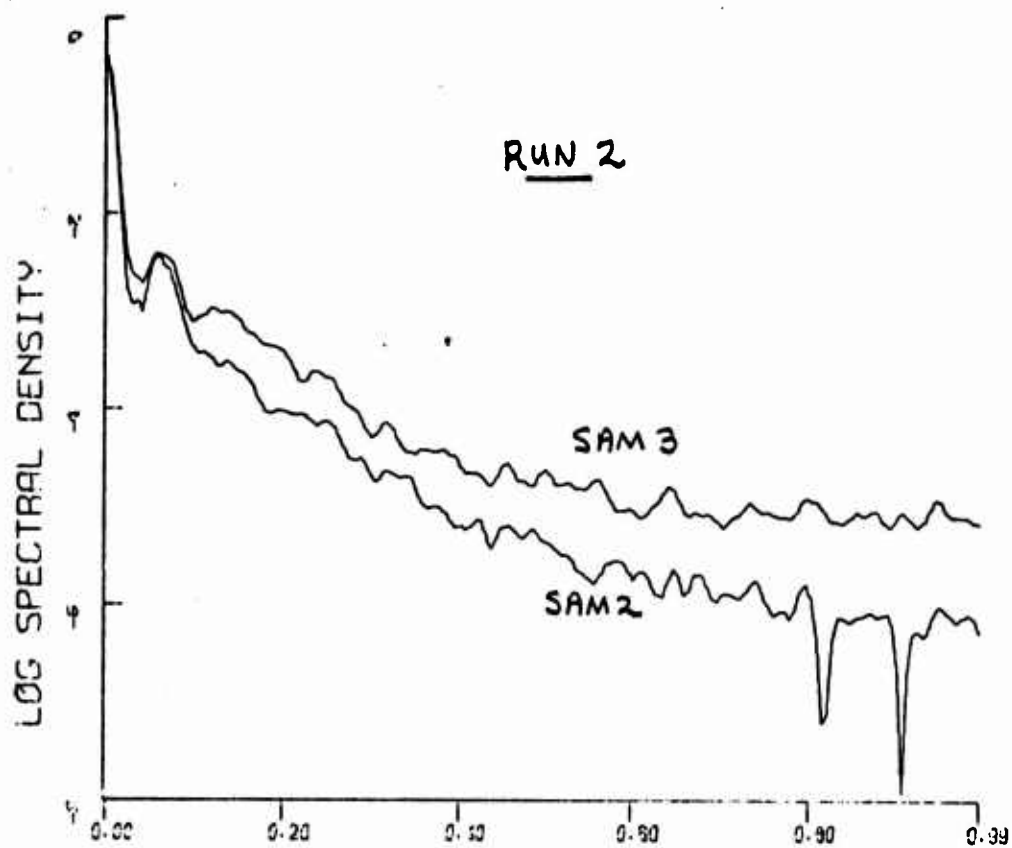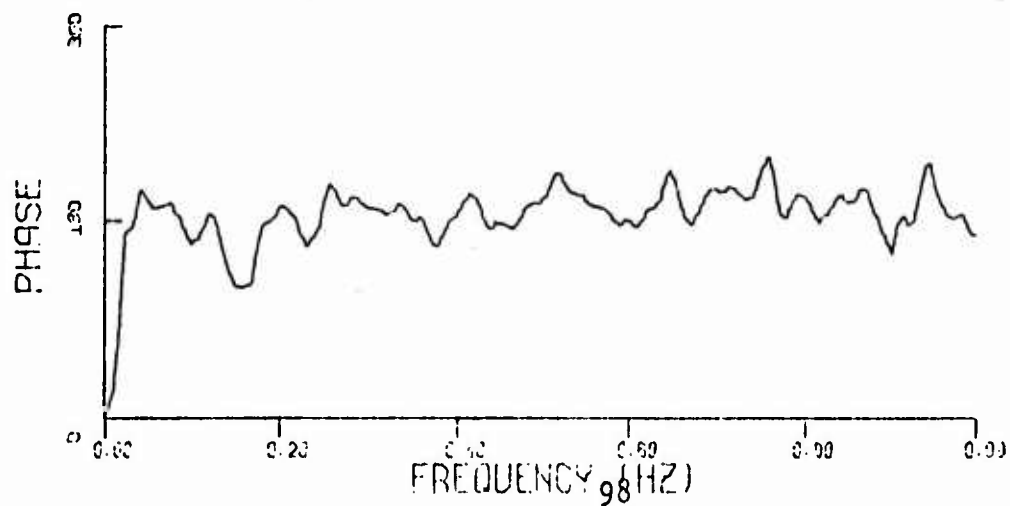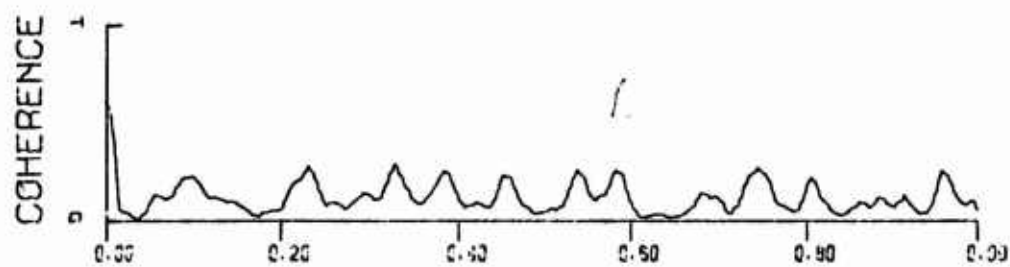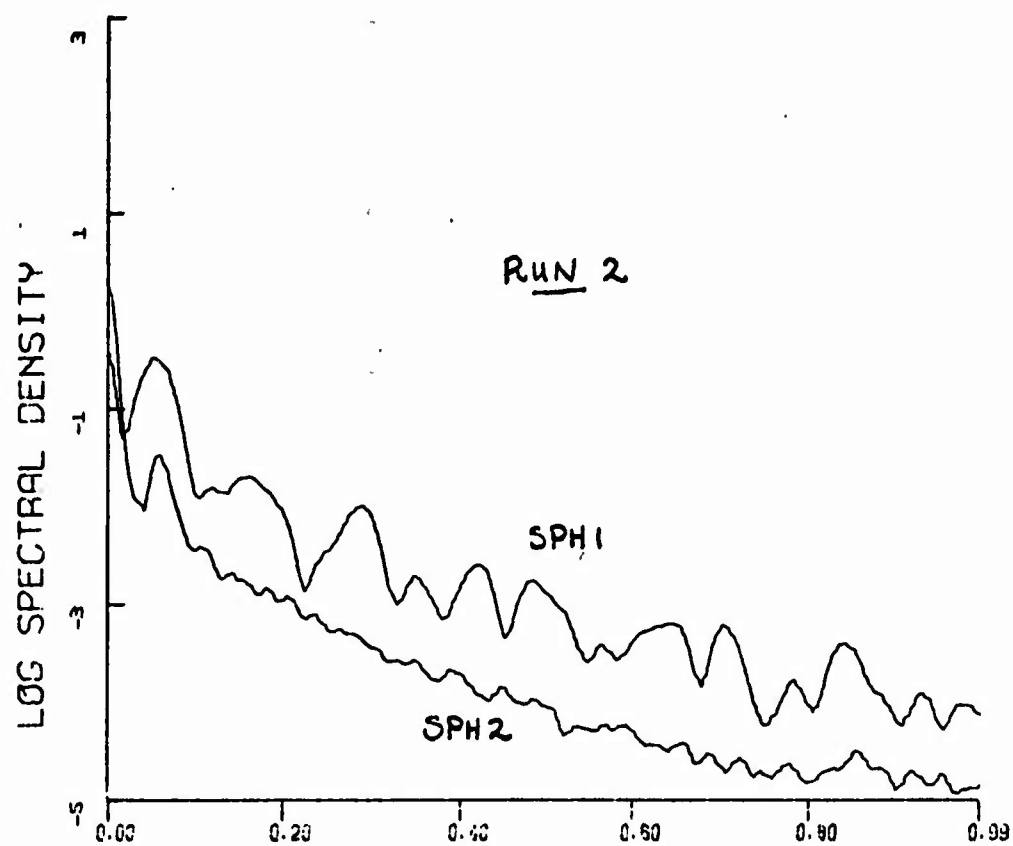
PHASE

FREQUENCY (HZ)

97

Run 2

APPENDIX B

Analyses of Variance Regressions

Variances of 56 sec samples of data which included 1400 data points each were calculated along 26.67 min segments of certain channels of runs one, two and 12. Regression analyses for sound amplitude and phase versus temperature were computed using these variances. The resultant plots of the variances with the regression curves are shown after Table B5. A summary of the regression equations is given in Table B1. The following mean variance equations were computed from the average of the regression equations listed for runs one and two:

$$V^2(\text{SAM1}) = 3.2 \times 10^{-3} \; V^2(T) \tag{B1}$$

$$V^2(\text{SAM2}) = 1.6 \times 10^{-3} \; V^2(T) \tag{B2}$$

$$V^2(\text{SAM3}) = 4.1 \times 10^{-4} \; V^2(T) \tag{B3}$$

If $V^2(T)$ is eliminated from the above equations (stationary assumption), then because SAM1 and SAM2 are 30 cm apart and 60 cm separates SAM2 and SAM3:

$$V^2(\text{SAM}) \propto (\tfrac{1}{2})^{-L/30} \; \text{cm} \tag{B4}$$

where L = sound path length.

This equation can be checked by comparing the sound amplitude variances for specific 56 sec samples (where the sample is stationary) and similarly deriving the relationship

$$V^2(SAM) \propto (\tfrac{1}{2})^{-L/x} \tag{B5}$$

where x is the distance required to reduce $V^2(SAM)$ by 0.5. This is done in Tables B3 - B5. The following equations result:

$$\text{Run 1:} \quad V^2(SAM) \propto \tfrac{1}{2}^{-L/34.5} \text{ cm} \tag{B6}$$

$$\text{Run 2:} \quad V^2(SAM) \propto \tfrac{1}{2}^{-L/42} \text{ cm} \tag{B7}$$

Conversion from base $\tfrac{1}{2}$ to base e and placing the path length reference at 1m vice 2m yields (from equations B1, B4, and B5):

$$V^2(SAM) = (0.34\mu b^2/{}^\circ c^2)V^2(T)e^{-L/x} \tag{B8}$$

where:

L = acoustic path length in meters,

x = temperature spatial scale for which

100

$$V^2(\text{SAM}) = V^2(\text{SAM})_{x=0}/2$$

$$V^2(T) = \text{temperature variance}$$

$$V^2(\text{SAM}) = \text{variance of sound amplitude.}$$

And the spatial scales in (B4), (B6) and (B7) become 43cm, 50cm and 61cm, respectively.

Since $V^2(\text{SAM})$ is known to be a function of α^2, the variance of the index of refraction, and $\alpha = 2.1 \times 10^{-3}$ for run two (which had the best regression fits):

$$V^2(\text{SAM}) = 7.7 \times 10^4 \, \alpha^2 \, V^2(T) \, e^{-L/x} \qquad \text{(B9)}$$

Assuming that $x \ll L$, the following approximation can be made:

$$e^{-L/x} \approx \frac{x}{x+L} \approx \frac{x}{L} \qquad \text{(B10)}$$

Substituting Equation B(10) into Equation B(9) and multiplying by L^2 to compensate for the spherical spreading loss yields:

$$V^2(\text{SAM}) = 7.7 \times 10^4 \, \alpha^2 \, V^2(T) \, xL \qquad \text{(B11)}$$

101

which is similar to the exponential form of the Born approximation:

$$V^2 = k_o{}^2 \; \alpha^2 \; aL \tag{B12}$$

if k_o is similarly included in Equation (B11):

$$V^2(SAM) = 1.1 \times 10^{-5} \; k_o{}^2 \; \alpha^2 \; V^2(T) \; xL. \tag{B13}$$

The plots following Table B5 are included to allow qualitative comparisons of conditions between runs and of the variances between channels during the same run. For each run analyzed the variance versus time plots are given followed by regression plots between various channels.

TABLE B1. Regression Equations for Sound Versus Temperature Variances

AMPLITUDE

Channel	Run#	Equation
SAM1	1	$V^2(\text{SAM1}) = [3.4V^2(T)] \times 10^{-3}$
	2	$V^2(\text{SAM1}) = [3.0V^2(T)] \times 10^{-3}$
	12	$V^2(\text{SAM1}) = [4 - 2V^2(T)] \times 10^{-4}$
SAM2	1	$V^2(\text{SAM2}) = [2.0V^2(T)] \times 10^{-3}$
	2	$V^2(\text{SAM2}) = [1.2V^2(T)] \times 10^{-3}$
	12	$V^2(\text{SAM2}) = [0.7 + 1.5V^2(T)] \times 10^{-5}$
SAM3	1	$V^2(\text{SAM3}) = [4.8V^2(T)] \times 10^{-4}$
	2	$V^2(\text{SAM3}) = [3.3V^2(T)] \times 10^{-4}$
	12	$V^2(\text{SAM3}) = [0.2 + 4V^2(T)] \times 10^{-4}$

PHASE

Channel	Run#	Equation
SPH1	1	$V^2(\text{SPH1}) = 1 + 41V^2(T)$
	2	$V^2(\text{SPH1}) = 0.2 + 0.7V^2(T)$
	12	$V^2(\text{SPH1}) = 3.7 + 77V^2(T)$
SPH2	1	$V^2(\text{SPH2}) = 2 + 8V^2(T)$*
	2	$V^2(\text{SPH2}) = 2 + 22V^2(T)$
	12	$V^2(\text{SPH2}) = 2 - 25V^2(T)$

*From 20 minute record.

TABLE B2. Run 1 Variances

sample variance	Run 1 26 2/3 min	Run 1-18 56 sec	Run 1-13 56 sec	Run 1-25 56 sec
$V_T^2(°C^2)$	2.2×10^{-2}	16.1×10^{-2}	3.2×10^{-2}	0.43×10^{-2}
$V_{SAM1}^2(\mu b^2)$	11.0×10^{-5}	52.0×10^{-5}	12.0×10^{-5}	18×10^{-5}
$V_{SAM2}^2(\mu b^2)$	7.6×10^{-5}	39.0×10^{-5}	7.2×10^{-5}	13×10^{-5}
$V_{SAM3}^2(\mu b^2)$	2.5×10^{-5}	9×10^{-5}	3.3×10^{-5}	3.2×10^{-5}

TABLE B3. Sound Amplitude Distance Loss Factors (Run 1)

sample distance	Run 1* 26 2/3 min	Run 1-1 56 sec	Run 1-2 56 sec	Run 1-3 56 sec
30 cm	1.45	1.33	1.67	1.38
60 cm	3.04	4.33	2.18	4.06
90 cm	4.40	5.78	3.64	5.63

quantity distance	mean loss factors	standard deviation in loss factors	normalized loss factors	accepted loss factors
30 cm	1.46	0.18	1.00	1.15
60 cm	3.52	1.17	2.41	2.30
90 cm	5.02	1.19	3.44	3.45

*not included in mean loss factors
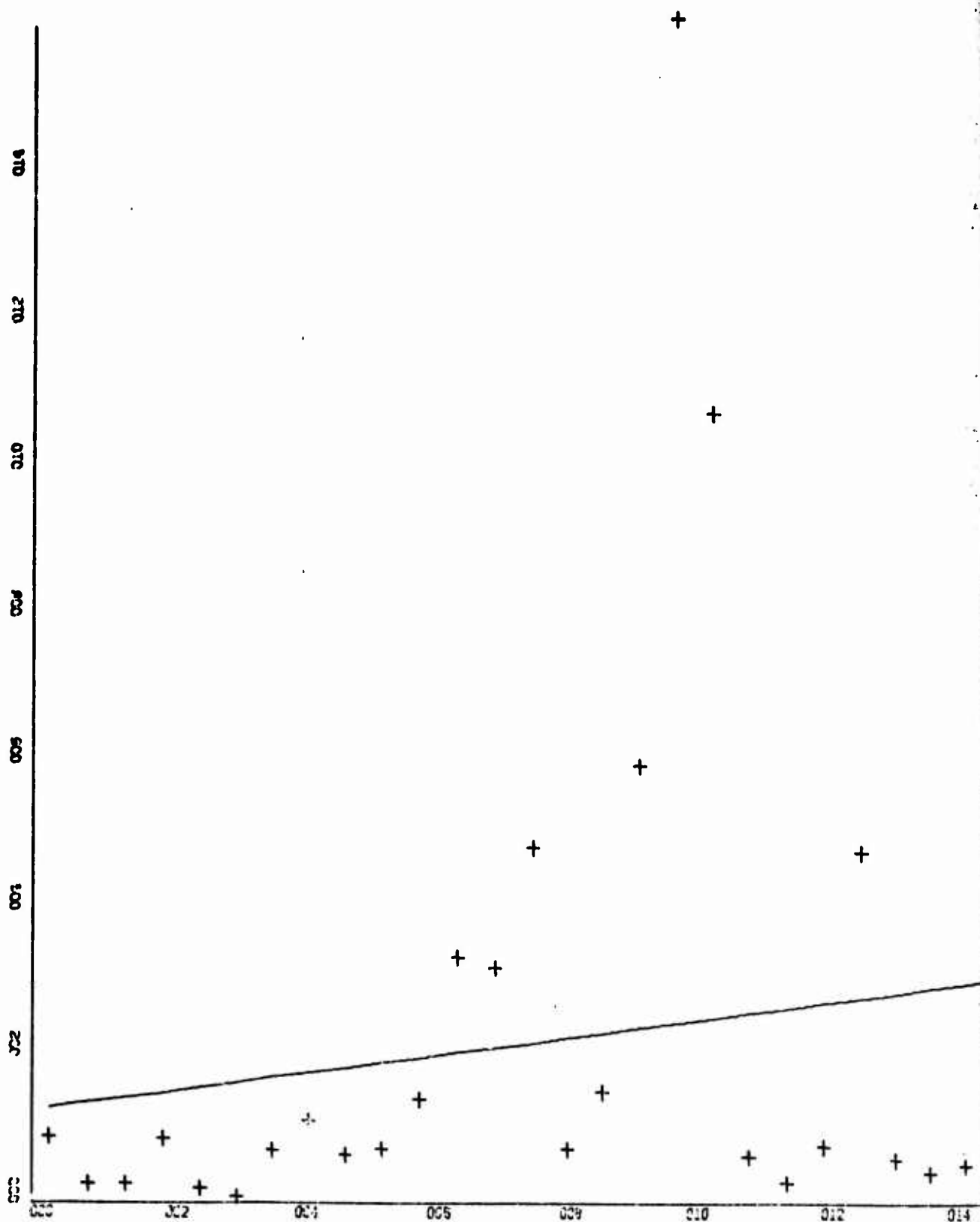
104

TABLE B4. Run 2 Variances

Sample variance	Run 2 26 2/3 min	Run 2-9 56 sec	Run 2-26 56 sec	Run 2-20 56 sec
$V_T^2(°C^2)$	46.2×10^{-2}	98.1×10^{-2}	143.4×10^{-2}	121.4×10^{-2}
$V_{SAM1}^2(\mu b^2)$	140×10^{-5}	311×10^{-5}	422×10^{-5}	420×10^{-5}
$V_{SAM2}^2(\mu b^2)$	56.0×10^{-5}	122×10^{-5}	146×10^{-5}	178×10^{-5}
$V_{SAM3}^2(\mu b^2)$	17.0×10^{-5}	30.5×10^{-5}	40.3×10^{-5}	460×10^{-5}

TABLE B5. Sound Amplitude Loss Factors with Distance (Run 2)

sample distance	Run 2* 26 2/3 min	Run 2-9 56 sec	Run 2-26 56 sec	Run 2-20 56 sec
30 cm	2.5	2.5	2.9	2.4
60 cm	3.29	4.0	3.62	3.9
90 cm	8.24	10.2	10.47	9.1

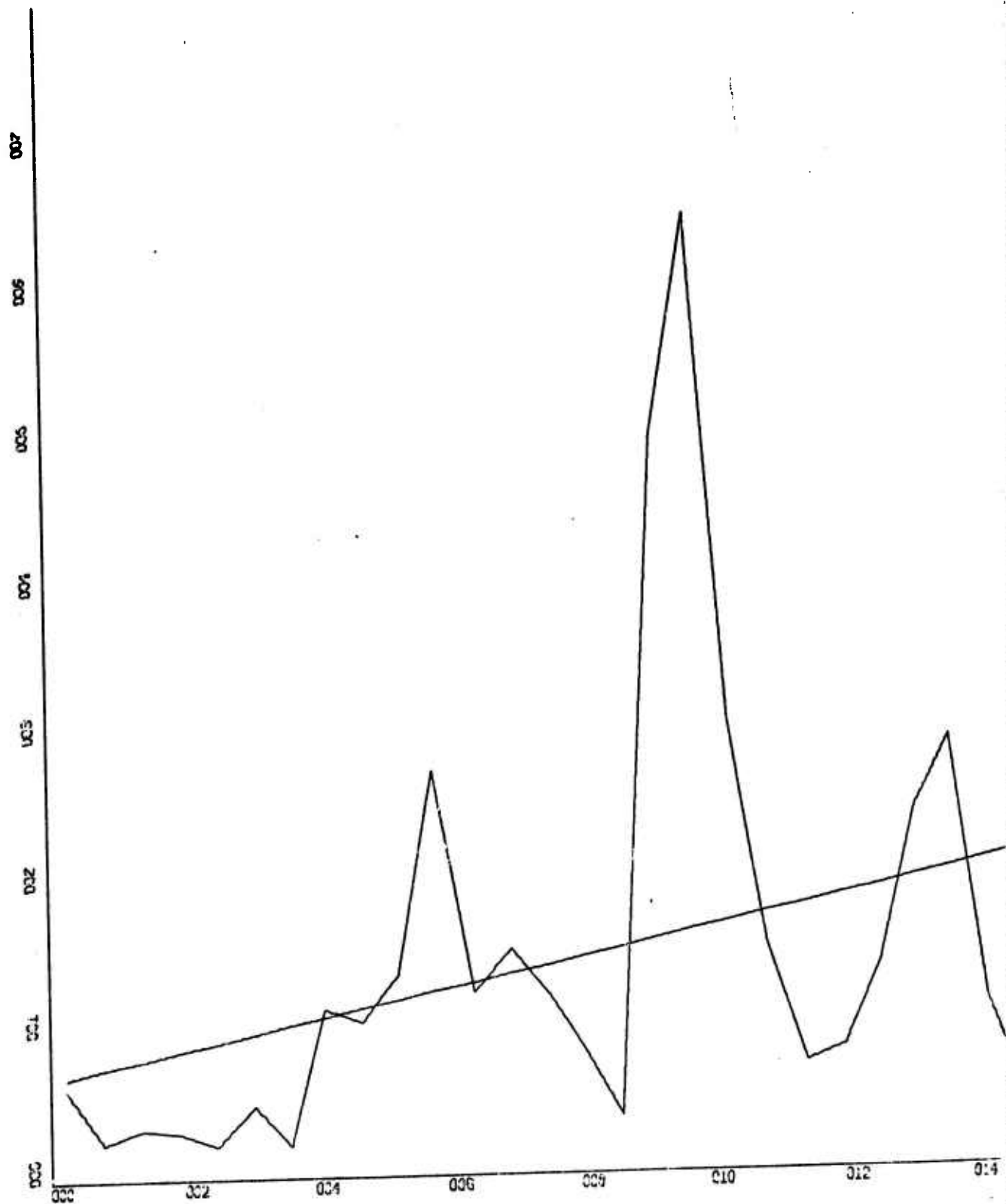| quantity distance	mean loss factors	standard deviation in loss factors	normalized loss factors	accepted loss factors
30 cm	2.6	0.3	1.0	1.4
60 cm	3.8	0.20	1.5	2.8
90 cm	9.9	0.73	3.8	4.2

*not included in mean loss factors.

RUN 1

X-SCALE 2.00E+02 UNITS INCH. = TIME (sec)
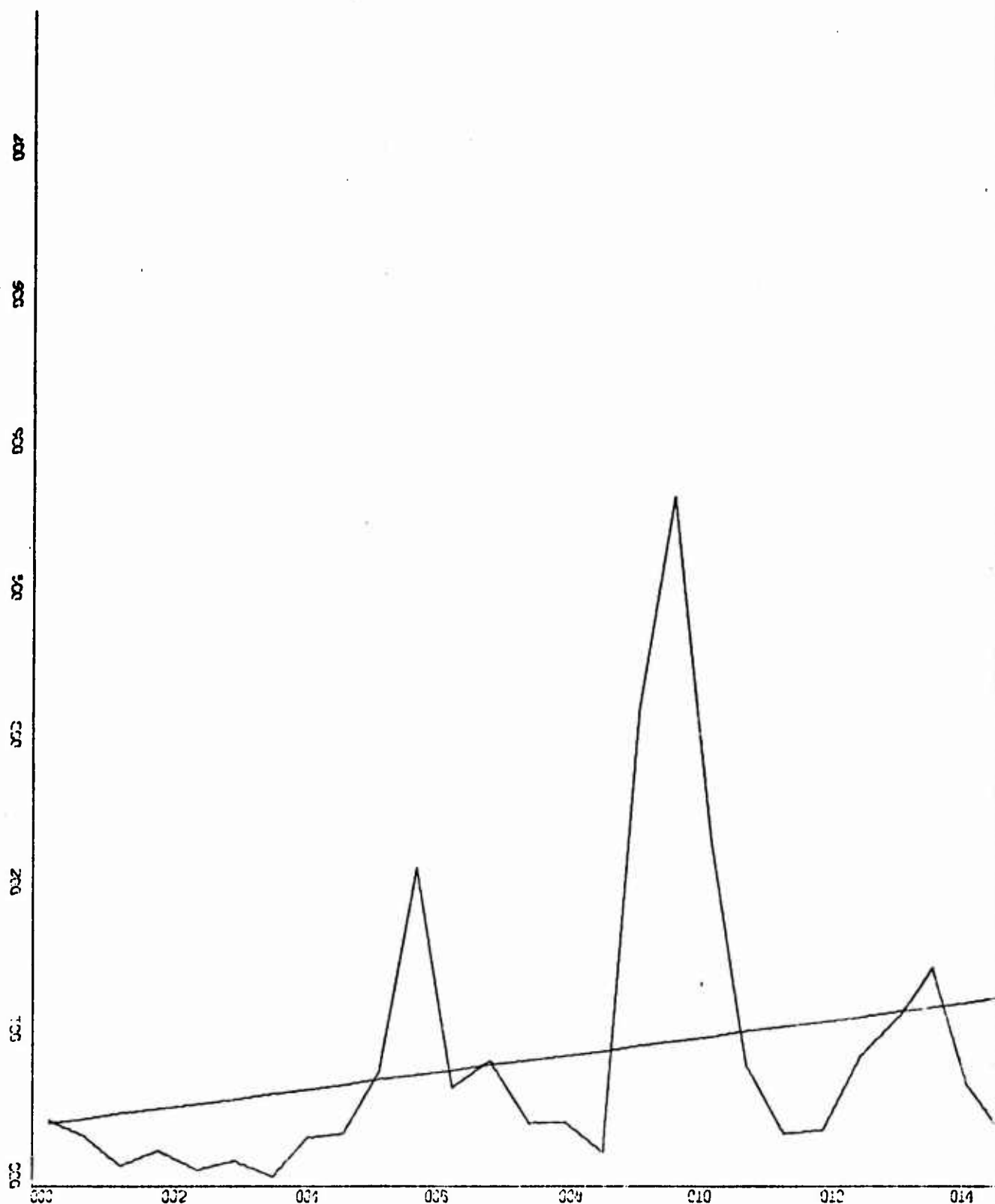Y-SCALE 5.00E-02 UNITS INCH. = V²(WAVE) (m²)

VARIANCE FIT

106

RUN 1

X-SCALE-2.00E+02 UNITS INCH. = TIME (SEC)
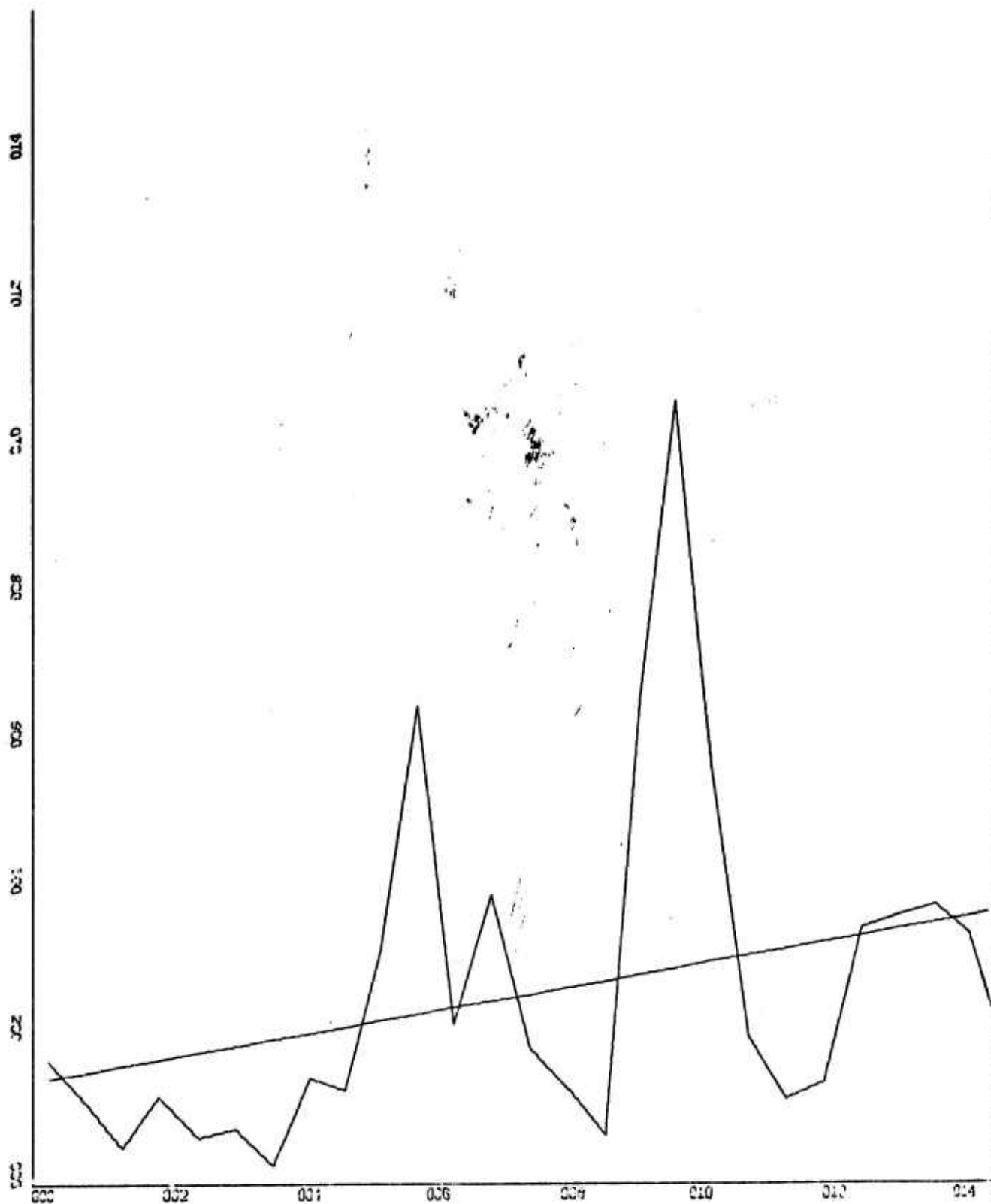Y-SCALE-2.00E-02 UNITS INCH. = V^2(TMH2) ($°C^2$)

VARIANCE FIT

RUN 1

X-SCALE: 2.00E+02 UNITS INCH. = TIME (SEC)
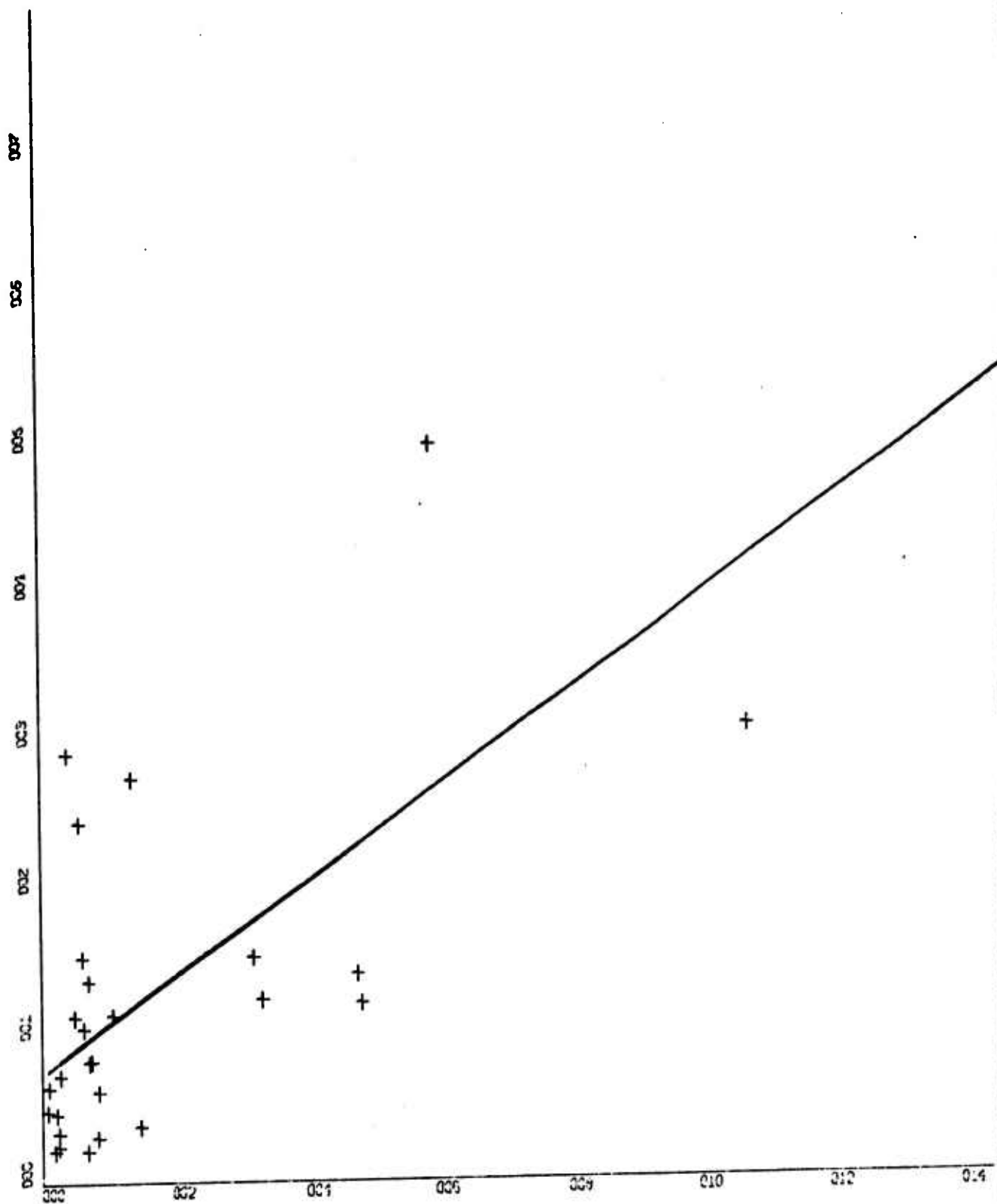Y-SCALE: 1.00E-05 UNITS INCH. = V^2(SAM1) (VOLTS^2)
VARIANCE FIT

RUN 1

X-SCALE-2.00E+02 UNITS INCH. = TIME (SEC)
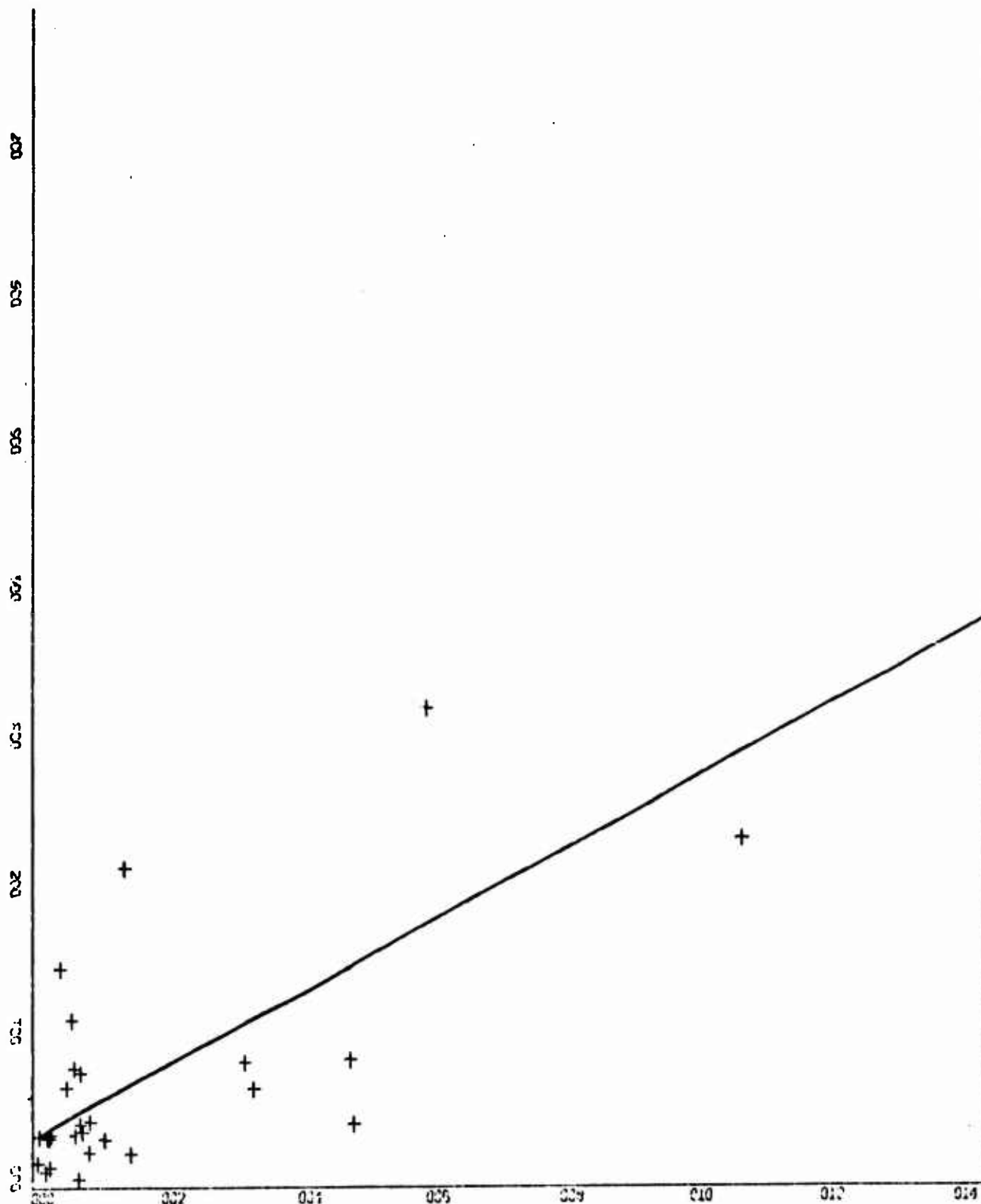Y-SCALE-1.00E-05 UNITS INCH. = V²(SAM2) (VOLTS²)

VARIANCE FIT

109

RUN 1

X-SCALE-1.00E+02 UNITS INCH. = TIME (sec)
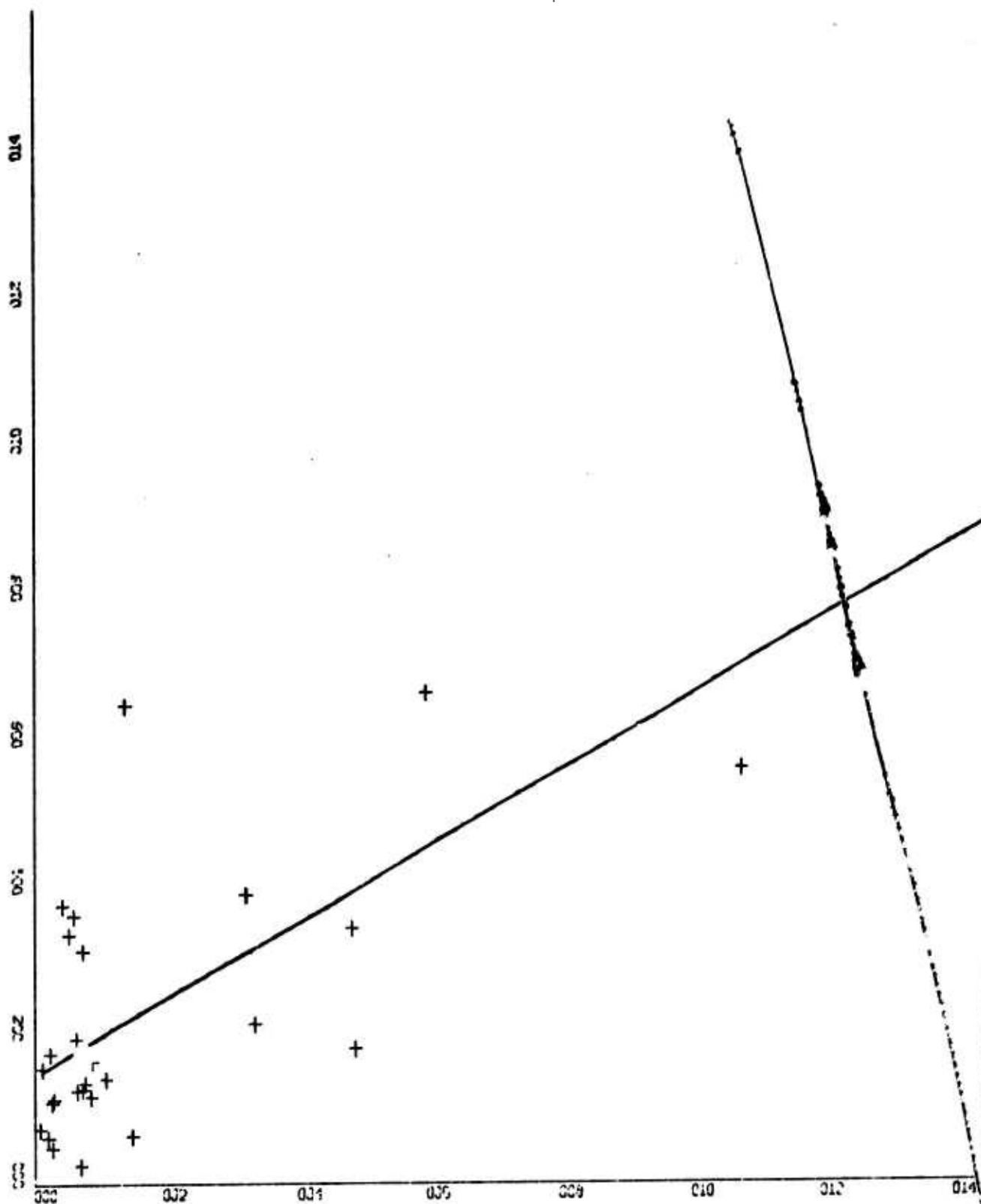Y-SCALE-2.00E-06 UNITS INCH. = V²(SAM3) (VOLTS²)

VARIANCE FIT

110

RUN 1

X-SCALE: 2.00E-02 UNITS INCH. = V^2 (TMH2) ($^{\circ}C^2$)
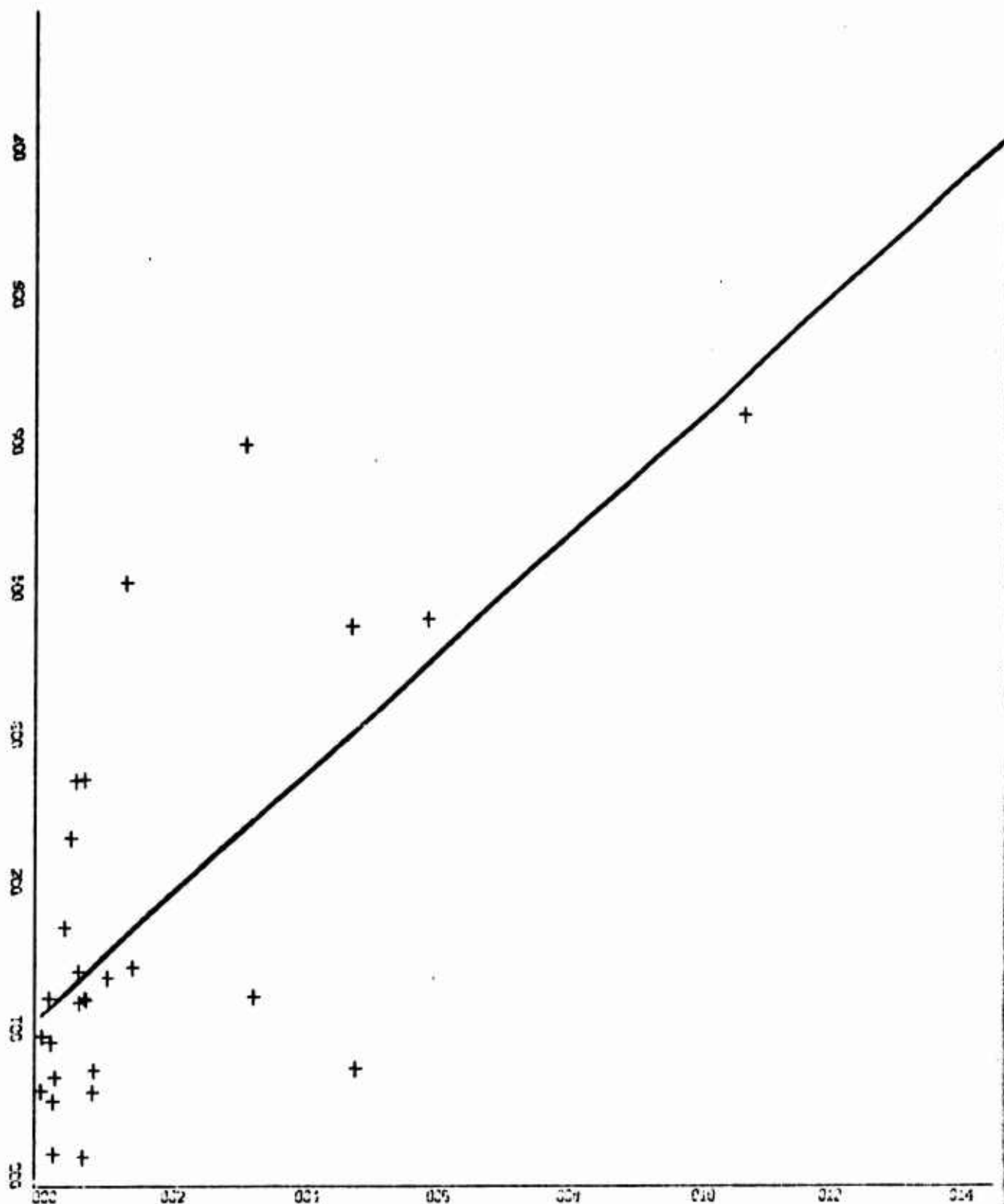Y-SCALE: 1.00E-05 UNITS INCH. = V^2 (SAM1) (VOLTS^2)
REGRESSION PLOT

111

RUN I

X-SCALE = 2.00E-02 UNITS INCH. = V^2 (TMH2) $(^\circ C^2)$
Y-SCALE = 1.00E-05 UNITS INCH. = V^2 (SHM2) (VOLTS^2)

REGRESSION PLOT 112

RUN 1

X-SCALE 2.00E 02 UNITS INCH. = $V^2(TMH2)(^oc^2)$
Y-SCALE 2.00E 06 UNITS INCH. = $V^2(SAM3)(VOLTS^2)$
REGRESSION   PLOT

113

RUN 1

X-SCALE 2.00E-02 UNITS INCH. = V² (TMH2) (°c²)
Y-SCALE 1.00E+00 UNITS INCH. = V² (SPH1) (degrees²)
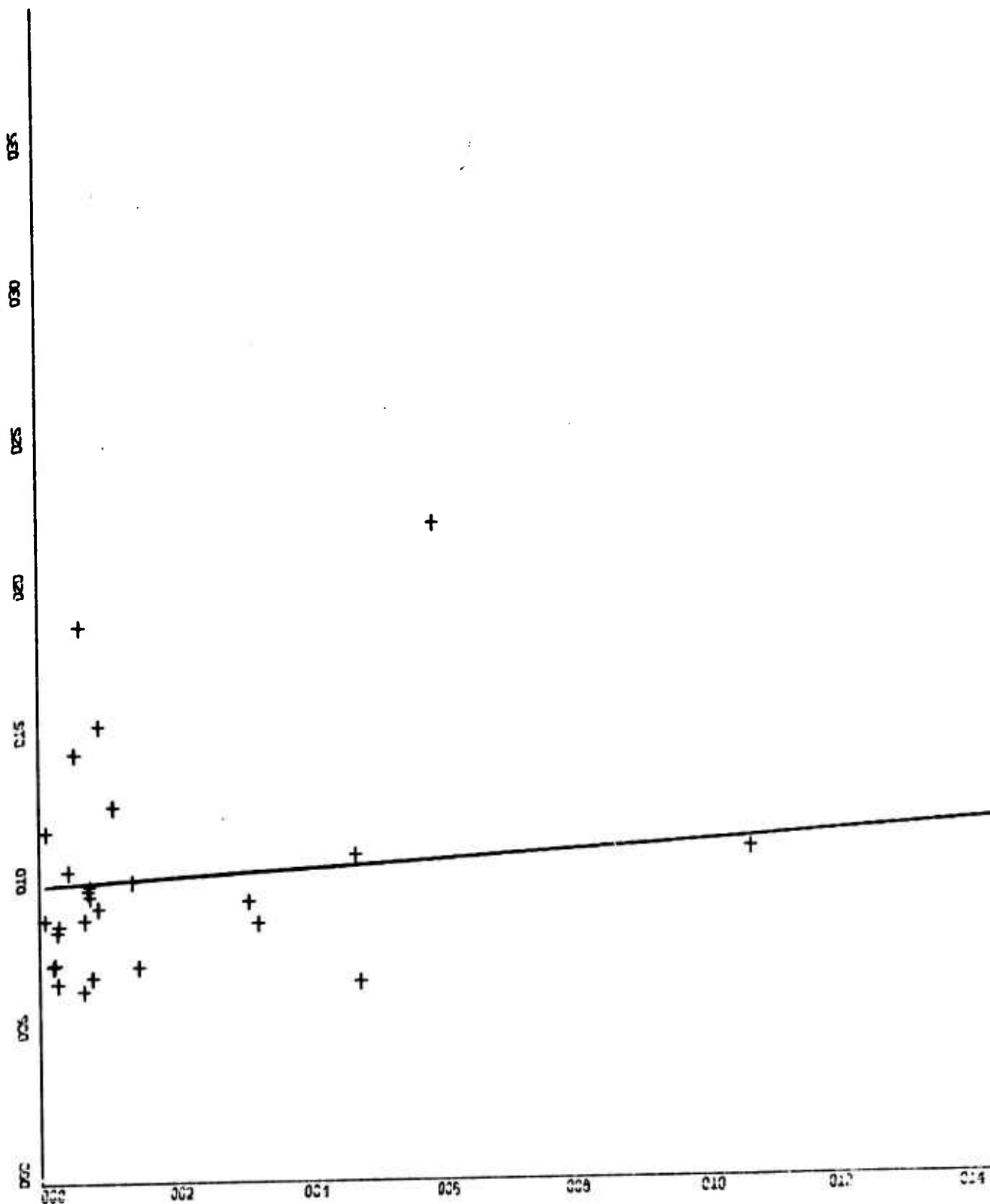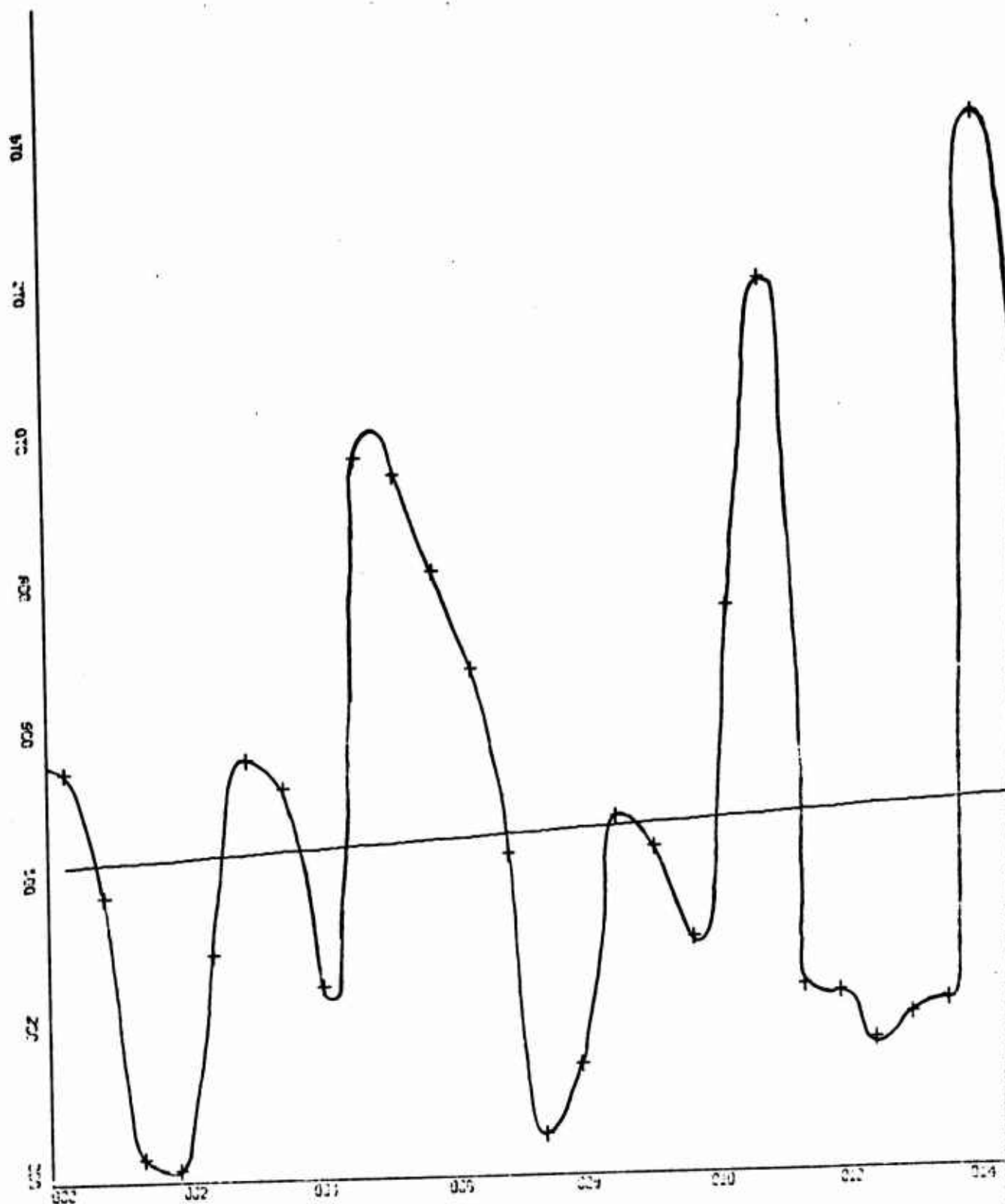REGRESSION PLOT

114

RUN 1

X-SCALE 2.00E-02 UNITS INCH. $= V^2(TMH2)(^\circ C^2)$
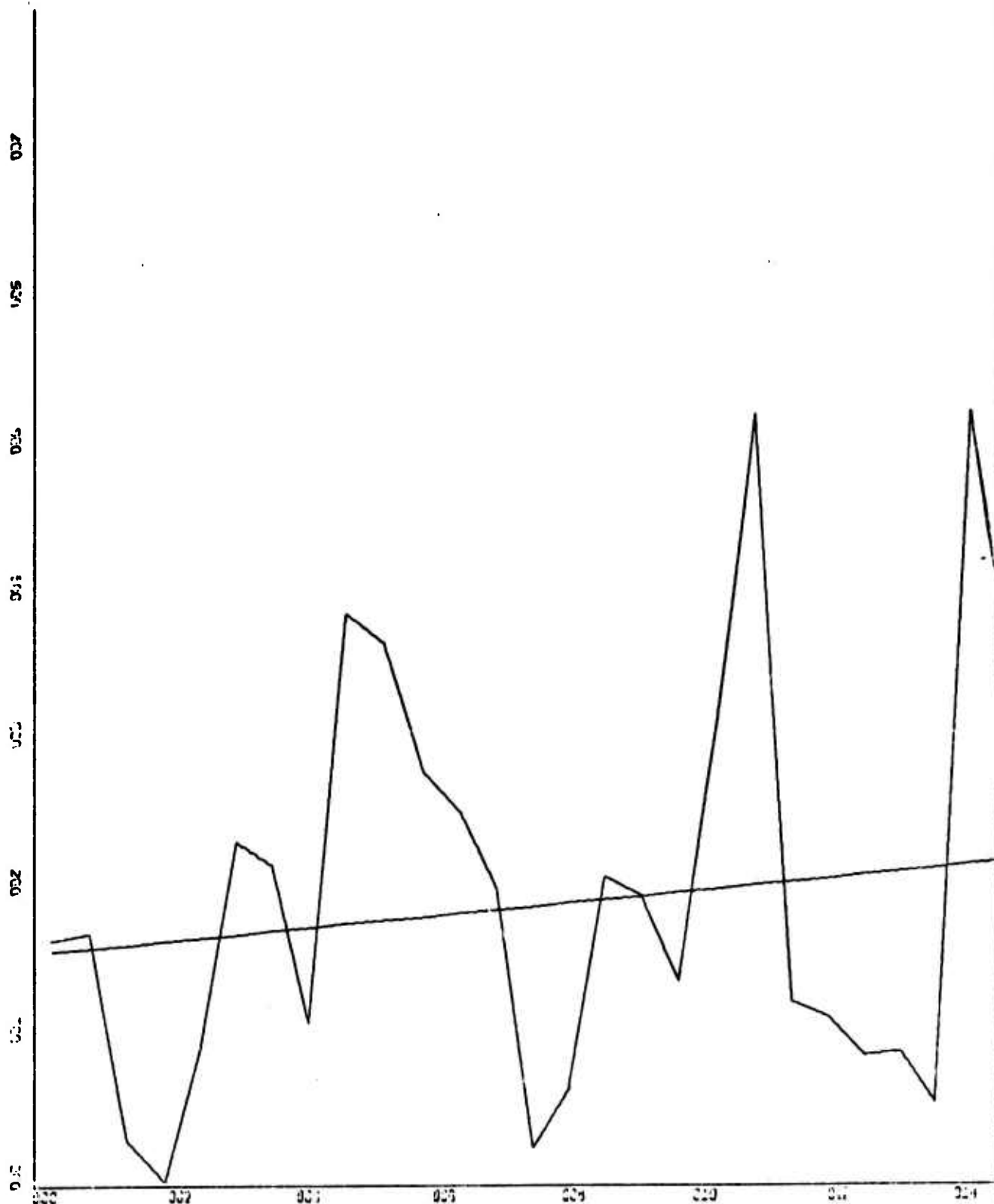Y-SCALE 5.00E-02 UNITS INCH. $= V^2(SPH2)(degrees^2)$

REGRESSION PLOT

115

RUN 2

X-SCALE 2.00E+02 UNITS INCH = TIME (SEC)
Y-SCALE 2.00E-02 UNITS INCH = V²(WAVE) (m²)

VARIANCE FIT

RUN 2

X-SCALE·2.00E+02 UNITS INCH = TIME (SEC)
Y-SCALE·2.00E 01 UNITS INCH = V^2 (TMH2) ($°C^2$)
VARIANCE FIT   117

RUN 2

X-SCALE 0.00E+02 UNITS INCH = TIME (SEC)
Y-SCALE 1.00E-04 UNITS INCH = V^2 (SAMI) (VOLTS^2)

VARIANCE FIT

RUN 2

X-SCALE=2.00E+02 UNITS INCH. = TIME (SEC)
Y-SCALE=1.00E-04 UNITS INCH. = V^2(SAM2) (VOLTS^2)
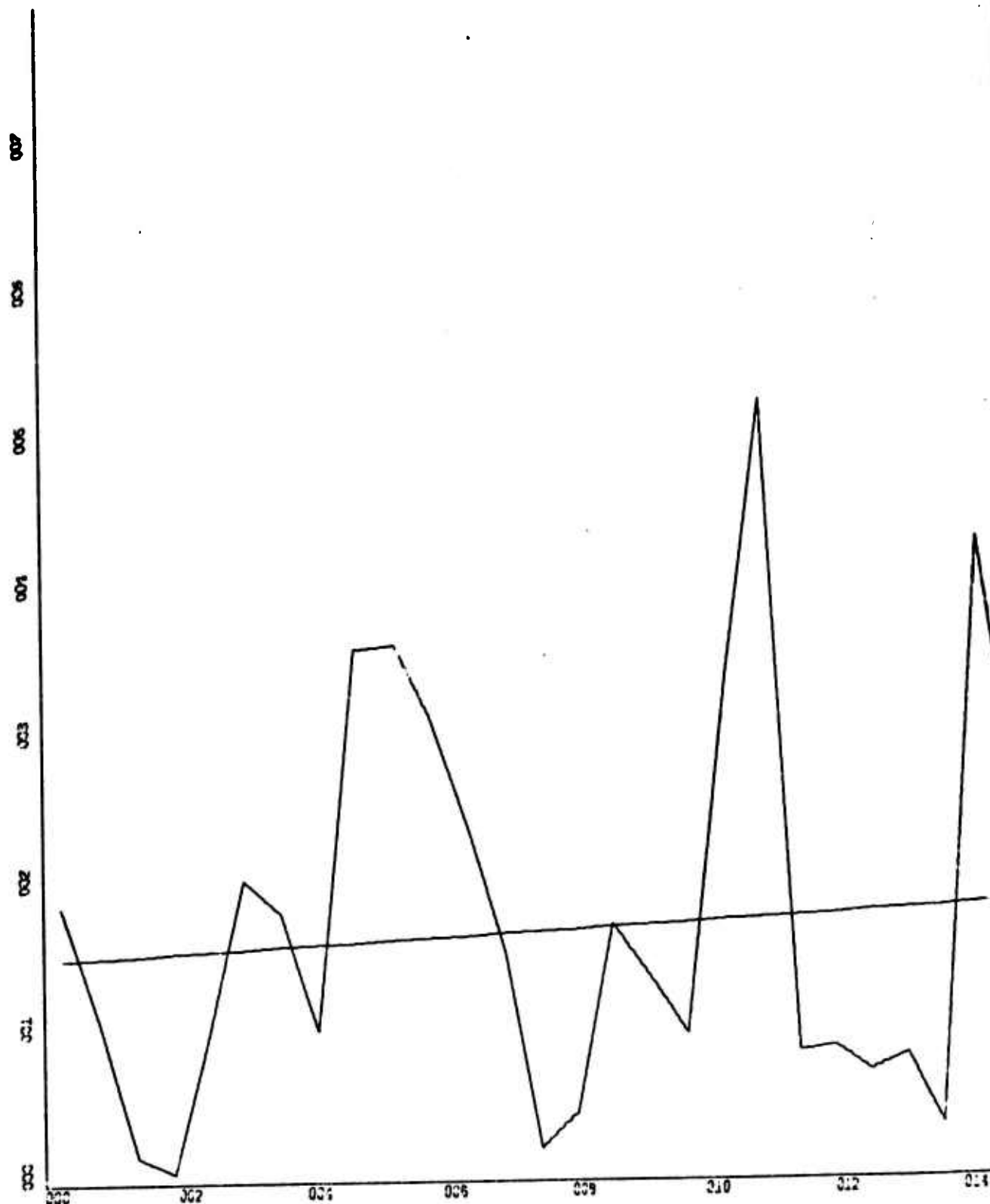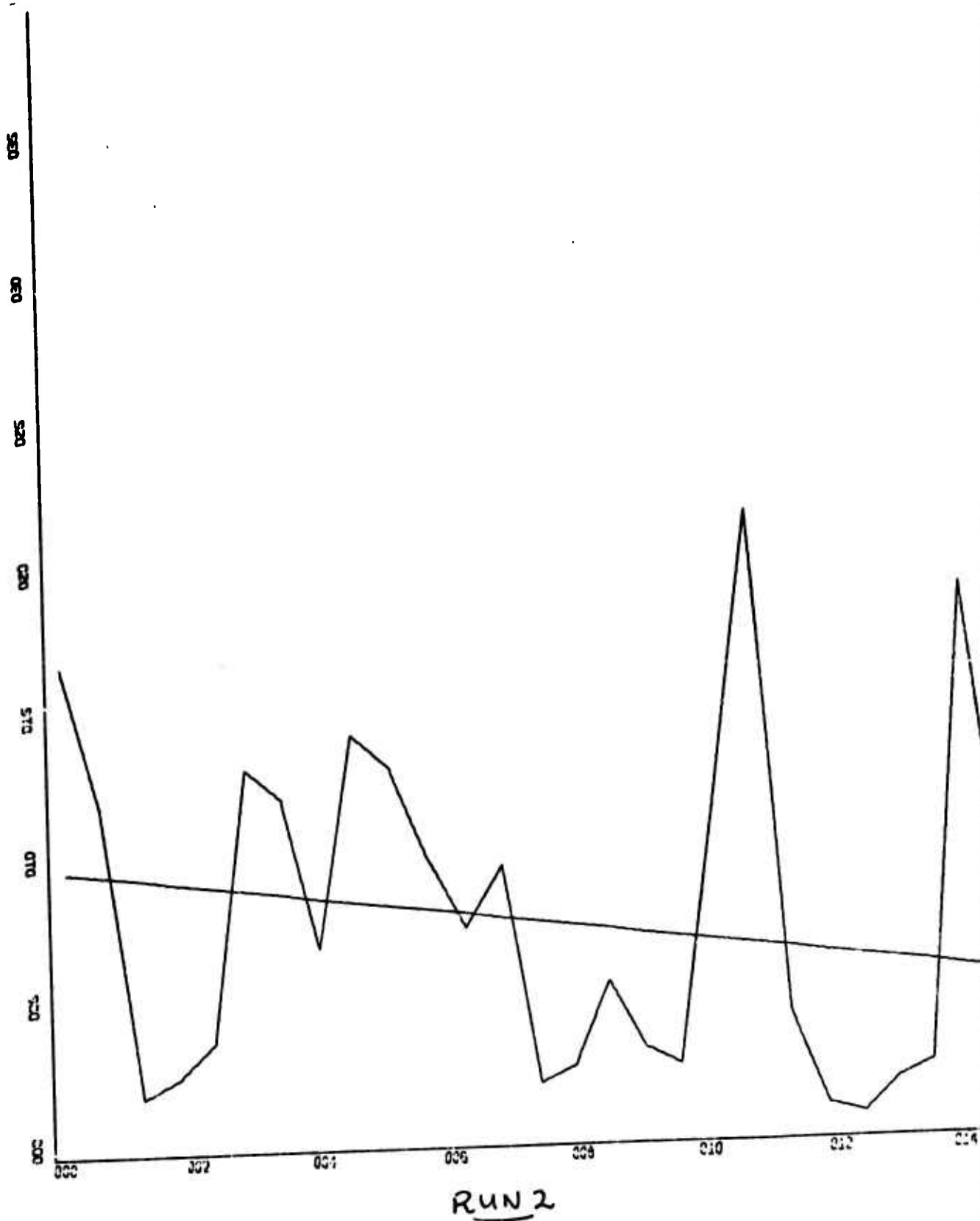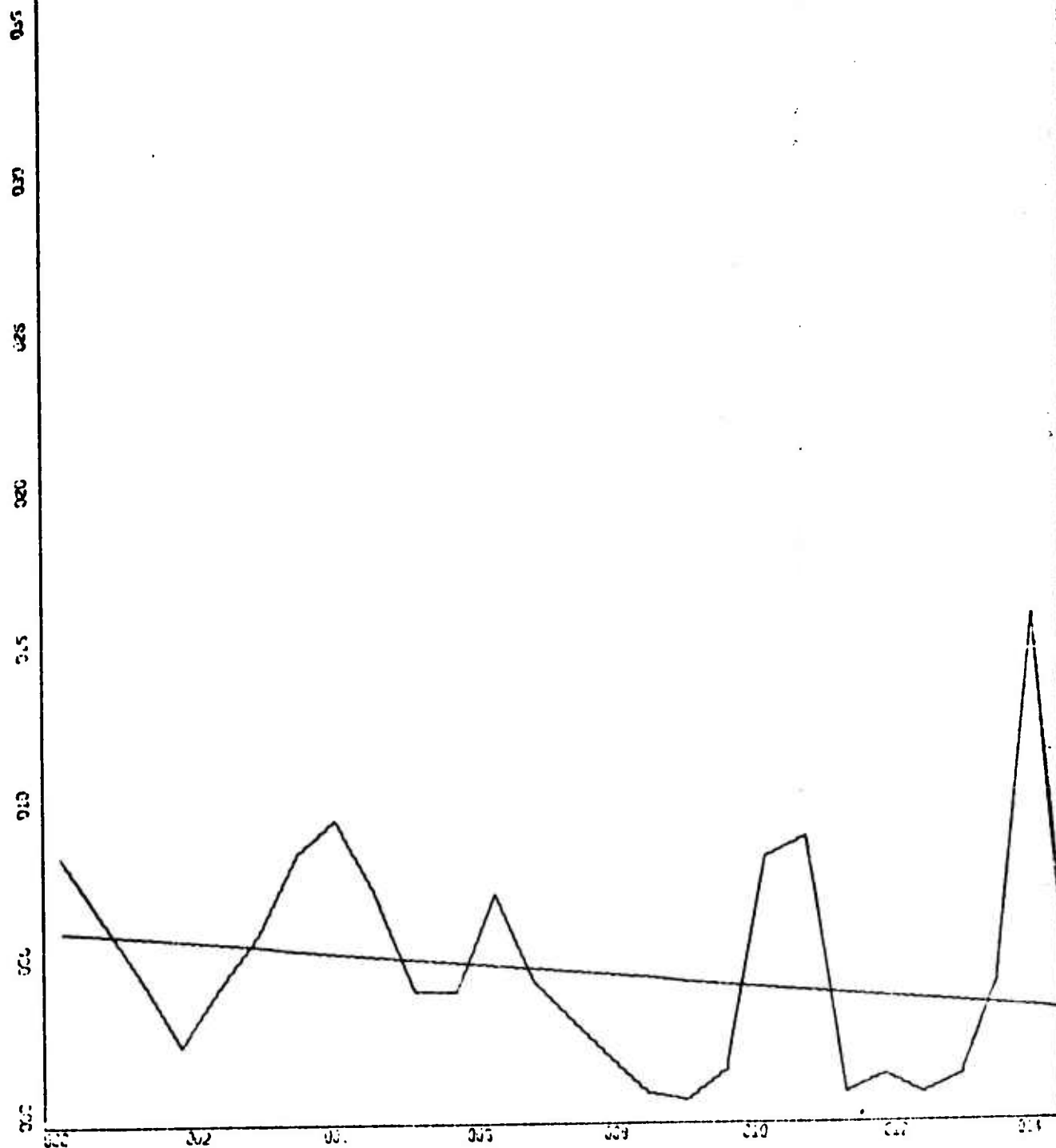VARIANCE FIT

119

RUN 2

X-SCALE:2.00E+02 UNITS INCH. = TIME (sec)
Y-SCALE:5.00E-06 UNITS INCH. = V²(SAM3) (VOLTS²)

VARIANCE FIT

120

RUN2

X-SCALE 2.00E+02 UNITS INCH. = $TIME(sec)$
Y-SCALE 5.00E-01 UNITS INCH. = $V^2(SPHI) (degrees^2)$

VARIANCE FIT

121

RUN 2

X-SCALE=1.00E+02 UNITS INCH. = TIME (SEC)
Y-SCALE=5.00E+00 UNITS INCH. = $V^2(SPH2)$ (degrees^2)
VARIANCE FIT   122

RUN 2

X-SCALE 2.00E-01 UNITS INCH = V^2 (TMH2) ($°C^2$)
Y-SCALE 1.00E-04 UNITS INCH = V^2 (SAMI) (VOLTS^2)
REGRESSION PLOT.

123

RUN 2

X-SCALE=2.00E-01 UNITS INCH. = $V^2(TMH2)$ ($°C^2$)
Y-SCALE=1.00E-04 UNITS INCH. = $V^2(SAM2)$ ($VOLTS^2$)
REGRESSION PLOT

124

RUN 2

X-SCALE: 2.00E-01 UNITS INCH. = V^2(TMH2)($°C^2$)
Y-SCALE: 5.00E-06 UNITS INCH. = V^2(SAM3)(VOLTS^2)
REGRESSION PLOT

RUN 2

X-SCALE=2.00E-01 UNITS INCH.= V^2(TMH2) ($^\circ c^2$)

Y-SCALE=5.00E-01 UNITS INCH.= V^2(SPHI) (degrees^2)

RECRESSION   PLOT

RUN 2

X-SCALE:-2.00E-01 UNITS INCH. = V^2(TMH2) (°C)
Y-SCALE:-5.00E+00 UNITS INCH. = V^2(SPH2) (degrees)
REGRESSION PLOT

RUN 2

X-SCALE 1.00E-04 UNITS INCH. = V^2 (SAMI) (VOLTS^2)

Y-SCALE 2.00E-02 UNITS INCH. = V^2 (WAVE) (m^2)

REGRESSION PLOT

RUN 12

X-SCALE=2.00E+02 UNITS INCH. = TIME (sec)
Y-SCALE=5.00E-02 UNITS INCH. = V² (WAVE)(m²)
VARIANCE FIT

129

RUN 12

X-SCALE=2.00E+02 UNITS INCH. = TIME (sec)
Y-SCALE=1.00E-01 UNITS INCH. = V^2 (TMH2) ($°C^2$)

VARIANCE FIT

130
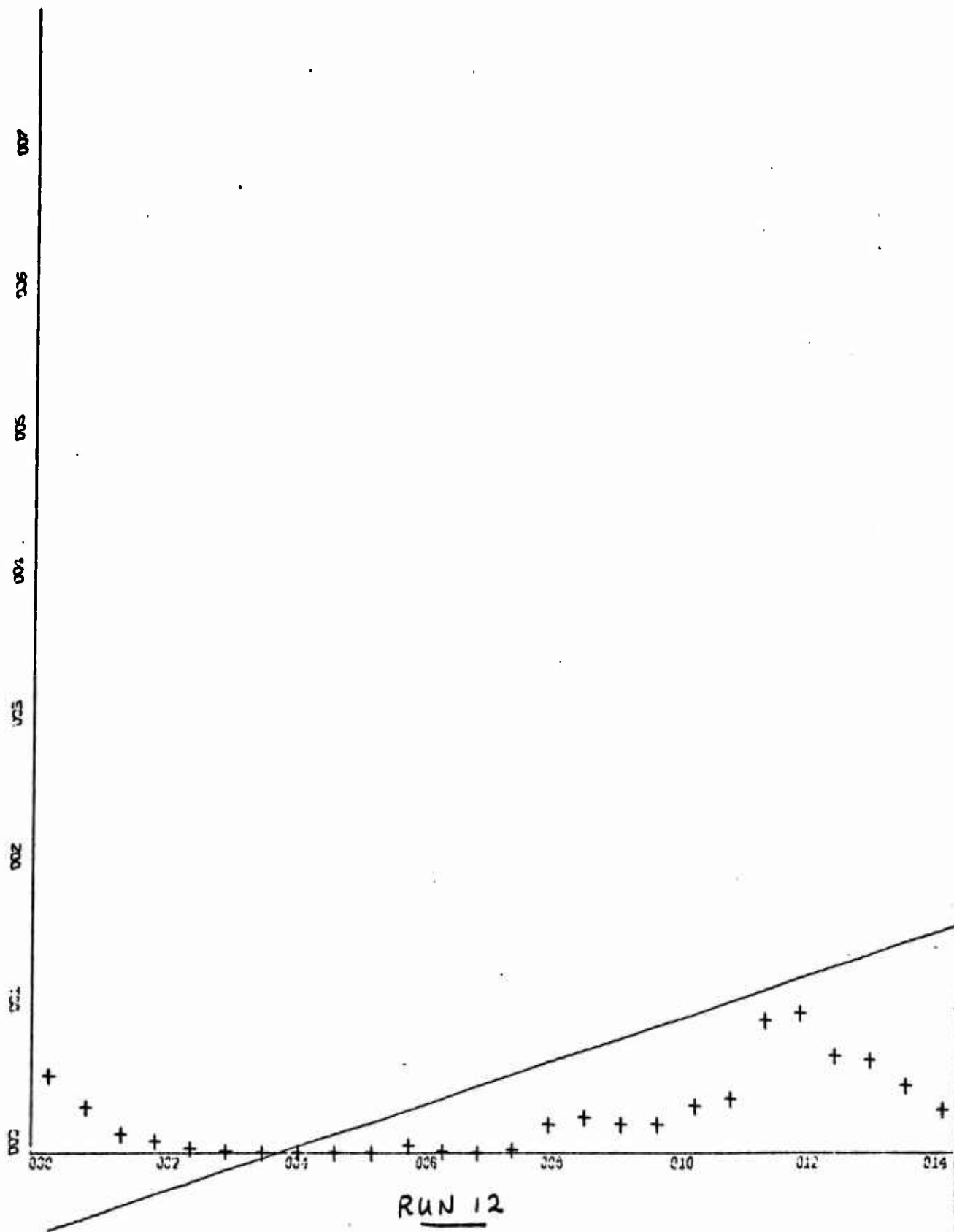
RUN 12

X-SCALE: 2.00E+02 UNITS INCH. = TIME (sec)
Y-SCALE: 5.00E-06 UNITS INCH. = V^2 (SHMI) (VOLTS^2)

VARIANCE FIT

RUN 12

X-SCALE 2.00E+02 UNITS INCH. = TIME (sec)
Y-SCALE 5.00E-02 UNITS INCH. = V^2 (SAM 2) (VOLTS^2)
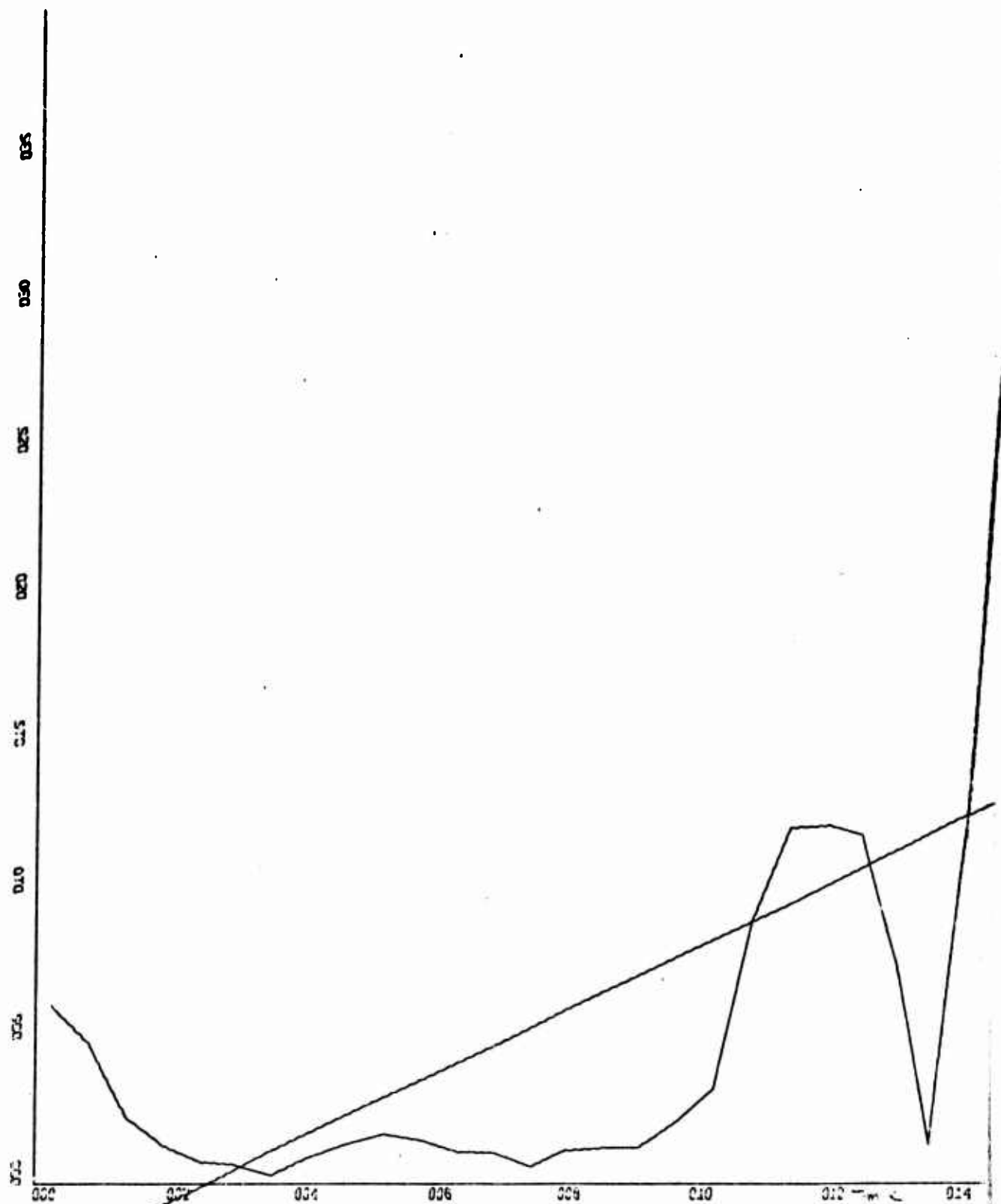
VARIANCE FIT

132

RUN 12

X-SCALE=2.00E+02 UNITS INCH. = TIME (SEC)
Y-SCALE=5.00E-05 UNITS INCH. = V² (SAM3) (VOLTS²)
VARIANCE FIT

X-SCALE:2.00E+02 UNITS INCH. = TIME (sec)
Y-SCALE:1.00E+01 UNITS INCH. = V²(SPHI)(degrees²)
VARIANCE FIT

134

RUN 12

X-SCALE: 2.00E+02 UNITS INCH. = TIME (sec)
Y-SCALE: 5.00E+00 UNITS INCH. = V²(SPH2) (degree²)
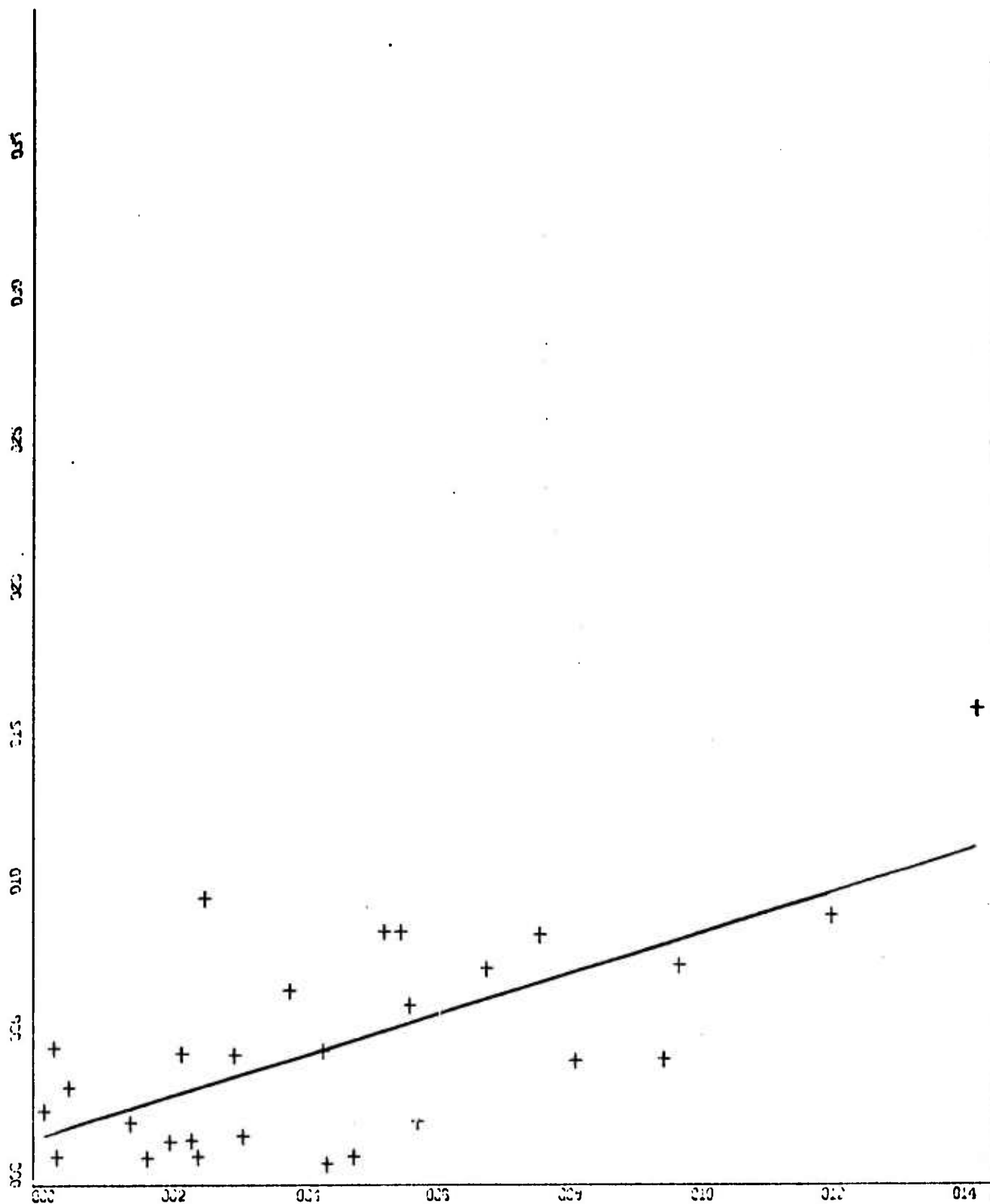VARIANCE FIT

135

RUN 12

X-SCALE: 1.00E-01 UNITS INCH. $= V^2(TMH2)\ (^{\circ}C^2)$
Y-SCALE: 5.00E-06 UNITS INCH. $= V^2(SAMI)\ (VOLTS^2)$
REGRESSION PLOT

136
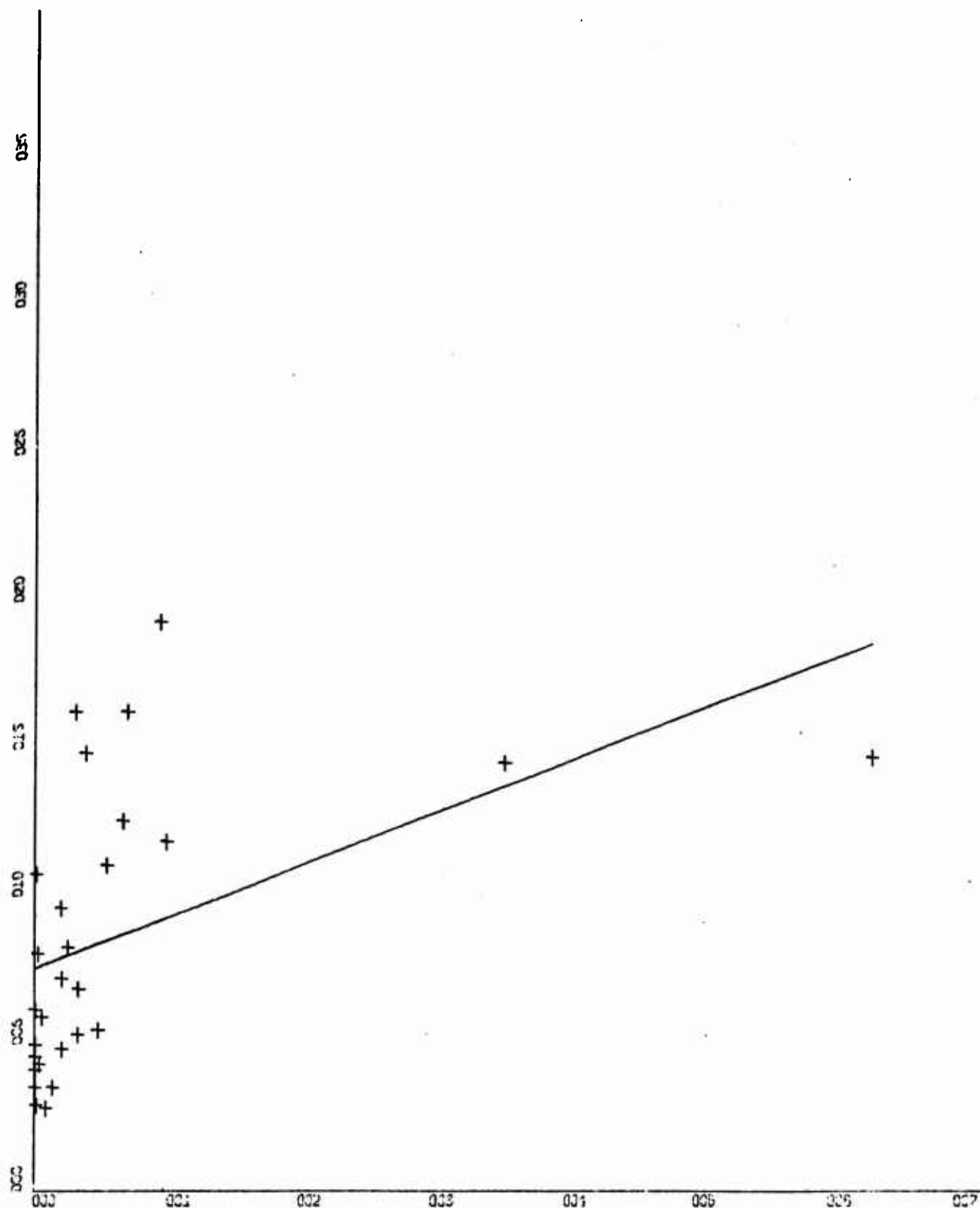
RUN 12

X-SCALE 1.00E-01 UNITS INCH. = V^2 (TMH2) ($°C^2$)
Y-SCALE 5.00E-07 UNITS INCH. = V^2 (SAM2) (VOLTS^2)
REGRESSION PLOT
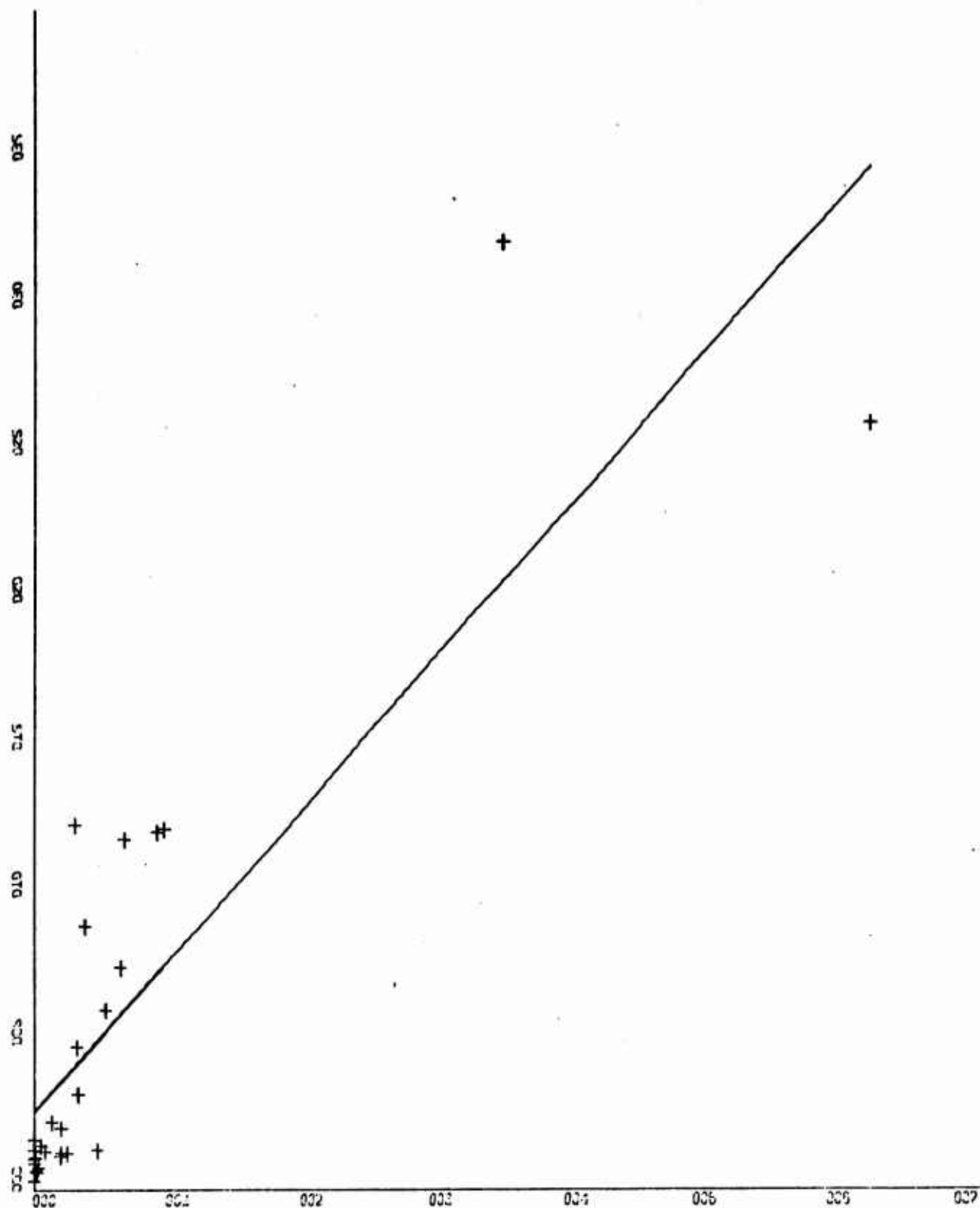
RUN 12

X-SCALE 1.00E-01 UNITS INCH. = V^2 (TMH2) $(°C^2)$
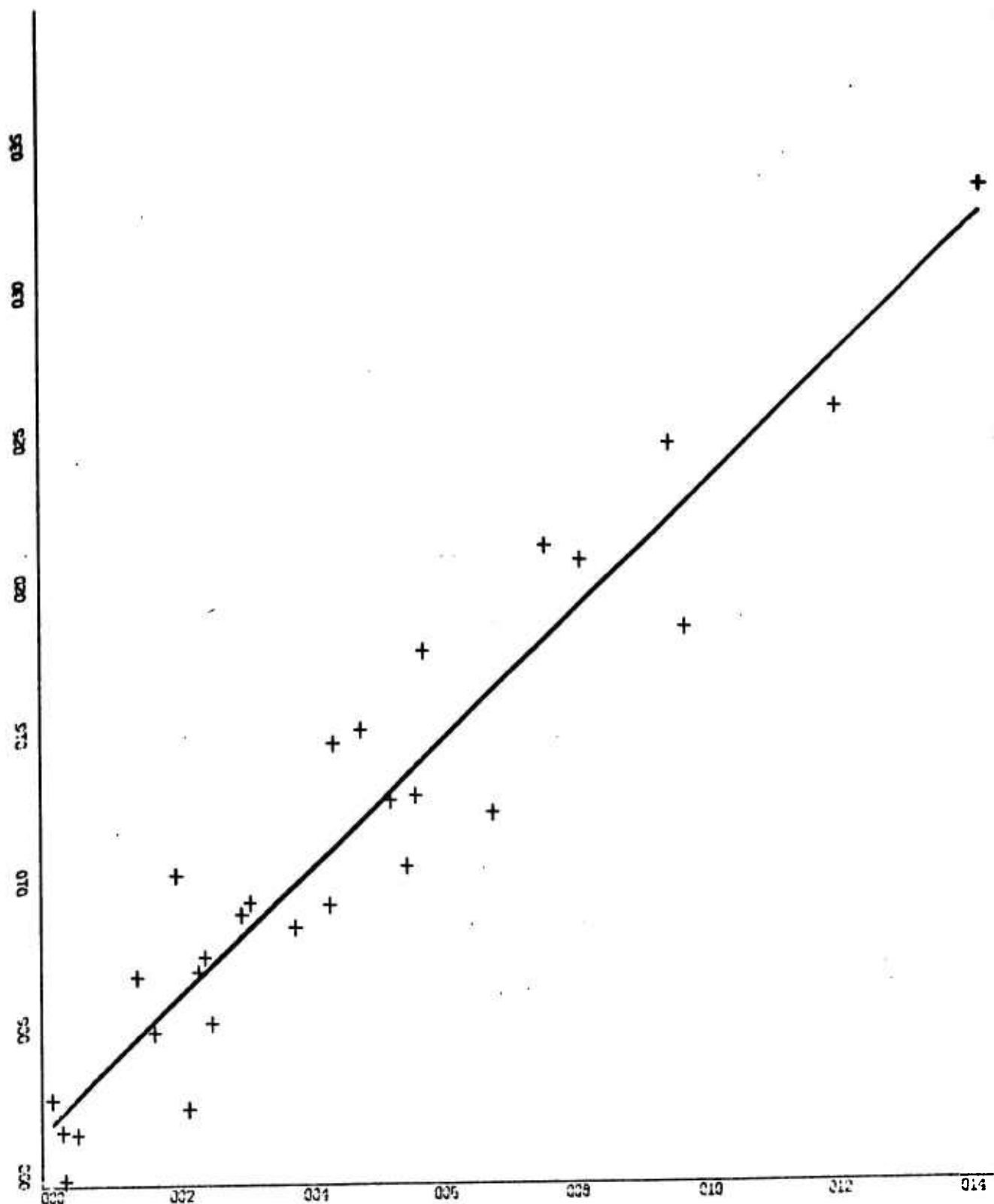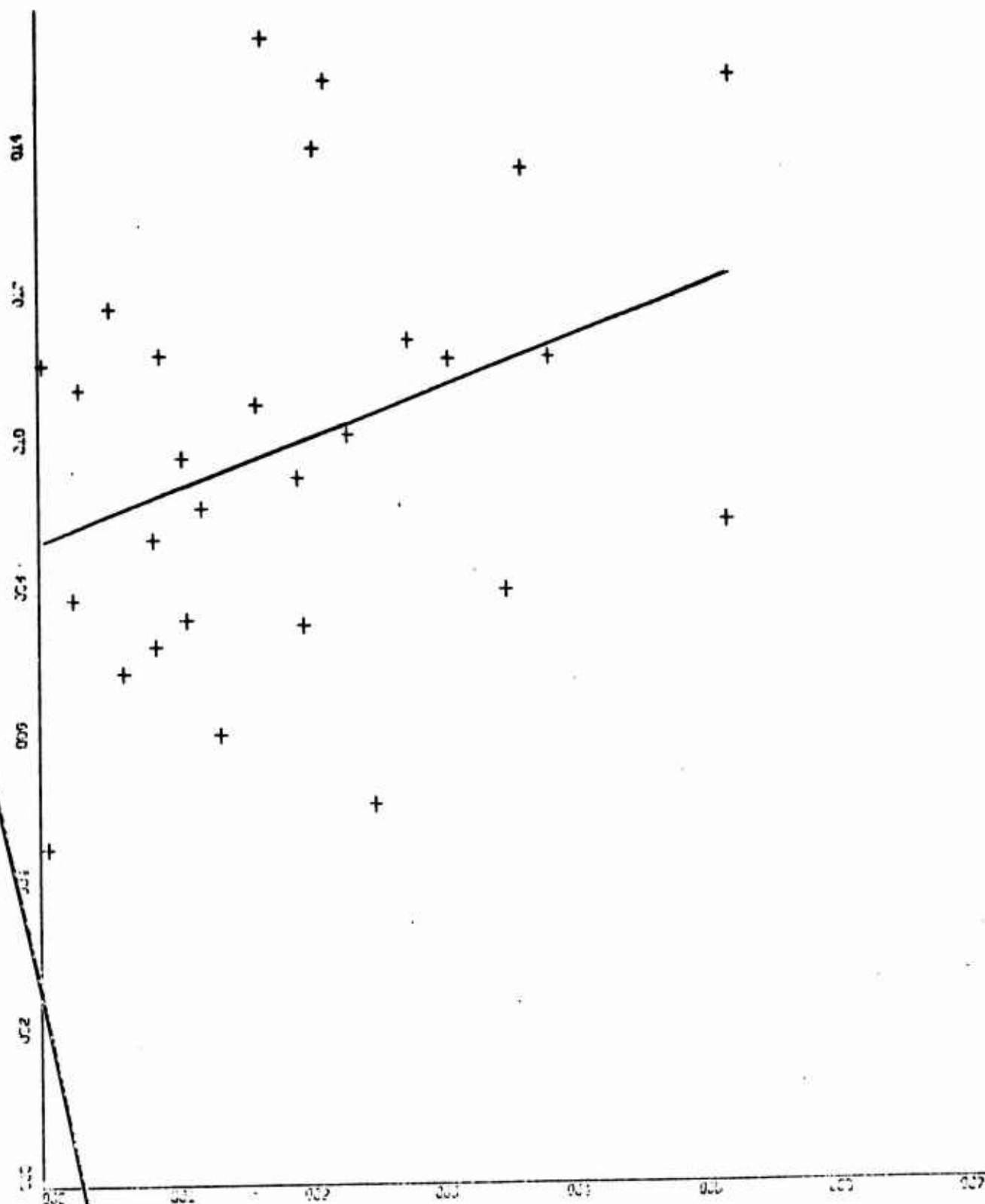Y-SCALE 5.00E-05 UNITS INCH. = V^2 (SAM3) (VOLTS^2)
REGRESSION PLOT
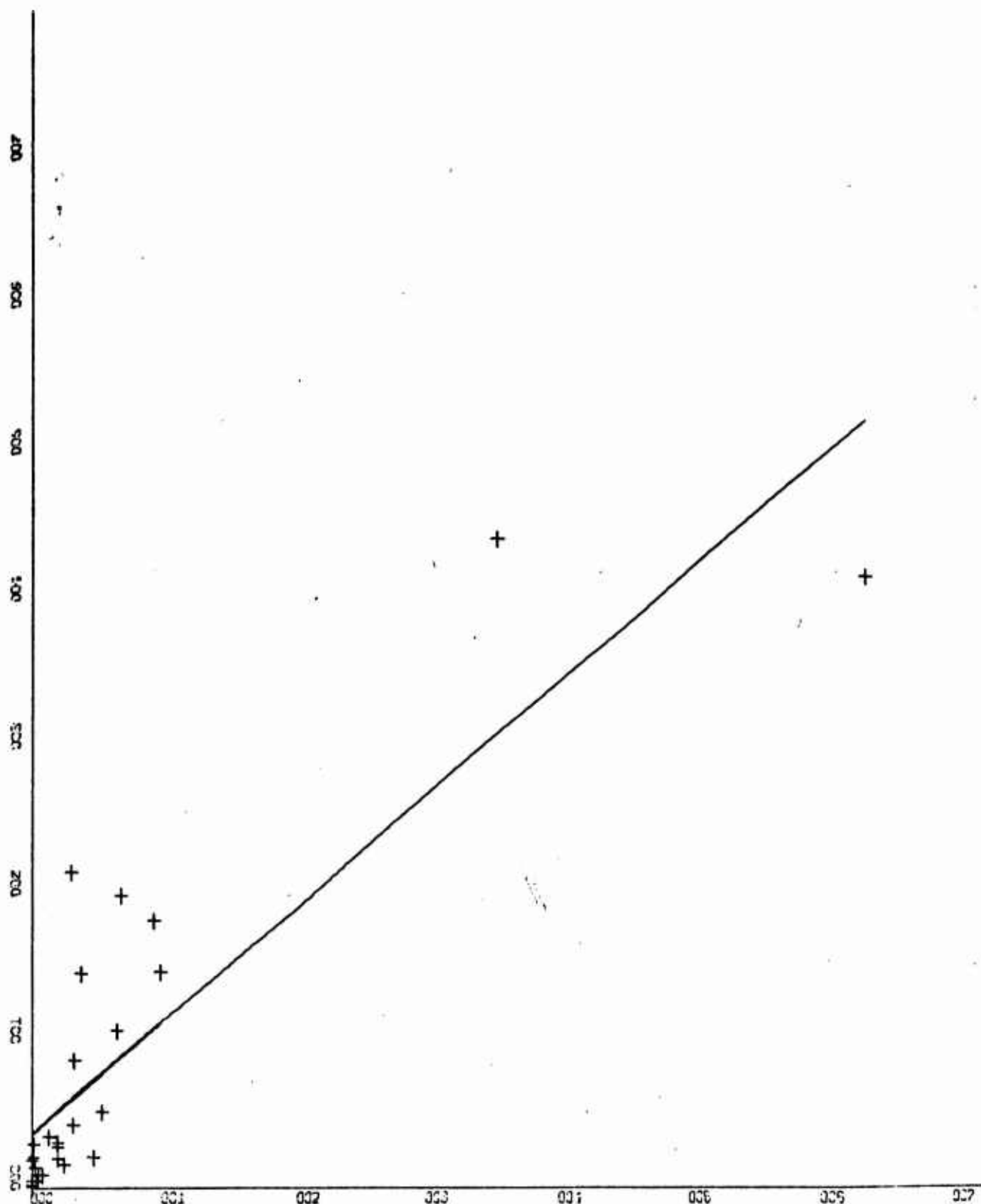
RUN 12

X-SCALE=1.00E-01 UNITS INCH. = V^2 (TMH2) ($^{o}c^2$)
Y-SCALE=1.00E+01 UNITS INCH. = V^2 (SPHI) (degrees^2)
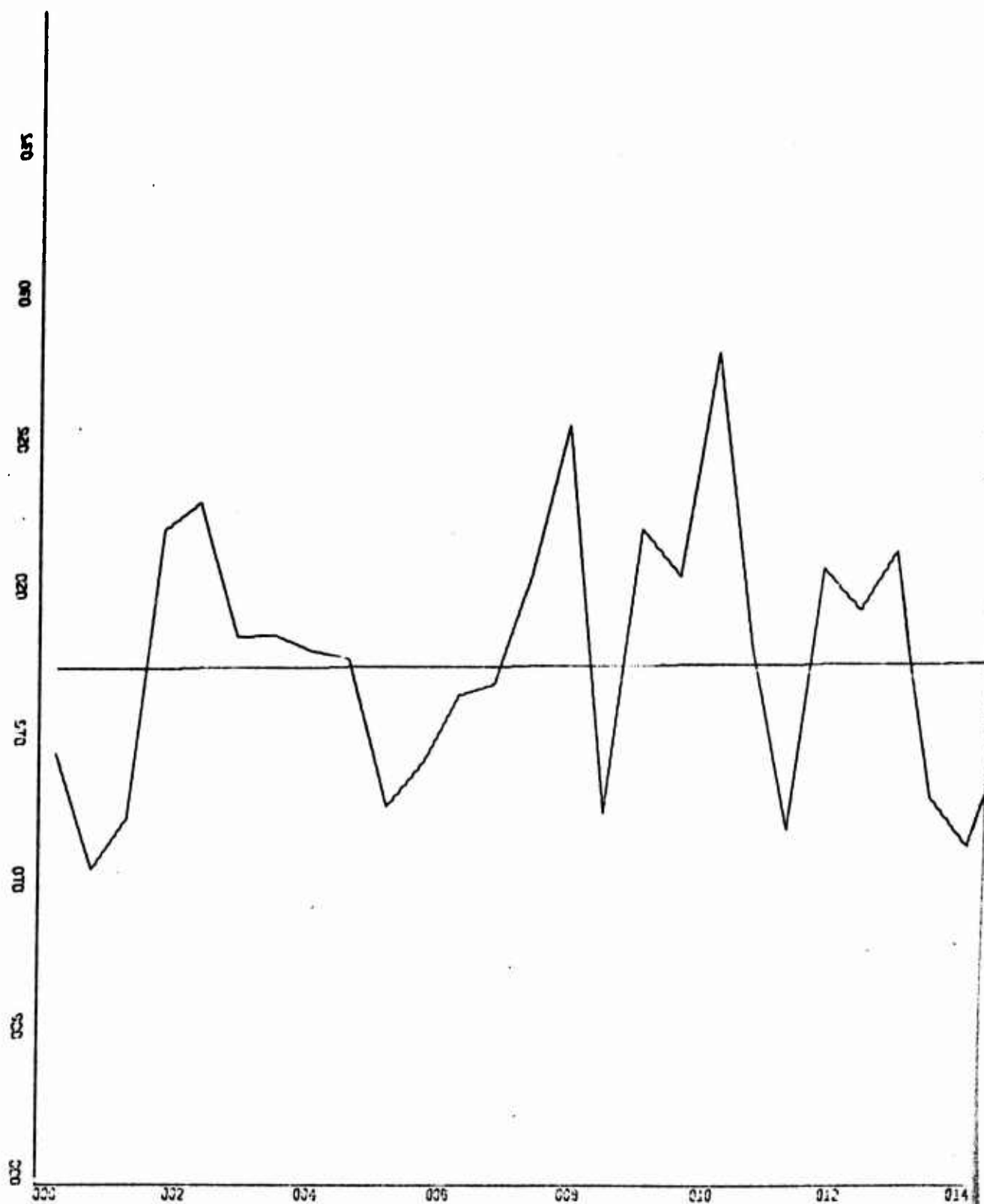REGRESSION PLOT
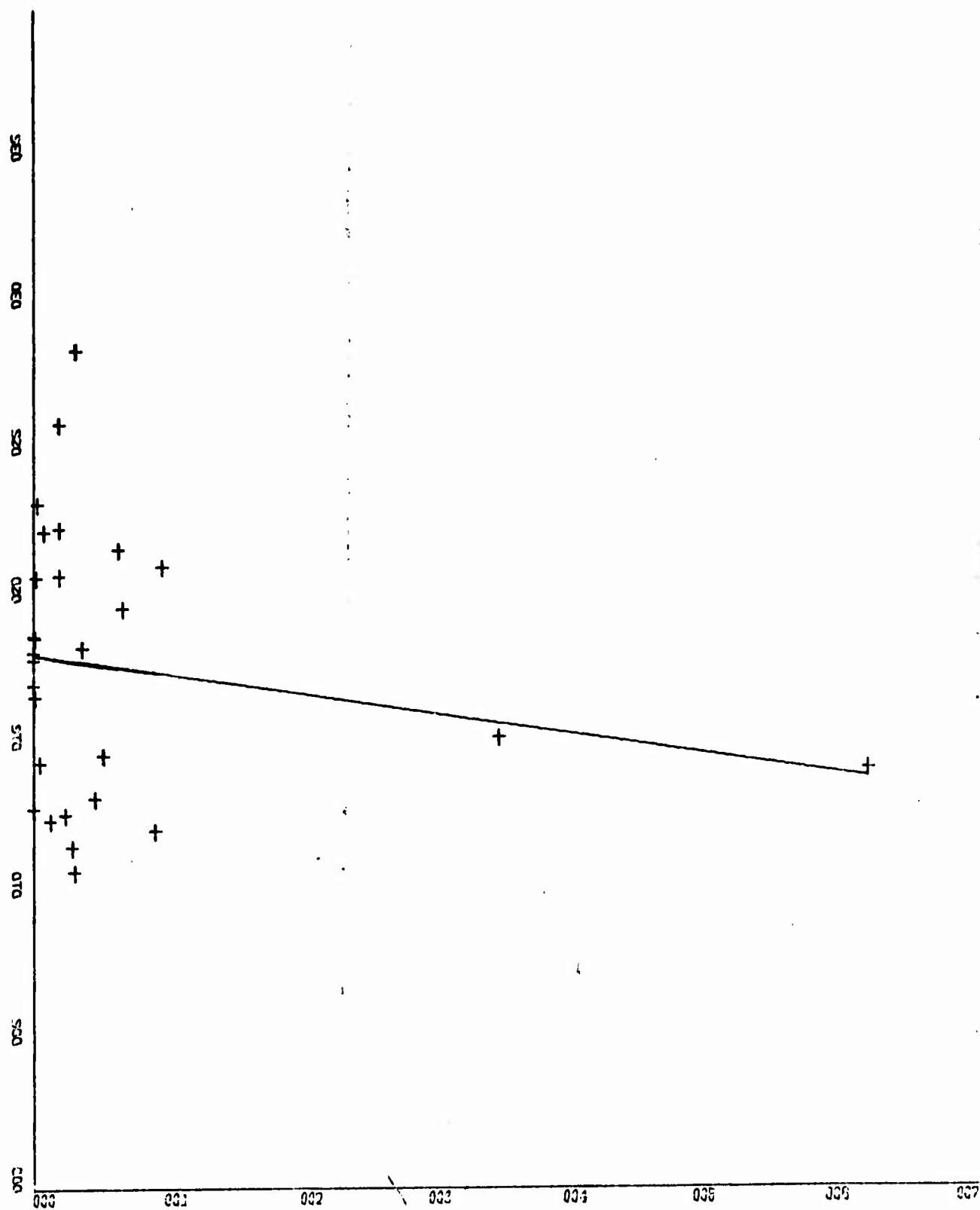
RUN 12

X-SCALE=1.00E-01 UNITS INCH. = $V^2(TMH2)$ $(°C^2)$
Y-SCALE=5.00E-02 UNITS INCH. = $V^2(SPH2)$ $(degrees^2)$

REGRESSION PLOT

140
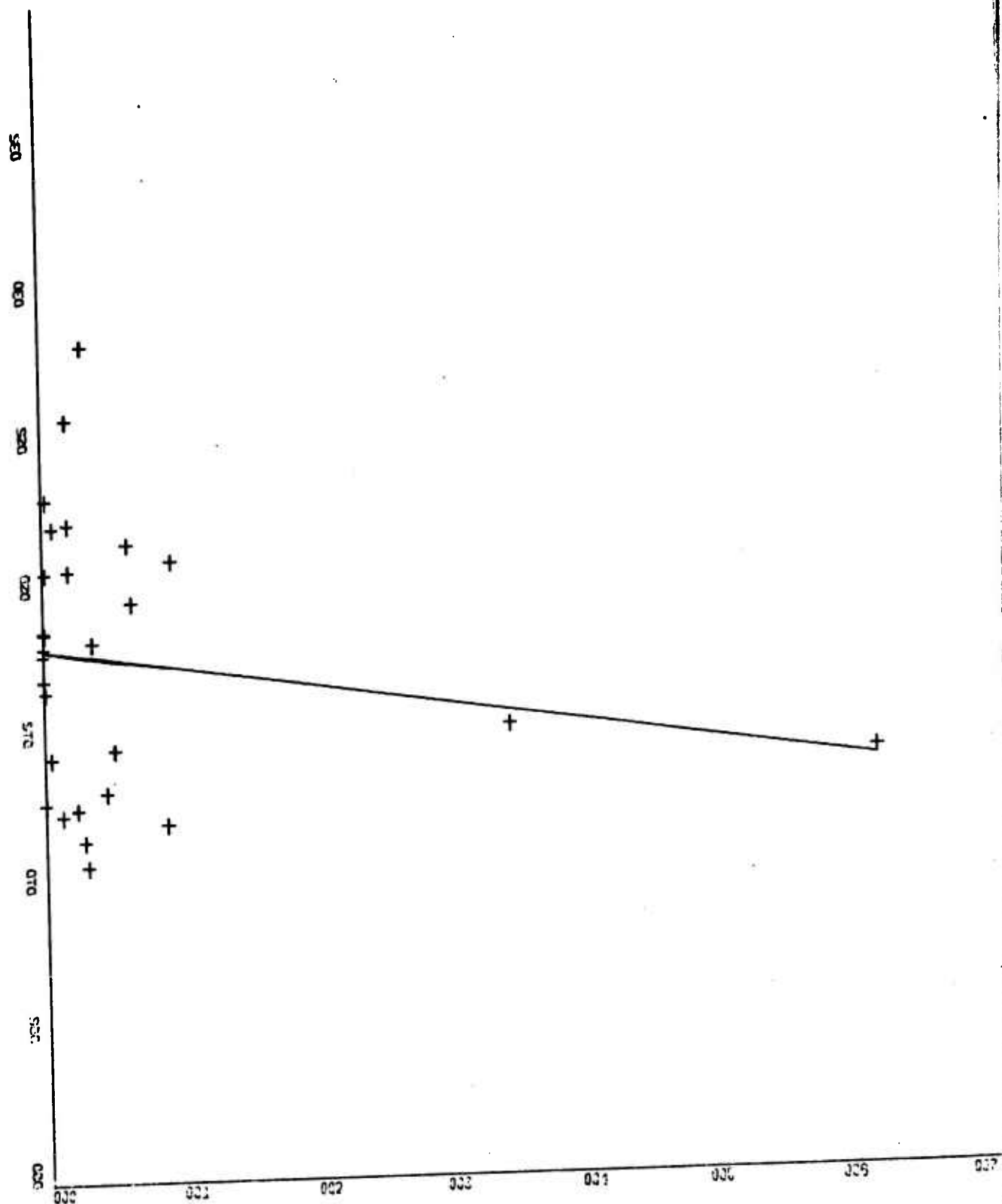
RUN 12

X-SCALE 1.00E-01 UNITS INCH. = V^2 (WAVE) (m^2)
Y-SCALE 5.00E-02 UNITS INCH. = V^2 (TMH2) ($^\circ C^2$)

REGRESSION PLOT 141

APPENDIX C

Spatial Correlation and Structure Functions

The values of the spatial correlation function and structure function calculated during spatial stochastic analyses are tabulated in Tables C1 - C6. The functions were calculated along the vertical thermistor array. The variance of the temperature at each thermistor over the ensemble is also given.

The Tables include:

Table #	Ensemble
C1	Run 1, 26.67 min
C2	Run 2, 26.67 min
C3	Run 3, 26.67 min
C4	Low turbulence intensity
C5	Middle turbulence intensity
C6	High turbulence intensity

TABLE C1. Run 1, Vertical Spatial Correlation and Structure Function.

Thermistor No.	Variance ($^\circ C^2$)
1	0.5999
2	1.0970
3	0.0540
4	0.3090
5	0.2722
6	0.1359
7	0.0747

Correlation Function	Structure Function	Lag
1.0000	0.0	0.0
0.9635	0.2081	5.0000
0.3745	0.5841	15.0000
0.3654	0.4673	20.0000
0.5507	0.3978	25.0000
2.6243	0.9860	25.0000
0.5208	0.5926	30.0000
0.1736	0.3503	45.0000
0.2716	0.2302	55.0000
0.2668	0.7407	80.0000
0.2430	0.9232	85.0000
0.0721	0.3287	100.0000
0.5209	3.1869	135.0000
0.9274	3.3103	150.0000
0.9724	3.0852	155.0000
0.3622	1.6778	160.0000
0.6725	1.9936	175.0000
0.6874	1.8289	180.0000
0.5094	3.5094	180.0000
0.3640	1.9750	205.0000
0.1944	3.9140	235.0000
0.1514	2.1753	260.0000

143

TABLE C2.   Run 2, Vertical Spatial Correlation and Structure Function

Thermistor No.	Variance ($°C^2$)
1	0.2154
2	0.1750
3	0.3544
4	0.5783
5	0.3910
6	0.4338
7	0.5170

Correlation Function	Structure Function	Lag
1.0000	0.0	0.0000
1.0592	0.3607	5.0000
1.0090	0.3676	15.0000
0.9452	0.0160	20.0000
1.0354	0.0388	25.0000
1.0891	0.4103	30.0000
0.9706	0.0749	45.0000
1.1503	0.1313	55.0000
1.0532	0.2159	80.0000
1.0844	0.6326	85.0000
0.9813	0.2662	100.0000
0.5463	0.2614	135.0000
0.6164	0.6939	150.0000
0.5559	0.3357	155.0000
0.5010	0.4553	160.0000
0.5551	0.9197	175.0000
0.4985	0.5539	180.0000
0.5580	0.4413	180.0000
0.4878	0.6848	205.0000
0.5458	0.6783	235.0000
0.4557	0.9619	260.0000

TABLE C3. Run 12, Vertical Spatial Correlation and Structure Function

Thermistor No.	Variance ($^\circ C^2$)
1	0.2792
2	0.2433
3	0.1690
4	0.1444
5	0.1275
6	0.0743
7	0.0083

Correlation Function	Structure Function	Lag
1.0000	0.0	0.0
1.0558	0.0211	5.0000
1.1642	0.1301	15.0000
1.0859	0.1540	20.0000
0.7096	0.1640	25.0000
1.5349	1.0283	25.0000
0.7463	0.2231	30.0000
0.7552	0.3984	45.0000
0.1447	0.3588	55.0000
0.1852	0.6946	80.0000
0.1969	0.8039	85.0000
0.1995	0.9920	100.0000
0.8057	1.6228	135.0000
0.6778	1.6854	150.0000
0.6295	1.6494	155.0000
0.6143	2.2873	160.0000
0.5148	2.2931	175.0000
0.4773	2.2355	180.0000
0.4121	1.6676	180.0000
0.2998	2.1737	205.0000
0.1487	1.6762	235.0000
0.1214	2.0123	260.0000

TABLE C4. Low-Intensity, Vertical Spatial Correlation and Structure Function

Thermistor No.	Variance ($°C^2$)
1	0.0666
2	0.0774
3	0.0062
4	0.0038
5	0.0028
6	0.0114
7	0.0014

Correlation Function	Structure Function	Lag
1.0000	0.0	0.0
1.0785	0.2173	5.0000
1.3019	0.9860	15.0000
1.0129	1.1896	20.0000
0.2793	4.5337	25.0000
9.4721	32.6599	25.0000
0.2274	5.0118	30.0000
0.0791	6.1497	45.0000
0.1556	4.2863	55.0000
0.4158	0.6737	80.0000
0.4850	0.9095	85.0000
0.6269	1.4669	100.0000
3.1748	23.5975	135.0000
1.6307	25.8445	150.0000
1.5337	25.6640	155.0000
2.9846	20.1207	160.0000
1.5724	22.1038	175.0000
1.1432	22.5880	180.0000
0.7332	30.3575	180.0000
-1.6798	31.3264	205.0000
0.5584	27.1199	235.0000
1.1856	22.0083	260.0000

TABLE C5. Mid-Intensity, Vertical Spatial Correlation and Structure Function

Thermistor No.	Variance ($°C^2$)
1	0.3603×10^{-5}
2	0.3726×10^{-3}
3	0.8536×10^{-1}
4	0.1329
5	0.1011
6	0.8996×10^{-1}
7	0.3400×10^{-1}

Correlation Function	Structure Function	Lag
1.0000	0.0	0.0
1.0345	0.2462	5.0000
0.9265	0.3068	15.0000
0.8702	0.1042	20.0000
0.8345	0.2212	25.0000
0.0002	0.0034	25.0000
0.8742	0.4570	30.0000
0.6962	0.3425	45.0000
0.2549	0.7168	55.0000
0.2131	0.9103	80.0000
0.2374	1.1769	85.0000
0.1709	0.8393	100.0000
0.0130	0.8224	135.0000
0.0205	1.2779	150.0000
0.0134	0.9769	155.0000
-0.0008	0.8464	160.0000
-0.0005	1.3162	175.0000
-0.0008	1.0017	180.0000
0.0149	0.8641	180.0000
-0.0004	0.8911	205.0000
0.0154	0.3093	235.0000
0.0005	0.3356	260.0000

TABLE C6. High-Intensity, Vertical Spatial Correlation and Structure Function

Thermistor No.	Variance ($^\circ C^2$)
1	0.1800×10^{-5}
2	0.2462×10^{-3}
3	0.4578×10^{-3}
4	0.1231×10^{-1}
5	0.1226×10^{-2}
6	0.5298×10^{-2}
7	0.2655×10^{-1}

Correlation Function	Structure Function	Lag
1.0000	0.0	0.0
0.6971	9.6513	5.0000
0.3813	9.6565	15.0000
0.5125	0.3485	20.0000
1.7985	1.7245	25.0000
0.0147	0.1730	25.0000
1.1782	12.0107	30.0000
0.8521	2.9908	45.0000
8.3755	9.2314	55.0000
3.7301	15.2006	80.0000
2.9532	25.7984	85.0000
1.9051	18.2240	100.0000
0.2184	0.1375	135.0000
0.2522	9.7420	150.0000
0.2551	0.6906	155.0000
0.0156	0.3438	160.0000
0.0156	10.0158	175.0000
0.0170	0.9675	180.0000
0.3564	3.8096	180.0000
0.0179	4.2871	205.0000
1.0541	19.7533	235.0000
0.0543	21.5538	260.0000

LIST OF REFERENCES

1. Batchelor, G.K., Kolmogorov's Theory of Locally Isotropic Turbulence, Proc. Camb. Phil. Soc. v. 43, p. 533, 1947.

2. Bendat, K.R. and Piersol, A.G., Random Data: Analysis and Measurement Procedures, Wiley-Interscience, 1971.

3. Bisset-Berman Corporation Report MJO-1049, The Turbulent Distribution of Temperature in the Ocean, by C.F. Black, 23 December 1965.

4. Born, M., Atomic Physics, Hafner Publishing Company, New York, 1933.

5. Chernov, L.A., Wave Propagation in a Random Medium, Translated by R.A. Silverman, McGraw-Hill, 1960.

6. Davidson, K.L., "An Investigation of the Influence of Water Waves on the Advacent Airflow," PH.D. Dissertation, University of Michigan 1970.

7. Denner, W.W., "The Layered Microstructure and Acoustic Propagation in the Arctic Ocean," U.S. Navy Journal of Underwater Acoustics, v. 21(1), p. 45-51, January 1971.

8. Enochson, L.D. and Otnes, R.K., Programming and Analysis for Digital Time Series Data, Navy Publication and Printing Service, 1968.

9. Frisch, U., Probabilistic Methods in Applied Mathematics, A.T. Bharucha-Reid, Ed., Academic Press, New York, 1968.

10. Grant, H.L. and others, "Turbulence Spectra from a Tidal Channel", J. Fluid Mech., v. 12, p. 241, 1962.

11. Gregg, M.C., "The Microstructure of the Ocean," Scientific American, v. 228(2), p. 65-77, February 1973.

12. Haley, M.C., "Small Scales Interactions in the Near Surface Ocean," M.S. Thesis, Naval Postgraduate School, December 1974.

13. Kane, L.K.II, Measurement and Analysis of Temporal Variations of Salinity in Shallow Water, M.S. Thesis, Naval Postgraduate School, September 1974.

14. Kolomogorov, A.N., "Local Structure of Turbulence in an Incompressible Fluid at Very High Reynolds Numbers," Doklady AN SSSR, v. 30(4), p. 299-303, 1941.

15. Liebermann, L., "The Effect of Temperature Inhomogeneities in the Ocean on the Propagation of Sound," Journal of the Acoustical Society of America, v. 23(5), p. 563-570, September 1951.

16. Lumley, J.L. and Panofsky, H.A., The Structure of Atmospheric Turbulence, p. 239, Wiley 1964.

17. Mintzer, D., "Wave Propagation in a Randomly Inhomogeneous Medium," Journal of the Acoustical Society of America, v. 25 part I, p. 922-927; and part II, 1107-1111, 1953.

18. Naval Postgraduate School Report NPS61Md73121A, Sound Speed Dispersion and Fluctuations in the Upper Ocean: Project BASS, by H. Medwin, October 1973.

19. Naval Postgraduate School Report NPS61Ms73111A, Predicting Sound Phase and Amplitude Fluctuations due to Microstructure in the Upper Ocean, by H. Medwin, November 1973.

20. Naval Postgraduate School Report NPS58TM74021, Separating Turbulent and Wave Induced Velocity and Temperature Fluctuations, by E.B. Thornton and N.E.J. Boston, December 1973.

21. Neubert, J.A., "Asymptotic Solution of the Stochastic Helmholtz Equation for Turbulent Water," Journal of the Acoustical Society of America, v. 48(5), part 2, p. 1203-1211, November 1970.

22. Neubert, J.A. and Lumley, J.C., "Derivation of the Stochastic Helmholtz Equation for Sound Propagation in a Turbulent Fluid," Journal of the Acoustical Society of America, v. 48, p. 1212-1218, November 1970.

23. Phillips, O.M., The Dynamics of the Upper Ocean, Cambridge University Press, 1966.

24. Pond, S. and others, "Turbulence Spectra in the Wind Over Waves," J. Atmos. Sci., v. 20, p. 319, 1963.

25. Powell, J.W., An Investigation of Surface and Internal Wave-Induced Turbulence in Shallow Water Thermal Microstructure, M.S. Thesis, Naval Postgraduate School March 1974.

26. Rytov, S.M., "Diffraction of Light by Ultrasonic Waves," Izv. Akol, Nauk SSSR, Ser. Fiz., v. 2, p. 233, 1937.

27. Sagar, F.H., "Fluctuations in Intensity of Short Pulses of 14.5-KC Sound Received from a Source at Sea," *Journal of the Acoustical Society of America*, v. 27 (6), p. 1092-1106, November 1955.

28. Sagar, F.H., "Comparison of Experimental Underwater Acoustic Intensities of Frequency 14.5 KC with Values Computed for Selected Thermal Conditions at Sea," *Journal of the Acoustical Society of America*, v. 29(8), p. 948-965, August 1957.

29. Sagar, F.H., "Acoustic Intensity Fluctuations and Temperature Microstructure in the Sea," *Journal of the Acoustical Society of America*, v. 32(1), p. 112-121, January 1960.

30. Sheehy, M.J., "Transmission of 24 KHZ Sound from a Deep Source," *Journal of the Acoustical Society of America*, v. 22(1), p. 24-28, 1950.

31. Stewart, R.W. and Grant, H.L., "Determination of the Rate of Dissipation of Turbulent Energy near the Sea Surface in the Presence of Waves," *Journal of Geophysical Research*, v. 67(8), p. 3177-3181, July 1962.

32. Stone, R.G. and Mintzer, D., "Range Dependence of Acoustic Fluctuations in a Randomly Inhomogeneous Medium," *Journal of the Acoustical Society of America*, v. 34 p. 647-653, 1962.

33. Stone, R.G. and Mintzer, D., "Transition REgime for Acoustic Fluctuatio.s in a Randomly Inhomogeneous Medium," *Journal of the Acoustical Society of America*, v. 38, p. 843-846, November 1965.

34. Strobehn, J.W., "Line-of-Sight Wave Propagation Through the Turbulent Atmosphere," *Proceedings of the IEEE*, v. 56(8), p. 1301-1318, August 1968.

35. Tatarski, V.I., "On Strong Amplitude Fluctuations of a Wave Propagating in a Medium with Weak Random Inhomogeneities," (in Russian), *Radiofiz.*, v. 10, p. 1, 1967.

36. Tatarski, V.I., *Wave Propagation in a Turbulent Medium*, Translated by R.A. Silverman, McGraw-Hill, 1961.

37. Thornton, E.B. and Krapohl, R.F., "Water Particle Velocities Measured Under Ocean Waves," *Journal of Geophysical Research*, v. 79(6), p. 847-852, February 1974.

38. Urick, H.J., _Principles of Underwater Sound for Engineers_, McGraw-Hill, 1967.

39. Woods, J.D. and Wiley, R.L., "Billow Turbulence and Ocean Microstructure," _Deep Sea Research_, v. 19, p. 87-121, Pergamon Press, 1972.

40. Whitmarsh, D.C., and others, "Forward Scattering of Sound in the Sea and its Correlation with the Temperature," _Journal of the Acoustical Society of America_, v. 29(10), p. 1124-1143, October 1957.